# NASA CONTRACTOR REPORT

NASA CR-2766

NASA CR-2766
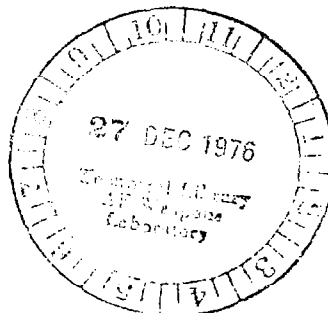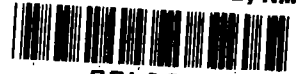
# ANALYSIS OF PRESSURE DISTORTION TESTING

*K. E. Koch and R. L. Rees*

*Prepared by*
GENERAL ELECTRIC COMPANY
Cincinnati, Ohio 45215
*for Lewis Research Center*

27 DEC 1976

NATIONAL AERONAUTICS AND SPACE ADMINISTRATION • WASHINGTON, D. C. • DECEMBER 1976

| 1. Report No. NASA CR-2766 | 2. Government Accession No. | 3. Recipient's Catalog No. |
|---|---|---|
| 4. Title and Subtitle ANALYSIS OF PRESSURE DISTORTION TESTING | | 5. Report Date December 1976 |
| | | 6. Performing Organization Code |
| 7. Author(s) K. E. Koch and R. L. Rees | | 8. Performing Organization Report No. 76AEG272 |
| 9. Performing Organization Name and Address General Electric Company 1 Jimson Road Cincinnati, Ohio 45215 | | 10. Work Unit No. |
| | | 11. Contract or Grant No. NAS3-19522 |
| 12. Sponsoring Agency Name and Address National Aeronautics and Space Administration Washington, D.C. 20546 | | 13. Type of Report and Period Covered Contractor Report |
| | | 14. Sponsoring Agency Code |

15. Supplementary Notes

16. Abstract

The development of General Electric's distortion methodology, Method D, was documented, and its application to steady-state and unsteady data was demonstrated. Three methodologies based upon DIDENT, a NASA-LeRC distortion methodology based upon the parallel-compressor model, were investigated by applying them to a set of steady-state data. The best formulation was then applied to an independent data set. The good correlation achieved with this data set showed that Method E, one of the above methodologies, it is a viable concept. Unsteady data were analyzed by using the Method E methodology. This analysis pointed out that the Method E sensitivities are functions of pressure defect level as well as corrected speed and pattern. No compressor "critical time" could be determined because the unsteady pressure defect levels were beyond the range of the steady-state data base used to define the sensititivites. One of the requirements of the Method E methodology is that the basic pattern type must be recognized by the computer program employing Method E. Two pattern recognition techniques were developed and investigated. Neither one proved completely satisfactory. Independent work at NASA-LeRC showed one recognition technique to be successful. It is documented in this report and was used in the correlation of the independent data set. Method E was shown to be an acceptable approach to correlation of inlet distortion for compressors with a uniform discharge total pressure under distorted inflow conditions. It was estimated that 17 patterns are necessary to define completely the Method E sensitivities at each corrected speed. However, one screen could produce acceptable patterns over a range of corrected speeds.

| 17. Key Words (Suggested by Author(s)) Inlet flow distortion Distortion methodology Unsteady distortion | 18. Distribution Statement Unclassified - unlimited STAR category 05 | | |
|---|---|---|---|
| 19. Security Classif. (of this report) Unclassified | 20. Security Classif. (of this page) Unclassified | 21. No. of Pages 102 | 22. Price* $5.50 |

# TABLE OF CONTENTS

# LIST OF ILLUSTRATIONS

# LIST OF ILLUSTRATIONS (Concluded)

# SUMMARY

The development of General Electric's distortion methodology, Method D, has been documented. Method D was then used to correlate steady-state and unsteady data sets. A modification of Method D, known as Method D+ was documented and applied to a steady-state data set.

A NASA-LeRC distortion methodology formulation, DIDENT, was investigated for accuracy of its correlation capability, ease of implementation, and applicability. Three different formulations of DIDENT were investigated. The first provided a correlation of loss of surge pressure ratio at constant corrected speed. The second formulation correlated loss of surge airflow at constant corrected speed. This was then combined with the first formulation to result in a correlation of loss of surge pressure ratio at constant corrected airflow. The third formulation provided a direct correlation of loss of surge pressure ratio at constant corrected airflow. These three formulations were applied to steady-state data.

One of the aspects of DIDENT is that a distortion pattern recognition technique is needed to properly choose the sensitivity parameter used in predicting loss of surge pressure ratio or loss of surge airflow. Three different pattern recognition techniques were investigated. Two, developed during this work, are based upon radial and circumferential pressure defect terms. The third, developed by NASA-LeRC, is based upon maximization of the loss of surge pressure ratio.

It was concluded that the formulation of DIDENT that provided a direct correlation of loss of surge pressure ratio at constant corrected airflow was the best DIDENT approach. This conclusion is based on applicability and usefulness in all phases of engine design. This formulation of DIDENT provides a correlation quality that is comparable to Method D.

Of the three pattern recognition techniques, the NASA-LeRC technique provided the best results. The first two techniques suffered because too many combined screen patterns were recognized as circumferential while the test engine saw them as radial patterns.

The recommended formulation of DIDENT using the NASA-LeRC pattern technique was then applied to an independent steady-state data set. The good correlation resulting from this indicates that DIDENT is a viable approach to distortion methodology. This formulation of DIDENT is not related to parallel-compressor theory. Because of this, to avoid confusion in the report, it will be referred to as Method E.

An attempt was made to use the recommended formulation of Method E to correlate the unsteady data set used with Method D. Analysis of this work showed that the Method E sensitivities are functions of pressure defect level. In the general use of Method E, the levels of distortion used to define sensitivities must cover the range of anticipated distortion levels from flight tests.

# INTRODUCTION

Engine inlet distortion has long been recognized as a source of aero-dynamic instability that can lead to engine surge. In recent years data from high performance inlet/engine systems have shown that engines can be sensitive to unsteady distortions that only exist for milliseconds.

Various correlations have been developed to predict a given engine's tolerance to distortion. These have primarily been empirical in nature. Typically, pressure defect parameters are defined to describe the distortion. These parameters are then related to surge pressure ratio loss by defining various coefficients, or sensitivities. Using these sensitivities, then, for any given distortion pattern, a surge pressure ratio loss can be predicted to assess an engine's stability with that pattern. Unsteady distortion analyses have typically been deterministic in that surge pressure ratio loss is computed as a function of time. It is assumed that the steady-state-derived sensitivities apply to the unsteady analysis. The one unknown parameter then is the data frequency content required to make calculated peaks in surge pressure ratio equivalent to known available surge pressure ratio. The individual unsteady pressures are filtered by analog or digital means to define the data frequency content. This process leads to the concept of critical time or critical frequency in that a time or frequency can be used to describe the filter characteristics. When the filter characteristics necessary to correlate data from a given type of engine or compressor are known, a set of unsteady data can be used to generate a prediction of surge pressure ratio loss.

The foregoing approach to predicting surge pressure ratio losses is used with General Electric's Method D. This methodology has been in use at General Electric since 1970. It has shown reasonable correlation capability for both steady-state and unsteady total pressure distortion data. This report describes the effort that generated Method D and presents examples of its application to both steady-state and unsteady data.

A different concept of relating engine inlet distortion to surge pressure ratio loss has been developed by NASA-LeRC. This concept, called DIDENT, has its basis in the parallel-compressor modeling technique. The mathematical formulation is quite simple. Also, the coefficients, or sensitivities, required by the DIDENT formulation have the potential of being defined by a relatively small data set. The implementation of the DIDENT concept follows similar techniques used for Method D.

Various formulations of DIDENT are analyzed, using steady-state data sets as a basis of verification. The best, most useful, formulation is then applied to a new data set for further verification. This formulation is also applied to a set of unsteady data. These results are used to discuss the applicability of the DIDENT formulation to engine inlet total pressure distortion analysis. Aspects of unsteady data analysis, such as analog or digital analyses and input or output filtering are addressed and the advantages of each are noted.

## ANALYSIS APPROACH

Some of the factors to be considered in the evaluation of a distortion methodology are:

- The correlation capability of the methodology must be sufficiently accurate to allow confidence in its prediction. The current goal in the industry is an error band of ±0.02 when the correlated parameter is surge pressure ratio loss.

- The correlated parameter should be readily related to surge margin. Without such a relationship, it is difficult, if not impossible, to use a distortion methodology in stability assessments of engines early in their design phase. An accepted practice is to define loss of surge pressure ratio and surge margin at constant corrected airflow. With these parameters, the designer is able to relate objective operating lines, surge lines and distortion sensitivities prior to any detailed component design. This freedom is considered to be an important aspect of a distortion methodology's usefulness.

- The methodology should be easy to implement. That is, the definition of methodology sensitivities should not require an inordinately large data base.

- The methodology should be applicable to any compression system (i.e., fans, boosters or compressors). Further, it cannot show variations of sensitivity from engine to engine. For example, the sensitivities desired from a cell test must be applicable to flight tests using two different engines of the same design.

With these criteria, then, Method D and DIDENT can be evaluated. Method D has been applied to steady-state data and to unsteady data. The unsteady data analysis includes a comparison of analog and digital analyses. A refinement of Method D is discussed and is applied to steady-state data. Three formulations of DIDENT are applied to steady-state data. The most applicable formulation is then applied to an independent steady-state data set and to unsteady data. This unsteady analysis uses analog techniques.

Five data sets have been used in this evaluation and are briefly described here. A more detailed description can be obtained from the references cited with each description.

1. Data Set A – A set of 11 drift surges from a NASA-LeRC J85-13/axisymmetric inlet wind-tunnel test. The data are characterized by high turbulence levels, up to 8%, with no particular class of pattern (circumferential, radial) being predominant. These data are described in Reference 1.

4

2. Data Set B - A set of 102 surges from a NASA-LeRC J85-13 screen test. The data set consists primarily of circumferential, tip-radial, and hub-radial screens. Only 4 screens can be classified as combined. Reference 2 gives a description of these data.

3. Data Set C - A set of 84 surges from a NASA-LeRC J85-13/screen test. The data set is characterized by a large number of combined patterns. Two engines were used within this set of data. Reference 3 gives a description of these data.

Data Sets B and C are defined by a set of six equally-spaced rakes. Some screen positions were such that rakes were located at the edge of the screen rake. This tended to artificially suppress face average pressure and increase pressure defect extents. These rake values were corrected using NASA-LeRC-supplied correction factors during the DIDENT analyses.

4. Data Set D - A set of screen test data from a variety of GE tests along with Data Set B. Data Set D was used in the development of the General Electric Method D. Reference 4 gives a description of these data.

5. Data Set E - A set of 36 surges from a General Electric low pressure compressor component screen test. The data are described in Appendix I.

Two different definitions of loss of surge pressure ratio have been used. Figure 1 shows the relationships between the various terms for these two definitions. The loss of surge pressure ratio defined at constant corrected airflow ($\Delta$PRSW) is:

$$\Delta PRSW = \frac{PR_C - PR_B}{PR_C}$$

The loss of surge pressure ratio defined at constant corrected speed ($\Delta$PRSN) is:

$$\Delta PRSN = \frac{PR_A - PR_B}{PR_A}$$

A loss of surge airflow at constant corrected speed ($\Delta$WS) is also defined as:

$$\Delta WS = \frac{\left.\dfrac{W\sqrt{\theta}}{\delta}\right)_A - \left.\dfrac{W\sqrt{\theta}}{\delta}\right)_B}{\left.\dfrac{W\sqrt{\theta}}{\delta}\right)_A}$$

5

# DISCUSSION OF RESULTS

## DEVELOPMENT OF METHOD D

The General Electric Method D is an empirical approach to correlating pressure distortion to loss of surge pressure ratio. It was developed from other empirical methodologies (referred to here as Methods A, B, and C). Method D and its predecessors are outlined in Reference 4. The equations used by Methods A, B and C and their implementation are included here to provide a background for the development of Method D. The methodologies A, B, C, and D are defined in Figures 2 through 5. Method A, shown in Figure 2, uses a Fourier series to describe each ring's circumferential pressure variation. Each ring is weighted inversely to diameter so that hub circumferential distortion contributes more heavily than tip circumferential distortion. Radial distortion is a function of ring average pressure, again weighted inversely to diameter. Pressures are normalized by inlet dynamic pressure, q, in an attempt to collapse speed effects. Complex patterns use a direct linear superposition of circumferential and radial contributions.

Method B is shown in Figure 3. All pressures are normalized by face-average pressure. Here the circumferential variation in pressure is described by a Fourier series. The series coefficients are summed and ring-weighted to define a circumferential index, $A_C$. This is made equivalent to surge pressure ratio loss, $\Delta PRS$, for pure circumferential test data:

$$K_C = \Delta PRS_{AVAIL}/A_C$$

Thus, the circumferential parameter

$$ND_C = K_C * A_C$$

is equivalent to $\Delta PRS_{AVAIL}$.

The radial distortion parameter is similarly defined. Ring average pressures are described by a Fourier series. The series coefficients are summed and weighted to define a radial index, $A_R$. This is related to $\Delta PRS$ for pure radial test data:

$$K_R = \Delta PRS_{AVAIL}/A_R$$

and

$$ND_R = K_R * A_R$$

Complex patterns are treated with a linear superposition factor of 1.0:

$$ND_T = ND_C + ND_R$$

Note that $ND_T$ is equivalent to $\Delta PRS_{AVAIL}$.

Method C is shown in Figure 4. This technique relies on level parameters rather than Fourier coefficients. The circumferential ring level parameter is:

$$IDC = \frac{P_{ring\ avg} - P_{ring\ min}}{P_{Face\ avg}}$$

This level parameter is modified by shape, extent and multi-per-rev function $(1/n)^\omega$, factors to define a sensitivity. This is, in turn, summed and weighted to develop a $\Delta PRS_{circum}$. Radial data are similarly processed. The radial level parameter is defined:

$$IDR = \frac{P_{Face\ avg} - P_{ring\ avg}}{P_{Face\ avg}}$$

This parameter is weighted with extent factors k and separate tip and hub sensitivities are defined. Complex patterns are processed by using a linear superposition factor of 1.0. The final parameter, $\Delta PRS_{Total}$ is equivalent to $\Delta PRS_{AVAIL}$.

Method D, which is an extension of Method C in that pressure defect definitions are similar, is shown in Figure 5. Here $\Delta PRS_{circum}$ for each ring is defined by the same level parameter used in Method C, modified by a "multi-per-rev" factor, a shape factor, an extent factor and a sensitivity. $\Delta PRS_{circum}$ is then chosen as the maximum of the average of the two tip ring $\Delta PRS$ values or the two hub ring $\Delta PRS$ values.

Radial data are handled by an extent coefficient and a sensitivity. They are, in general, different for the hub and tip regions. The largest $\Delta PRS$ is chosen as representative of stall margin loss due to radial distortion. Method D is unique in that complex patterns are processed using a nonlinear superposition factor. It is a function of the ratio $\Delta PRS_{RAD}/\Delta PRS_{circum}$ and operates on the $\Delta PRS_{circum}$ term:

$$\Delta PRS_{Comb} = b \ * \ \Delta PRS_{circum} + \Delta PRS_{RAD}$$

Again, $\Delta PRS_{comb}$ is equivalent to $\Delta PRS_{AVAIL}$ so that a prediction of surge pressure ratio loss is computed.

It is estimated in Reference 4 that Method D requires 22 patterns at each speed to completely define the sensitivities.

The correlation of each methodology with the General Electric Data Set D, which includes Data Set B, is shown in Figures 6 through 14. Only the bounds of Data Set B are shown. Note that Method A derives a correlation with $\Delta PRS_{Avail}$ that is related only to a given data set. The parameter $K_A$ is not universally related to $\Delta PRS_{AVAIL}$. For this reason, Method A data are shown on individual figures for each subset of data in Data Set D. This is not the case with Methods B, C and D. All of these derive a number (NDT or $\Delta PRS_{Calc}$) that is universally related to $\Delta PRS_{AVAIL}$, regardless of the data set used. For these methodologies, the entire Data Set D is presented on one figure.

A qualitative comparison of these correlations can be made through the use of the standard deviation of each subset. This is shown in Table I, derived from data in Reference 4. The standard deviation, $\sigma$, is defined as:

$$\sigma = \sqrt{\frac{\sum\limits_{i=1}^{N} \left( (\Delta PRS_{Test})_i - X_i \right)^2}{N-1}}$$

where N is the number of points

X is the methodology parameters NDT or $\Delta PRS_{Calc}$. For $K_A$, the standard deviation is that obtained from a straight line fit of $K_A$ vs $\Delta PRS_{Test}$.

Table I. Standard Deviation.

| Subset | A | B | C | D | No. of Points |
|--------|------|------|------|------|---------------|
| GE4 (72T, 85T) | 0.0345 | 0.0244 | 0.0141 | 0.0073 | 9 |
| GE4 (72P, W85, Va5) | 0.0138 | 0.0168 | 0.0237 | 0.0167 | 13 |
| GE-F100 BU/6 | 0.0295 | 0.0342 | 0.058 | 0.0190 | 19 |
| GE-F100 BU/7 + IGV | 0.012 | 0.0197 | 0.0075 | 0.0067 | 13 |
| GE-F100 BU/7 + IGV + OS | 0.020 | 0.0052 | 0.0074 | 0.011 | 18 |
| NASA-J85 (set B) | 0.04 | 0.0268 | 0.0234 | 0.0185 | 100 |
| Overall | 0.0337 | 0.0248 | 0.0270 | 0.0165 | 172 |

These data show that Method D provides the best correlation on 4 of the 6 subsets and is the best method of those shown on the overall basis.

The development of the empirical constants used in Method D for the NASA Data Set B are shown in Figures 15 through 23. Circumferential sensitivies $K_C$, are the slopes of the straight lines in Figure 15. These parameters define $K_C$ as a function of corrected speed and extent of the low pressure region. These values are tabulated in Table II.

Table II.  Data Set B Values of $K_C$.

| Corrected Speed | Angular Extent, Degrees | | |
|---|---|---|---|
| | 215 | 141 | 100 |
| 87% | 2.32 | 1.65 | 1.10 |
| 90% | 3.18 | 2.39 | 1.90 |
| 93% | 2.40 | 1.50 | 1.37 |
| 97% | 1.00 | 1.34 | 1.88 |
| 100% | 1.4 | 0.93 | 0.93 |
| Screen Angular Extent | $180°$ | $90°$ | $60°$ |

The above values were plotted as a function of extent in Figure 16.  The value of $K_C$ at 20° extent is assumed to be zero.  These curves are shown as straight line segments between data points in accordance with the General Electric Distortion Analysis Program (GE DAP) method of interpolation between data points.  Note also that the value of $K_C$ at 180° has been interpolated using faired curves, rather than straight line segments between 140° and 216°.

The extent function, EF, is derived from these data since

$$EF = \frac{K_C)_\theta}{K_C)_{180°}}$$

The extent function is plotted in Figure 17.  These values of extent function were input to the GE DAP program along with $K_C$ at 180° to completely define the circumferential sensitivity.

The "multi-per-rev" function, MR, was defined from data shown in Figure 18.  The data are limited and the scatter is large so that the "multi-per-rev" function was chosen to be 1.0 for all speeds.

Radial sensitivities are defined by two parameters, $K_R$ and $\alpha$.  These are interrelated through the equations:

$$\Delta PRS_{TIP} = K_{R_{TIP}} \left[ \Delta P/P)_5 + \alpha_{TIP} * \Delta P/P)_4 \right]$$

$$\Delta PRS_{HUB} = K_{R_{HUB}} \left[ \Delta P/P)_1 + \alpha_{HUB} * \Delta P/P)_2 \right]$$

$$\Delta PRS_{RAD} = MAX\ OF\ \left( \Delta PRS_{TIP}, \Delta PRS_{HUB} \right)$$

$K_{RTIP}$, $\alpha_{TIP}$, $K_{RHUB}$ and $\alpha_{HUB}$ were computed from the first two equations using a linear least squares multiple regression analysis with $\Delta PRS)_{test} \equiv \Delta PRS)_{rad}$. The resulting values of these four coefficients were used to construct the lines in Figures 19 and 20. The data in these figures show a reasonable fit with the constructed lines.

The data from these figures were then used to define the variation of $K_{RH}$, $K_{RT}$, $\alpha_H$ and $\alpha_T$ with speed. The results of this are shown in Figures 21 and 22.

The preceeding circumferential and radial sensitivities were used to define $\Delta PRS_{CIRC}$ and $\Delta PRS_{RAD}$ for the various combined patterns in the data set. These were, in turn, used to develop the superposition factor. b. b is defined as:

$$b \equiv \frac{\Delta PRS_{AVAIL} - \Delta PRS_{RAD}}{\Delta PRS_{CIRC}}$$

It is a function of $\dfrac{\Delta PRS_{RAD}}{\Delta PRS_{CIRC}}$ and corrected speed.

The data shown in Figure 23 define the b-factor for these data. Note that they are not a function of speed in this case. The addition of any radial distortion makes the J85-13 compressor less sensitive to the imposed circumferential distortion.

The correlation of all points in Data Set B, using these constants, is shown in Figure 24. From Table I, the standard deviation is 0.0185.


REFINEMENT OF METHOD D

In 1972, General Electric evaluated Method D with the objective of refining its correlation capability. This evaluation was based upon the Data Set C. The result of this work has become known as Method D+. As with Method D and its predecessors, Method D+ is an empirical approach. The primary difference between Methods D and D+ is the inclusion of radial weighting terms in Method D+. The formulation of Method D+ is as follows:

- Circumferential

$$\frac{\Delta P}{P}\bigg)_{C_i} = \frac{P_{ring\ avg_i} - P_{ring\ min_i}}{P_{face\ avg}} \qquad i\ is\ \underline{i}th\ ring$$

$$\left(\overline{\frac{\Delta P}{P}}\right)_C = \frac{1}{N} \sum_1^N \frac{\Delta P}{P}\Bigg)_{C_i} \quad \text{for rings where } \frac{\Delta P}{P}\Bigg)_i \geq .75 \frac{\Delta P}{P}\Bigg)_{i_{max}}$$

$$\Delta P/P\Big)_E = \left(\overline{\frac{\Delta P}{P}}\right)_C \times CEF \times REF \times MRF$$

$$K_C = \Delta PRS_{AVAIL} / (\Delta P/P)_E$$

$$\Delta PRS_{CIRC} = K_C * \left(\frac{\Delta P}{P}\right)_E$$

- Radial

$$\frac{\Delta P}{P}\Bigg)_{R_i} = \frac{P_{face\ av} - P_{ring\ av_i}}{P_{face\ av}} \quad i \text{ is } i\underline{th} \text{ ring}$$

$$\Delta P/P\Big)_{R_i} \geq 0$$

$300°$ or more of ring must be below $P_{face\ av}$ for $\Delta P/P)_{R_i}$ to be $> 0$.

$$\Delta PRS_{RAD} = \sum_1^5 \alpha_i * \Delta P/P\Big)_{R_i}$$

$$\alpha_i = \frac{\Delta PRS)_{avial}}{\Delta P/P}\Bigg)_{R_i}$$

- Combined

$$\Delta PRS_{CALC} = A * (\Delta PRS_{CIRC}) + \Delta PRS_{RAD}$$

$$A = f (\Delta PRS_{RAD})$$

The application of Method D+ to Data Sets B and C has been limited to 87, 93, and 100% corrected speeds where the bulk of the test data are located.

The circumferential data are analyzed by first plotting $\overline{(\Delta P/P)}_C$ versus $K_C$, where $K_C = \Delta PRS_{AVAIL}/\overline{(\Delta P/P)}_C$ for 180°, full-span screens. This develops the basic circumferential sensitivity, to which all circumferential data are normalized. The first normalization considers angular extent. Full span screens of extents less than 180° are plotted as the 180° screens were. This is shown in Figure 25 for the three speeds analyzed. The ratio of slopes between 180° and any other extent is the circumferential extent factor, CEF, which is plotted versus angular extent in Figure 26. The second normalization considers radial extent of circumferential screens (the partial extent tip and hub radials in Data Set C, for example). Here, $K_C$ is plotted versus $\overline{(\Delta P/P)}_C$ X CEF.

The result, shown in Figure 27, allows a definition of radial extent factor, REF, as the ratio of slopes between the radial extent = 1 and any other radial extent. REF is plotted versus radial extent in Figure 28. This defines the circumferential screen sensitivities, all normalized to 180°, full span sensitivity.

Radial data are considered on a ring-by-ring basis. That is, a sensitivity, $\alpha_i = \Delta PRS_{AVAIL}/(\Delta P/P)_{R_i}$ is plotted versus $(\Delta P/P)_{R_i}$ for each ring. Data where more than one ring has a contribution $[(\Delta P/P)_{R_i} > 0]$ are considered by assuming that the rings contribute to $\Delta PRS$ linearly. For example:

$$\alpha_{ik} = \Delta PRS_{AVAIL}\Big)_k / (\Delta P/P)_{R_{ik}}$$

where i is ith ring – the only ring to contribute to $\Delta PRS$ in this data point

k is kth data point

$$\alpha_{j1} = \left[\Delta PRS_{AVAIL}\Big)_1 - \alpha_{ik} \times (\Delta P/P)_{R_{i1}}\right] \Big/ (\Delta P/P)_{R_{j1}}$$

where i is same ring as above
j is another ring
k is same data point as above
1 is new data point where ith and jth rings contribute to $\Delta PRS$.

This process can be used to completely define the $\alpha_i$'s as shown in Figure 29. The gain in $\Delta PRS$ with hub radial screens causes some negative values of $\alpha_i$.

The circumferential and radial data so far analyzed can now be used for combined patterns, using a superposition function:

$$A = f(\Delta PRS_{RAD})$$

where

$$PRS_{CALC} = A\ \Delta PRS_{CIRC} + \Delta PRS_{RAD}$$

The superposition function was determined by solving the above equation for A and plotting these values versus $\Delta PRS_{RAD}$, as shown in Figure 30. Note that, in order to calculate $\Delta PRS$ for circumferential-only data, $A \equiv 1$ at $\Delta PRS_{RAD} = 0$.

There is a high degree of scatter in the data in Figure 30. The curves drawn through these data are considered the best fit to the data.

Putting all of these sensitivities together produces the correlation shown in Figure 31. Here $\Delta PRS_{CALC}$ is plotted versus $\Delta PRS_{AVAIL}$. There are some rather large deviations from the main correlation band. While they are limited in number, the underlying data must be considered valid and these points represent a failing of Method D+.

The standard deviation is 0.025 for this work. However, when comparing Methods D and D+, the comparison must be on an individual data set basis because Method D coefficients were developed on the individual data sets. This is shown in Table III where the various standard deviations are tabulated.

### Table III

#### Comparison of Methods D and D+

|  | Method D | Method D+ |
|---|---|---|
| Data Set B | 0.018 | 0.011 |
| Data Set C | 0.036 | 0.039 |
| Combined | 0.027 | 0.025 |

This table shows that Method D+ provides a better correlation for the Data Set B, largely pure circumferential and radial patterns. However, when combined patterns are introduced with Data Set C, it is no better than Method D.

The conclusion has been reached that Method D+ is not preferred over Method D because it provides a correlation no better than Method D and requires more detailed information (i.e., more screen patterns) than Method D.

## APPLICATION OF METHOD D TO UNSTEADY DATA

This section discusses the analysis of NASA-LeRC Data Set A using
Method D as programmed in the General Electric Dynamic Distortion Analysis
Program (DAP). The analysis technique used in DDAP processes the unsteady
pressure data time-slice by time-slice to compute surge pressure ratio loss
($\Delta$PRS) via the Method D equations. The output, then, is $\Delta$PRS as a function
of time (DDAP can plot up to six parameters on up to six plots for a total
of 36 parameters versus time).

Input pressure data are digitally low-pass filtered using a sliding
window average. The amplitude characteristics of this type of filter are
shown in Figure 32 where this filter is compared to a 5-pole linear phase analog
filter. They are seen to be quite similar in character. Note that two
characteristic frequencies are defined in Figure 32 - the 3 dB down point,
and the pole, or zero amplitude ratio point. The pole frequency is not
realizable in an analog filter and comparisons between analog and digital
filters are best made using the -3 dB frequency. However, in DDAP , and
in this report, the pole frequency is the implied frequency of the filter
in that:

$$\text{Averaging Time} = \frac{1}{f_{pole}}$$

For the filter employed in DDAP the relationship between the pole and -3 dB
frequencies is:

$$f_{(-3 \text{ dB})} = 0.45 \ f_{(pole)}$$

This input filtering is the control over the time dimension of the unsteady
analysis. Because all Method D sensitivities and coefficients in DDAP are
just those derived from steady-state screen data (Data Set B), the input
filter is the only independent variable that controls the amplitude and
frequency characteristics of $\Delta$PRS. This leads to the concept of "critical
time." Each data point, consisting of a digital record of pressure time
histories leading to engine surge, is successively processed with different
filter averaging times. The $\Delta$PRS time histories for each averaging time
will typically show a peak just prior to surge. The amplitude of this peak
is compared to the known surge pressure ratio margin ($\Delta$PRS$_{AVAIL}$). The
"critical time" is just that filter averaging time that causes the peak
$\Delta$PRS$_{CALC}$ prior to surge to be equal to $\Delta$PRS$_{AVAIL}$. When a group of data
points are available for analysis, the "critical time" is chosen so that
the standard deviation of $\Delta$PRS$_{CALC}$ compared to $\Delta$PRS$_{AVAIL}$ is minimized.

The DDAP analysis has been used with Data Set A and Method D sensi-
tivities derived from steady-state analysis of Data Set B. A typical time
history of loss in surge pressure ratio ($\Delta$PRS$_{CALC}$) is shown in Figure 33.
The measured value of $\Delta$PRS$_{AVAIL}$ and the peak in $\Delta$PRS$_{CALC}$ that induced surge
are shown. This figure shows an apparent shift of the data in time as a
function of averaging time. This is most easily seen by examination of the

14

peak in $\Delta PRS_{CALC}$ that occurs after compressor surge. This apparent shift is due to the way in which the averaging is implemented. The value of any individual pressure (and, therefore, $\Delta PRS_{CALC}$) at a given point in time is the average of that pressure from the given point in time to the leading edge of the average window. In equation form:

$$P_T(t_i) = \frac{1}{N} \sum_{t_i}^{t_i + N-1} P_j$$

$t_i$ is time slice being analyzed
N  is time slices being averaged
$P_j$ is individual values of pressure at each
    time slice.

In general, there would be an additional phase shift due to the number of time slices advanced between averaging processes. For all data reported herein, the advance was one time-slice. It has no effect in these data.

This apparent shift in time has no effect on the analyses performed on Data Set A, but in comparisons of wave shapes, it must be considered.

In Data Set A, the location of surge was chosen as that point where face average began to rise above the previous fluctuations of face average. This is the first indication of the surge overpressure. An analysis window was then defined from this surge location. The highest peak of $\Delta PRS$ within this window represents the peak stall pressure ratio loss for a given averaging time. The peak, in general, moves within the window as averaging time is varied. That is, one unique peak in $\Delta PRS$ is not maximized for all averaging times. This is because the wave shape of $\Delta PRS$ may be, in part, composed of nearly simultaneous minima from different probes. Input fitering then, will affect the waveshape of $\Delta PRS$ through the filtering effect on individual probes. In any analysis of unsteady distortion, the criteria used to define the peak $\Delta PRS_{CALC}$ must be defined. The approach used for these data is to assume that the engine surged due to some distortion that created a $\Delta PRS$ of sufficient magnitude and duration to induce the surge. The time required to propagate a disturbance from the measurement plane to the compressor discharge, allow one compressor revolution, and propagate a disturbance forward to the measurement plane is conservatively estimated to be no greater than 20 milliseconds. The peak $\Delta PRS$ that induced surge, then, should occur no further than 20 milliseconds prior to surge. Peaks in $\Delta PRS$ that occur at times greater than 20 milliseconds prior to surge have no effect on engine surge, regardless of their amplitude or duration. They represent an error in the correlation capability of the methodology used in the unsteady analysis. The peak values of $\Delta PRS$, obtained within 20 milliseconds of surge, are shown in Table IV. Averaging times are normalized by the time required for one compressor rotor revolution at its design speed of 16,500 rpm.

Table IV

## Data Set A Surge Pressure Ratio Losses

| Point | $\Delta PRS)_{AVAIL}$ | $\Delta PRS)_{.125_{REV}}$ | $\Delta PRS)_{.25_{REV}}$ | $\Delta PRS)_{.5_{REV}}$ | $\Delta PRS)_{1_{REV}}$ | $\Delta PRS)_{2_{REV}}$ |
|---|---|---|---|---|---|---|
| 82 | 0.147 | 0.168 | 0.15 | 0.145 | 0.137 | 0.132 |
| 103 | 0.156 | 0.248 | 0.202 | 0.215 | 0.162 | 0.055 |
| 141 | 0.079 | 0.16 | 0.13 | 0.09 | 0.055 | 0.027 |
| 148 | 0.183 | 0.293 | 0.25 | 0.18 | 0.111 | 0.078 |
| 154 | 0.216 | 0.303 | 0.237 | 0.15 | 0.113 | 0.065 |
| 162 | 0.238 | 0.355 | 0.332 | 0.294 | 0.263 | 0.241 |
| 164 | 0.237 | 0.166 | 0.160 | 0.153 | 0.141 | 0.140 |
| 200 | 0.066 | 0.147 | 0.118 | 0.078 | 0.050 | 0.043 |
| 214 | 0.009 | 0.113 | 0.107 | 0.103 | 0.087 | 0.073 |
| 219 | 0.008 | 0.132 | 0.128 | 0.118 | 0.097 | 0.057 |
| 261 | 0.244 | 0.282 | 0.268 | 0.233 | 0.196 | 0.177 |

The data shown in Table IV were used to develop a histogram of the number of surges where:

$$\Delta PRS_{CALC})_{A.T.} \geq \Delta PRS_{AVAIL} \geq \Delta PRS_{CALC})_{A.T. + \Delta A.T.}$$

This is shown in Figure 34. The peak of the histogram is at 0.25 to 0.5 rotor revolutions, but it is not conclusive that this time is the critical time of the J85-13 compressor. The histogram shows data points that do not agree with the basic distribution of the histogram. Referring back to Table IV, these data can be grouped and qualified as follows:

o   Points 82, 103, 141, 154, 200 and 261 are described by $\Delta PRS)_{.125} > \Delta PRS_{AVAIL} > \Delta PRS)_2$. These points indicate that the critical time is between 0.125 and 2 rotor revolutions.

o   Point 164 is described by $\Delta PRS_{AVAIL} > \Delta PRS)_{.125}$. Because of the eight points mentioned above, and the low senitivity to 30° extent per rev screens, it is highly unlikely that a realistic critical time less than 0.125 rotor revolution exists within these data. This point is interpreted as one containing an error in either $\Delta PRS_{AVAIL}$ or $\Delta PRS_{CALC}$, or both. It is not considered further in this analysis.

o   Points 162, 214, and 219 are described by $\Delta PRS_{AVAIL} < \Delta PRS)_2$. Because of the extremely low $\Delta PRS_{AVAIL}$ for 214 and 219, either the engine should have surged using a steady-state analysis or the $\Delta PRS_{AVAIL}$ is in error. These 2 points (214 and 219) out of the 11 drift surges from Data Set A will not be considered further. Point 162 would indicate a critical time slightly greater than 2 rotor revolutions. This point is eliminated because of the preponderance of the data lying well below 2 rotor revolutions.

With these "outlayers" eliminated from the data, the critical time can be investigated. This has been done by computing the standard deviation of the data set at each averaging time analyzed. The standard deviation compares the peak $\Delta PRS_{CALC}$ to $\Delta PRS_{AVAIL}$ at each averaging final.

The results are plotted in Figure 35 as a function of rotor revolutions. The data show a definite minimum in $\sigma$ at 0.5 revolution. Because points 162 and 164 cannot be eliminated from the analysis on grounds other than they do not show a critical time between 0.125 and 2 revolutions, the standard deviations were computed including these points. The results are also shown in Figure 35. Again, the standard deviation shows a minimum at 0.5 revolution.

The value of the standard deviation at 0.5 revolution is a measure of the accuracy of the methodology used in correlating the unsteady data. From Figure 35, $\sigma = 0.037$ at 0.5 revolution, while $\sigma = 0.0185$ for the steady-state Data Set B. This would indicate an accuracy for Data Set A of ~0.5 that for Data Set B. However, the difference in the number of points within each data set could cause these standard deviation comparisons to be misleading. Figure 36 shows the basic correlation of $\Delta PRS_{AVAIL}$ with $\Delta PRS_{CALC}$ for Data Sets A and B. The data from Data Set A are seen to correlate quite well except for two points. It can only be concluded that Data Set A is not large enough to statistically compare its fit to Data Set B. Figure 36 would indicate that the quality of the fit of Set A is equivalent to the fit obtained with Data Set B.

Figure 36 also demonstrated an important difference between Data Sets A and B. Values of $\Delta PRS$ for Data Set A are sometimes larger than those for Data Set B. This is important because Set B defines the sensitivity coefficients used in DDAP to analyze Set A. There is no assurance that these sensitivities may be accurately extrapolated to higher values of distortion as has been done in this analysis. However, referring back to Table IV, it can be seen that 0.5 rotor revolution will still provide the minimum standard deviation for those data points in Set A with $\Delta PRS_{AVAIL}$ values within the bounds of Data Set B.

It can be stated that the analysis of Data Set A shows that the J85-13 has a "critical time" of 0.5 rotor revolution using the following assumptions:

● The sensitivities defined by Data Set B can be extrapolated to the higher distortion levels of Data Set A.

● The peak $\Delta PRS_{CALC}$ that induced surge occurred within 20 milliseconds prior to the surge.

● The concept of "critical time" is valid. That is, sensitivities based upon steady-state data can be applied to unsteady data.

17

## ANALOG VS. DIGITAL ANALYSIS

The analog analysis of Data Set A was performed in General Electric's Stability Measurements Analysis Laboratory (SMAL). A photograph of the equipment used for the analysis of Data Set A is shown in Figure 37. The computers were programmed as shown in Figure 38. The objective of the analysis at the time it was done was to screen the data records for peaks in the Method D parameters $\Delta P/P)_C$ and $\Delta P/P)_R$. This analysis will form the basis of the discussions in this section.

Referring back to Figure 38, the analog data were low-pass filtered at the playback discriminators to 200 Hz (-3 dB) and then summed with steady-state values to make up the 30 filtered time-unsteady pressures. These were then processed to compute the various parameters shown in Figure 38.

Figure 39 shows typical digital and analog analyses for a point in Data Set A. The data were processed with comparable input filters. Each figure contains 250 millisecond records of $\Delta P/P)_{C_{max}}$, $\Delta P/P)_{R_{max}}$ and $\Delta P/P)_{C_{max}} + \Delta P/P)_{R_{max}}$. Visual inspection of these wave forms show that the wave shapes of digital and analog analyses are quite similar. One measure of the similarity is a comparison of peak values. This is shown in Figure 40 where a peak value for all three of the above parameters in each of nine digital records is plotted against the corresponding peak value in its companion analog record. The difference between analog and digital analyses is seen to be ± 0.01 of $\Delta P/P)_C$ or $\Delta P/P)_R$.

When comparing cost and time required for analysis, some assumptions must be made as to the starting point. It will be assumed that the digital computer use is charged to the analysis, the analog computer use is free, the data are on an analog magnetic tape, and that 10 data points are to be processed to determine peak $\Delta PRS_{CALC}$ prior to stall. With this starting point, the following table of required steps and the estimated cost of each may be made. A rate of $25/man hour is assumed.

Table V

Comparison of Unsteady Data Processing Costs

| Digital | | | Analog | | |
|---|---|---|---|---|---|
| Item | Manhours | Cost | Item | Manhours | Cost |
| Digitize Data | 20 | 500 | Prog. Analog | 16 | 400 |
| Qualify Digital Data | 10 | *450 | Checkout | 8 | 200 |
| Process Data | 20 | *1200 | Process Data | 20 | 500 |
| | Total | $2150 | | Total | $1100 |

\* Includes digital computer usage charges
\* Based on assumed rates and times

This table serves to estimate costs. Overall timing must be estimated separately due to turnaround time in the digital computer. The estimate is two points per day for qualification and processing of digital data, run in parallel. Digitation could be performed in two days, qualification and processing would require six days, for a total of eight days to process the data. Analog analysis is a serial procedure through the steps in Table V – a total of 5-1/2 days. Analog analysis is about 1.4 times faster and 2 times cheaper than digital analysis. Assuming that digital data are "truth", analog analysis has an error of ±0.01, based upon the analysis of Data Set A.

With all data analysis efforts, engineering judgement is necessary to determine the best procedure. However, a good philosophy is to perform as much analysis as possible on the analog system and resort to digital analysis only when its capabilities offset its increased cost.


## INPUT VS. OUTPUT FILTERING

The effect of input as opposed to output filtering on $\Delta$PRS can be seen by considering the Method D equations as programmed in the Dynamic Distortion Analysis Program (DDAP).

$$P_{min_j} = \frac{1}{N} \sum_{k=1}^{N} P_{xjk}$$

$$P_{avg_j} = \frac{1}{LN} \sum_{i=1}^{L} \sum_{k=1}^{N} P_{ijk}$$

$$P_{Face} = \frac{1}{LMN} \sum_{i=1}^{L} \sum_{j=1}^{M} \sum_{k=1}^{N} P_{ijk}$$

i is $i_{th}$ probe in ring

j is $j_{th}$ ring

k is $k_{th}$ time slice

L is probes in ring

M is rings in face

N is number of slices in average time

x is probe whose average over N is minimum in $j_{th}$ ring.

$$\left. \frac{\Delta P}{P} \right)_{C_j} \right)_I = \frac{P_{avg_j} - P_{min_j}}{P_{Face}} \qquad I = \text{input filtering}$$

$$= \frac{\frac{1}{LN} \sum_{i=1}^{L} \sum_{k=1}^{N} P_{ijk} - \frac{1}{N} \sum_{k=1}^{N} P_{xjk}}{\frac{1}{LMN} \sum_{i=1}^{L} \sum_{j=1}^{M} \sum_{k=1}^{N} P_{ijk}} \qquad \text{(Eqn. 1)}$$

19

If the same equation is output filtered the form is:

let: $\dfrac{1}{L}\sum\limits_{i=1}^{L} P_{ijk} = \bar{P}_{R_{jk}} = \bar{P}_{R_{ss}} + \bar{P}'_{R_k}$

$$\left.\frac{\Delta P}{P}\right)_{C_j}\right)_o = \frac{1}{N}\sum_{k=1}^{N} \left.\frac{\Delta P}{P}\right)_{C_j}\right)_k = \frac{1}{N}\sum_{k=1}^{N}\left[\frac{\frac{1}{L}\sum\limits_{i=1}^{L}P_{ijk} - P_{min_{jk}}}{\frac{1}{LM}\sum\limits_{i=1}^{L}\sum\limits_{j=1}^{M}P_{ijk}}\right]$$

(Eqn. 2)

$\dfrac{1}{LM}\sum\limits_{i=1}^{L}\sum\limits_{j=1}^{M} P_{ijk} = \bar{P}_{Face_k} = \bar{P}_{F_{ss}} + \bar{P}'_{F_k}$

$P_{min_{jk}} = \bar{P}_{min_{ss}} + P'_{min_k}$

where subscript ss is steady-state component and (') is unsteady component.

$$\left.\frac{\Delta P}{P}\right)_{C}\right)_o = \frac{1}{N}\sum_{k=1}^{N}\frac{(\bar{P}_{R_{ss}} - P_{min_{ss}}) + (\bar{P}'_{R_k} - P'_{min_k})}{\bar{P}_{F_{ss}} + \bar{P}'_{F_k}} = \frac{1}{N}\sum_{k=1}^{N}[(\bar{P}_{R_{ss}} - P_{min_{ss}}) + (\bar{P}'_{R_k} - P'_{min_k})][\bar{P}_{F_{ss}}]^{-1}[1 + \frac{\bar{P}'_{F_k}}{\bar{P}_{F_{ss}}}]^{-1}$$

for $(1 + \varepsilon)^{-1} \simeq 1 - \varepsilon$ where $\varepsilon = \dfrac{\bar{P}'_{F_k}}{\bar{P}_{F_{ss}}} \ll 1$

$$\frac{1}{N}\sum_{k=1}^{N}\left[\frac{\bar{P}_{R_{ss}} - P_{min_{ss}}}{\bar{P}_{F_{ss}}}\right]\left[1 + \frac{(\bar{P}'_{R_k} - P'_{min_k})}{(\bar{P}_{R_{ss}} - P_{min_{ss}})}\right]\left[1 - \frac{\bar{P}'_{F_k}}{\bar{P}_{F_{ss}}}\right] = \left(\frac{\bar{P}_R - P_{min}}{\bar{P}_F}\right)_{ss} + \frac{1}{N}\sum_{k=1}^{N}\frac{\bar{P}'_{F_k}(\bar{P}'_{R_k} - P'_{min\,k})}{(\bar{P}_{F_{ss}})^2}$$

(Eqn. 3)

where $\Sigma$ of first order $P'$ terms are zero by stationarity.

Equations (1) and (3) are different in formulation because summations are not distributive. In Equation (1), individual terms are averaged over N samples. In Equation (2) N ratios are averaged. While this certainly effects the results, perhaps the largest difference in input versus output filtering is due to the treatment of minima. Equation (1) uses a minimum from one probe whose average over N samples is minimum. Equation (2) uses a minimum that is the average of N minima – not necessarily from one probe. One would expect that the average of N minima will be less than the minimum probe averaged over N samples. That is:

$$\left.\frac{\Delta P}{P}\right)_{C_i}\right)_o \geq \left.\frac{\Delta P}{P}\right)_{C_i}\right)_I$$

This inequality is demonstrated in Figure 41 where $\Delta P/P)_C$ for each ring is plotted for data point 148. Output averaged data are seen to be equal to or greater than input averaged data.

A similar relationship may be obtained for the Method D radial parameter, $\Delta P/P)_R$. That is:

$$\left.\frac{\Delta P}{P}\right)_{R_i}\right)_o \geq \left.\frac{\Delta P}{P}\right)_{R_i}\right)_I$$

However, because of the nonlinear relation of the basic circumferential and radial distortion parameters with $\Delta PRS_{CALC}$, the inequalities noted above do not hold when comparing $\Delta PRS_{CALC}$ for input and output filtering.

This is shown in Figure 42 where $\Delta PRS_{CALC}$ is plotted for data point 103. Here $\Delta PRS_{CALC})_O$ is generally, but not always, greater than $\Delta PRS_{CALC})_I$. The only conclusion to be drawn is that input and output filtering are not equivalent. Further, the proper technique is input filtering because the basic premise is that the engine is responsive to pressure defects that exist for some length of time. Input filtering is the control over that length of time.


## DIDENT FORMULATION

One of the disadvantages of most of the distortion methodologies currently used is that a significant number of screen patterns must be tested to define the methodology coefficients. An approach developed by NASA-Lewis Research Center (LeRC) called DIDENT (Distortion Identity) shows promise in that, potentially, the number of screen patterns can be significantly reduced and still correlate complex patterns. A description of the approach is given in Reference 5.

DIDENT is based on the parallel-compressor model and, for the J85-13 data analyzed herein, assumes that the compressor discharge total pressure is uniform for any inlet distortion pattern. Following the parallel-compressor model then, equations have been developed in Reference 5 that relate distortion level to loss in surge pressure ratio at constant corrected speed ($\Delta PRSN$). These equations are:

$$\Delta PRSN_{AVAIL} = \left(1 - \frac{(\bar{P}_3/\bar{P}_2)D}{(P_3/P_2)_c}\right) \qquad N/\sqrt{\theta} = \text{const.}$$

$$K_i = \frac{\left[\bar{P}_3/(P_{min},60°)_{2,r}\right]D}{(\bar{P}_3/\bar{P}_2)_c} \Bigg) \qquad N/\sqrt{\theta} = \text{const.}$$

$$\Delta PRSN_{CALC} = 1 - \frac{(P_{min},60°)_{2,r}}{\bar{P}_2} \times K_i$$

$\bar{P}_3$ - discharge total pressure          $D$ = distorted surge line

$\bar{P}_2$ - inlet average pressure          $C$ = clean surge line

$(P_{min},60°)_{2,r}$ - inlet minimum pressure averaged over 60° in rings 1 or 5

$K_i$ - sensitivity, a function of speed, pattern and engine.

Reference 5 has indicated that pattern effects are limited to circumferential, hub- or tip-radial effects. Thus, three separate curves, $K_C$, $K_H$, and $K_T$ can be defined as speed functions for each engine. These curves, from Reference 5, are shown as Figure 43. Note that $K_C = 1.0$, just the value predicted by parallel-compressor theory.

The data in this curve show a strong engine-to-engine variation of the hub- and tip-radial sensitivities. This effect of an individual engine on the DIDENT sensitivities will be noted for all correlations of the DIDENT approach in this effort. It is discussed later in the report.

A problem in using the DIDENT approach is the development of a pattern recognition technique to understand which $K_i$ should be employed for any given complex pattern.

In order to compare various pattern recognition techniques, it is necessary to know the data scatter inherent in DIDENT resulting from scatter in the $K_i$ curves. This has been done for the $\Delta$PRSN correlation by manually choosing the $K_i$ for each pattern. The $\Delta$PRS scatter is due only to $K_i$ scatter, since we have an identity.

The results are shown in Figure 44 for Data Set B and Data Set C. The standard deviations of each correlation are noted in the figure. With this figure as a baseline correlation, pattern recognition techniques may be defined and investigated as to accuracy.

Two different techniques have been investigated in this analysis. The first is based upon the radial pressure defect terms in Method D. This technique is:

$$\frac{\Delta P}{P}\bigg)_C = 1 - \frac{\bar{P}_{min \ rake}}{\bar{P}_{Face}} \geq 0$$

$$\frac{\Delta P}{P}\bigg)_T = 1 - \frac{\bar{P}_{Tip \ Ring}}{\bar{P}_{Face}} \geq 0$$

$$\frac{\Delta P}{P}\bigg)_H = 1 - \frac{\bar{P}_{Hub \ Ring}}{\bar{P}_{Face}} \geq 0$$

The maximum value of $\Delta P/P)_C$, $\Delta P/P)_T$, or $\Delta P/P)_H$ selects the corresponding value of $K_C$, $K_T$, or $K_H$. Data Sets B and C, correlated with this technique, are shown in Figure 45. The Data Set B, with its many pure patterns, is reasonably correlated. Notably, the two screens that differ from the baseline correlations are both combined patterns. Screen 24, a partial-extent

tip-radial pattern, was seen as a circumferential pattern at all speeds by this pattern recognition technique. The engine reacted to screen 24 as if it were a tip-radial pattern. Screen 26, a tip radial plus one-per-rev circumferential, was viewed by the pattern recognition technique as a tip-radial. The engine reacted to it as a circumferential screen pattern.

Investigation of Data Set C shows similar results. Screens 17, 18, 19, 21, 23, and 25 were viewed by the pattern recognizer as circumferential patterns. The engine reacted to screens 17, 18, 19 and 21 as hub-radial patterns – they are all partial hub-radials. The engine reacted to screens 23 and 25 as tip-radial patterns – they are both partial tip-radials.

The first technique, then, is not capable of resolving all of the patterns in Data Sets B and C such that the loss of surge pressure ratio at constant speed is predicted for all patterns.

The second technique employed to discriminate the pattern characteristics was designed to view combined patterns as if they were pure circumferential or radial patterns. This technique uses the following equations:

$$\left. \frac{\Delta P}{P} \right)_{C_i} = \frac{\overline{P}_{rad_i} - P_{min, 60_i}}{P_{Face}}$$

$$\left. \frac{\Delta P}{P} \right)_{R_i} = \frac{\overline{P}_{rad_i}}{P_{Face}} \geq 0 \quad i \text{ is } i\underline{th} \text{ ring}$$

$$\overline{P}_{rad_i} = 2 \, P_{RingAvg_i} - P_{min, 60_i}$$

$P_{min, 60_i}$ is minimum pressure integrated over $60°$ in $i\underline{th}$ ring

$P_{RingAv_i}$ is ring average pressure of $i\underline{th}$ ring

$P_{Face}$ is face average pressure

With these definitions, $\Delta P/P)_C$ and $\Delta P/P)_R$ reduce to those used in Method D for pure circumferential and radial patterns, respectively. Combined patterns have either $\Delta P/P)_C$ or $\Delta P/P)_R$ suppressed, depending upon details of the pattern. This tends to make most combined patterns appear "pure."

These equations were employed to compute the above circumferential and radial parameters in each ring. The circumferential parameters were then summed as follows:

$$\overline{\frac{\Delta P}{P}}\Big)_C = \frac{1}{A} \frac{1}{N} \sum_{i=1}^{N} \frac{\Delta P}{P}\Big)_{C_i} \quad \text{for N rings whose } \overline{\frac{\Delta P}{P}}\Big)_C \text{ is}$$

$$\text{greater than } .5 \frac{\Delta P}{P}\Big)_{C_{i_{max}}}$$

$$A = 1 \text{ for } N \geq 3$$
$$A = 2 \text{ for } N < 3$$

The maximum of:

$$\overline{\frac{\Delta P}{P}}\Big)_C , \quad \frac{\Delta P}{P}\Big)_{R_1} , \quad \frac{\Delta P}{P}\Big)_{R_5} \quad \text{was then used to select } K_C, K_H, \text{ or } K_T.$$

The resulting correlations for Data Sets B and C are shown in Figure 46. Technique number two differed from the baseline correlation similarly to technique number one. The same screens noted for technique number one were viewed in the same way as technique number one did. In addition, technique number two viewed screen 23, Data Set B, as a circumferential pattern while the engine reacted as if it were a hub-radial pattern. Screen 23 is a partial extent hub-radial pattern. It also saw screens 15 and 24, Data Set C, as circumferential patterns while the engine reacted to them as if they were tip-radials. Both screens are partial tip-radials, with screen 15 having two-per-revolution 90° extent tip sectors and 20° extent circumferential sectors; screen 24 is a 120° one-per-revolution tip sector.

The second technique proves to be less acceptable than the first. This technique did as anticipated - it viewed many combined screens as a pure pattern. However, too many patterns were viewed as pure circumferential rather than pure radial. This could be modified by changing the definition of $\Delta P/P_C$. This was not done because, as later discussed, the utility of $\Delta PRSN$ as an engine design program is limited.

In general, the engine reacts to partial radial patterns as if they were pure radial patterns. The engine reacts to combined patterns with full-span circumferential components as if they were circumferential. Neither technique was capable of fully resolving the patterns in Data Sets B and C in this manner. Of the two techniques investigated, the first is best for $\Delta PRSN$ correlation.

## CORRELATION OF LOSS OF SURGE AIRFLOW

As a continuation of the work on correlating Data Sets B and C using loss of surge pressure ratio at constant speed, a correlation of loss of surge airflow at constant speed has been obtained. These two correlations were

combined to predict the loss of surge pressure ratio at constant corrected airflow. Both pattern recognition techniques previously discussed were carried through these correlations.

The method used in correlating loss of surge airflow is very simple, but was arrived at only after many other methods were investigated. These will be discussed, but no complete correlations of these attempts have been presented.

The first approach was to utilize the parallel-compressor model as used in the basic DIDENT formulation. The sketch in Figure 47 for a two-sector parallel compressor shows the typical results of this effort. Here, the predicted airflow is that point on the straight line that crosses the predicted pressure ratio at surge. The calculated surge airflow was generally higher than the actual surge airflow. Further, this calculation would become rather complex for multisector parallel compressors required by complex patterns. The approach was discarded due to inaccuracy and complexity.

The second approach is based upon an observation that distorted speed lines may be derived from clean speed lines through the following technique. Define the coefficients:

$$R_1 = \left\{ \left[ \left( \bar{P}_3/\bar{P}_2 \right)_D \middle/ \left( \frac{W\sqrt{\theta}}{\delta} \right)_D \right] \middle/ \left[ \left( \bar{P}_3/\bar{P}_2 \right)_C \middle/ \left( \frac{W\sqrt{\theta}}{\delta} \right)_C \right] \right\}_{\eta_C = Max}$$

$$R_2 = \left[ \left( \frac{W\sqrt{\theta}}{\delta} \right)_D \middle/ \left( \frac{W\sqrt{\theta}}{\delta} \right)_C \right]_{\eta_C = Max}$$

Plot $R_1$ and $R_2$ versus distortion with corrected speed and pattern as bivariant parameters and fit curves through these data. These curves then give values of $R_1$ and $R_2$ for given distortion, pattern and corrected speed. These can be used to compute a distorted airflow and pressure ratio based upon the known clean surge airflow and pressure ratio. The computed values do tend to lie on the measured distorted speed line, but there was no correlation with the distorted surge airflow and pressure ratio. This approach was discarded as too inaccurate.

At this point, strictly empirical approaches were tried. They included curve-fits of the distorted maps which were too complex and inaccurate. The approach finally used, which resulted from the curve-fit work, was to simply define a loss of surge airflow as:

$$\Delta WS = 1 - \left[ \frac{W\sqrt{\theta}}{\delta} \right)_D \middle/ \frac{W\sqrt{\theta}}{\delta} \right)_C \right]$$

and plot it versus $1 - (P_{min}, 60)_2$, $r/\bar{P}_2$ for constant corrected speed and pattern type (circumferential, hub–radial, tip–radial). These plots are shown in Figures 48 through 50.

These correlations show that the J85–13 compressor tends to lose airflow with hub–radial patterns and gain airflow with circumferential, tip–radial, partial–hub–radial, and partial tip–radial patterns. Further, Data Sets B and C give different correlations, indicating a difference in engine-to-engine behavior which was also noted in the DIDENT sensitivities of Reference 5.

The curves shown in Figures 48 to 50 were then used to correlate $\Delta WS_{AVAIL}$ with $\Delta WS_{CALC}$. This was done by entering each curve with known values of distortion level, pattern type (as determined by identification techniques numbers 1 and 2, discussed earlier) and corrected speed. These allowed a prediction, $\Delta WS_{CALC}$ to be determined. The resulting correlations of $\Delta WS$ are shown in Figures 51 and 52 for Data Sets B and C using each identification technique.

The correlations achieved have standard deviations that compare favorably in level with previous $\Delta PRS$ values, so that this technique is not unreasonable. The best identification technique would appear to be number 2, based upon Data Set C with its many combined types of patterns. This is due to the previously noted trend of all pattern surge airflow losses appearing as circumferential patterns except the pure hub–radials. Identification technique number 2 tends to make most combined patterns appear as circumferential, thus providing the best correlation of $\Delta WS$.

These airflow correlations do not represent an end, but a step in the correlation of $\Delta PRS$ defined at constant airflow. The method used to combine $\Delta PRS$ defined at constant corrected speed ($\Delta PRSN$) and $\Delta WS$ to correlate $\Delta PRS$ defined at constant airflow ($\Delta PRSW$) is shown in the sketch in Figure 53. The following items are required known values:

- $N/\sqrt{\theta}$, pattern identity, distortion level

- Clean surge pressure ratio versus corrected speed

- Clean surge corrected airflow versus corrected speed

- Clean surge pressure ratio versus corrected airflow

- $\Delta PRSN_{CALC}$, $\Delta WS_{CALC}$

These are all typical outputs from a compressor distortion test series. They permit calculation of $\Delta PRSW_{CALC}$, as defined in Figure 53.

The results of these correlations are shown in Figures 54 and 55. Again, they represent Data Sets B and C for pattern identification techniques 1 and 2. These correlations have standard deviations that are greater than those obtained with the $\Delta$PRSN correlations of Figures 45 and 46. Both pattern recognition techniques produced similar levels of standard deviation. This is because the $\Delta$PRSN correlations were best with technique number 1, while $\Delta$WS correlations were best with technique number 2, resulting in $\Delta$PRSW correlations that are similar with both techniques.

DIRECT CORRELATION OF $\Delta$PRSW

At this point, it was desired that a correlation of loss of surge airflow at constant corrected airflow be done. This was implemented with the same equations defined for the DIDENT approach, namely:

$$\Delta PRSW_{CALC} = 1 - \frac{P_{(min, 60°)_{2,r}}}{\bar{P}_2} \times K_i$$

However, such an approach no longer uses the parallel-compressor model as a basis because of the definition of $\Delta$PRSW. Because of this basic difference, the methodology for this effort will be referred to as Method E to discriminate it from DIDENT. Because Method E is not related to the parallel-compressor model, the $K_i$ values are now simply empirically determined sensitivities. The curves defining $K_i$ are shown in Figures 56 and 57 for Data Sets B and C, respectively. There are some aspects of these curves worth noting. First, in Figure 56, for Data Set B, an effect of the radial extent of pure tip-radial patterns is seen. This was not the case with the previous sensitivities for $\Delta$PRSN. Also, the partial tip- and hub-radial patterns appear to fit the circumferential sensitivity curve better than they fit their respective pure radial sensitivity curves. The data in Figure 57, Data Set C, support the effect of partial hub-radial patterns appearing more like circumferential patterns at low corrected speeds. However, at ~100% speed, their sensitivity is different from both pure hub-radial and circumferential patterns. No pure tip radial patterns exist in Data Set C so that no conclusions as to extent effects can be drawn. The partial tip-radial patterns do not have sensitivities similar to circumferential patterns, as did Data Set B. Also, $K_C \neq 1$, shows the deviation from parallel-compressor theory.

In general, the radial sensitivities in Data Sets B and C are widely different from one another for $\Delta$PRSW and $\Delta$PRSN correlations. These differences are responsible for the apparent engine-to-engine variations previously noted when using the DIDENT approach.

The pure circumferential, tip-radial (not accounting for extent) and hub-radial sensitivity curves in Figures 56 and 57 were used to develop a correlation for $\Delta$PRSW. They are shown in Figures 58 and 59. Again, Data Sets B and C with pattern recognition techniques 1 and 2 are shown. The standard deviations obtained for Data Set B are very nearly the same as those obtained in Figures 54 and 55, where $\Delta$PRSW was derived from $\Delta$PRSN and

$\Delta WS$. This is due to the large number of pure patterns in Data Set B. In Data Set C, the direct correlation of $\Delta PRSW$ is better than the derived correlation for pattern recognition technique number 1, and worse for technique number 2.

All of these correlations can best be reviewed by referring to the following table of standard deviations.

### Table VI

#### Comparison of Methodology Results

| Parameter Pattern Recognition | Data Set B | | | Data Set C | | |
|---|---|---|---|---|---|---|
| | No. 1 | No. 2 | Manual | No. 1 | No. 2 | Manual |
| $\Delta PRSN$ | 0.0215 | 0.0220 | 0.0170 | 0.0293 | 0.0309 | 0.0259 |
| $\Delta WS$ | 0.0160 | 0.0134 | --- | 0.0155 | 0.0162 | --- |
| $\Delta PRSN + \Delta WS \rightarrow \Delta PRSW$ | 0.0299 | 0.0268 | --- | 0.0360 | 0.0360 | --- |
| $\Delta PRSW$, Method E | 0.0309 | 0.0263 | --- | 0.0344 | 0.0349 | --- |
| $\Delta PRSW$, Method D | --- | --- | 0.0185 | --- | --- | 0.0360 |

The values of standard deviation from the GE Method D analyses have been included as a reference. Interestingly, Data Set C correlates about as well with any one of the three approaches using $\Delta PRSW$. This is considered more significant than the standard deviations of Data Set B with its many pure patterns. Also, the correlations of $\Delta PRSN$ are consistently better than the correlations of $\Delta PRSW$ in the Method E analyses. Based upon the correlation standard deviations, the $\Delta PRSN$ approach certainly is best. However, the utility of this approach to engine programs must be considered in some detail prior to any recommendation.

The basic application of any distortion methodology is in the stability assessment, or audit, of a compression system. A methodology must be able to relate distortion level, sensitivity, and loss of surge pressure ratio. Further, loss of surge pressure ratio must be related to surge margin because a stability audit is the summation of all internal and external destabilizing influences to arrive at the amount of excess margin (or additional margin required) at a given operational condition. This process must be available to the designer during early phases of engine design so that an optimized target surge line, operating line, and control system may be defined. During this phase of the design, no design component maps may be available. Certainly, no test maps will be available.

Because of the fluid nature of all parts of the engine design in its early stages, a $\Delta PRSN$ value would be extremely difficult, if not impossible, to use in the design optimization. This difficulty precludes the recommendation of a $\Delta PRSN$ approach to distortion correlation.

The DIDENT correlations of ΔPRSW, as seen in Table I, are rather comparable in their standard deviations. Because of this, the ΔPRSN + ΔWS→ ΔPRSW approach cannot be recommended due to its complexity as compared to the direct empirical correlation of ΔPRSW. The recommended DIDENT formulation is the direct empirical correlation of ΔPRSW, Method E.

## APPLICATION OF METHOD E TO AN INDEPENDENT DATA SET

The Method E concept, as used in this contract, was developed from one engine - the J85-13. To show that the concept is viable, it is necessary to successfully correlate an independent data set from another compression system. This is the primary requirement for Data Set E. Data Set E is derived from a General Electric test of a low pressure compressor component and consists of 36 surge points. These surges and the various screens are described in Appendix I. The differences in design between the J85 compressor and the low-pressure compressor test vehicle are shown in Table VII.

### Table VII
### Compressor of J85-13 and Low-Pressure Compressor

| Parameter | J85-13 | Low-Pressure Compressor |
|---|---|---|
| Design Speed, rpm | 16500 | 13266 |
| Design Pressure Ratio | ~6.8 | 4.1 |
| No. Stages | 8 | 3 |
| Variable Stators | IGV's | IGV's S1, S2, S3 |
| Rotor Aspect Ratios | 2.64, 3.51, 3.58 3.24, 3.1, 2.89 2.79, 2.27 | 1.73, 1.598, 1.47 |

- S1, S2 only have inner platforms
- All stators have inner platforms

There are many design differences between these two machines so that a successful correlation of Data Set E should prove the validity of Method E.

The screens contained in Data Set E include 180° extent one per revolution, 50% area tip- and hub-radial, and simulated flight patterns. Other parameters varied in this data set include component builds and stator rigging. These have been included so that effects of aerodynamic variations within the test vehicle on Method E sensitivities can be observed.

Data Set E does not include any variation in extent of the pure circumferential screens. A direct evaluation of $\theta_{crit}$ was not possible because of this. The value of $\theta_{crit}$ was determined from the flight patterns to be 60°.

The data were then analyzed to define the $K_i$ curves. These are shown in Figure 60. These curves indicate only minor differences in $K_i$ between the builds and stator rigging variations. This is different from the behavior of the J85 compressor in Data Sets B and C where significant variations in $K_i$ were seen for the various engines tested. All the pure screens show consistent trends in the variation of $K_i$ with corrected speed. The combined screens are less straight forward. Screen 303 indicates a sensitivity typical of a tip-radial pattern at 100% speed while it is typical of a circumferential pattern at 105% speed. Screen 402 is midway between tip-radial and circumferential values of $K_i$. Both screens are combined tip-radial and circumferential patterns.

This behavior of the combined patterns has given further insight into the pattern recognition problem. Both recognition techniques previously used would fail to correlate these screens. NASA-LeRC has used a different technique with some success on Data Sets B and C. This technique is to compute the following:

$$\Delta PRS_T = 1 - \frac{P_{min, \text{ tip ring}}}{\bar{P}_2} \cdot K_T$$

$$\Delta PRS_H = 1 - \frac{P_{min, \text{ hub ring}}}{\bar{P}_2} \cdot K_H$$

$$\Delta PRS_C = 1 - \frac{P_{min \text{ rake}}}{\bar{P}_2} \cdot K_C$$

$$\Delta PRS_{CALC} = \text{Max of } \{\Delta PRS_T, \Delta PRS_H, \Delta PRS_C\}$$

For a pure circumferential screen pattern, the minima are approximately equal; that is:

$$\frac{P_{min, \text{ tip ring}}}{\bar{P}_2} = \frac{P_{min, \text{ hub ring}}}{\bar{P}_2} = \frac{P_{min \text{ rake}}}{\bar{P}_2}$$

In this case, the $\Delta PRS_i$ that is maximum will be the $\Delta PRS_i$ associated with the minimum $K_i$. Referring back to Figure 60, for $N/\sqrt{\theta} > 90\%$, $K_i$ minimum = $K_C$, for $N/\sqrt{\theta} < 90\%$, $K_i$ minimum = $K_T$. This would result in circumferential screens having an erroneous $\Delta PRS_{CALC}$ for $N/\sqrt{\theta} < 90\%$. To eliminate this, the following logic was installed in the NASA-LeRC pattern identification technique:

If $\left| \dfrac{P_{min,\ hub} - P_{min,\ tip}}{\bar{P}_2} \right| < 0.025,\ \Delta PRS_{CALC} = \Delta PRS_C$

Otherwise $\Delta PRS_{CALC} = $ Max of $\{\Delta PRS_T,\ \Delta PRS_H,\ \Delta PRS_C\}$

The resulting correlation for Data Set E is shown in Figure 61. Only two points are significantly far from the ± 0.02 band. These are the two points from screen 402 that lie midway between tip-radial and circumferential sensitivities in Figure 2. Neither tip-radial or circumferential sensitivity will adequately describe these points. It should be noted that screen 402 contains a solid plate. Past experience with screens containing a solid plate has been that test results are difficult to interpret and correlate with surge pressure ratio loss.

The successful correlation in Figure 61 demonstrates that the Method E concept is a viable approach to describing surge pressure ratio loss due to inlet distortion for a wide range of compression system design variables.

A very significant observation derived from this work is that the two separate builds and stator rigging variations have minimal effect on the correlation capability of Method E. This is in direct opposition to the J85-13 in Data Sets B and C. One must now pose the question of which data set is typical of all engines. If the J85-13 in Data Sets B and C is not representative, one of the significant potential limits to the applicability of Method E can be removed.

APPLICATION OF METHOD E TO UNSTEADY DATA

Data Set A has been analyzed using the recommended formulation of Method E. The sensitivities used were those derived from the analysis of Data Set B, shown in Figure 56. This is consistent with the process used for the Method D analysis of Data Set A.

The analysis was performed in the Stability Measurements Anlysis Laboratory (SMAL) on the analog computer. A block diagram of the analog program is shown in Figure 62. The analysis used two pattern recognition techniques. One was the NASA-LeRC technique; the second was that technique referred to as No. 1 in the development of the DIDENT formulation. The objective of the analysis was to determine a "critical time" for the J85-13 compressor using Method E. The data were analyzed at frequencies corresponding to 1, 1/2, 1/4, and 1/8 rotor revolution. Waveforms from data point 148 are shown in Figure 63.

As in the analysis of Data Set A with Method D, peak values of $\Delta PRS$ were chosen from the 20-millisecond time period prior to compressor surge. These values are shown in Figure 64 where $\Delta PRS_{CALC}$ is plotted versus averaging time for nine of the data points. Data points 214 and 219 were excluded from this analysis due to their inordinately low $\Delta PRS_{AVAIL}$ values.

Study of Figure 64 will show that most of the resulting $\Delta PRS_{CALC}$ values are quite low compared to $\Delta PRS_{AVAIL}$ or compared to $\Delta PRS_{CALC}$ by Method D. The results would indicate that the compressor's "critical time" is something less than 0.125 rotor rev. This is so far from all previous experience that such a conclusion is highly suspect. Furthermore, the curves in Figure 64 for the Method E analysis are rather flat, indicating that it is highly improbable that the $\Delta PRS_{AVAIL}$ levels could be achieved at any averaging time.

The data were examined in detail to find a possible explanation for this discrepancy. The analog program was verified – the computed pressure defects were correct. The program logic was investigated to determine how often the pattern recognition technique switched from one type of pattern to another. The pattern choice was always stable for the 20 milliseconds prior to surge. For some data points, it was stable for ~1 second prior to surge. These investigations showed that the analog analysis was mathematically correct.

The only variable left in the formulation is sensitivity. An assumption was made that sensitivity is also a function of pressure defect level. To verify that assumption, Method D and Method E were related in a simplistic fashion. Consider a pure 180° square wave circumferential distortion pattern so that:

$$\Delta PRS_{METH\ D} = K_C \cdot \frac{\Delta P}{P}_C \qquad\qquad SF=EF=MR=1.0$$

$$\Delta PRS_{METH\ E} = 1 - \frac{P_{min}}{P_{face}} \cdot K_C'$$

Then, equating $\Delta PRS_{METH\ D}$ and $\Delta PRS_{METH\ E}$

$$K_C \cdot \frac{\Delta P}{P}_C = 1 - \frac{P_{min}}{P_{Face}} \cdot K_C'$$

because $P_{ring\ av} = P_{Face}$

$$K_C \left( 1 - \frac{P_{min}}{P_{Face}} \right) = 1 - \frac{P_{min}}{P_{Face}} \cdot K_C'$$

$$K_C' = \frac{1}{\frac{P_{min}}{P_{Face}}} \left( 1 - K_C \left( 1 - \frac{P_{min}}{P_{Face}} \right) \right)$$

$$K_C' = \frac{1}{\frac{P_{min}}{P_{Face}}} \left( 1 - K_C \right) + K_C$$

With this relationship between Method D and Method E, it can be seen that, for a constant value of $K_C$, the Method E sensitivity, $K_C'$, would be expected to be an inverse function of pressure defect level. Figure 15, for example, shows $K_C$ (Method D) to be constant with defect level.

Similar relationships can be derived for radial sensitivities. The primary sensitivities in Method D are then relatable to Method E sensitivities.

With the Method E sensitivities shown to be functions of pressure defect level, along with corrected speed and pattern, Data Sets B and C were reinvestigated to determine this functional relationship. For this work, it was assumed that Data Sets B and C could be used as a single data set. For each corrected speed and type of pattern, sensitivity was plotted as a function of pressure defect level. The results are shown in Figure 65. The data in this figure from Data Set A were plotted by assuming that 0.5 rotor revolution was the correct "critical time" so that a sensitivity could be computed. Study of Figure 65 shows that Data Sets B and C are not unique, and can be considered as one data set. Further, Data Set A pressure defect levels are not all contained within the steady-state data. In order to analyze Data Set A using this DIDENT approach, one would need to extrapolate the sensitivity curves to defect levels typical of Data Set A. The results would be a function of the extrapolation chosen. For this reason, Data Set A was not further analyzed.

The most important observation is that Data Sets B and C can be considered as one data set. This explains the apparent engine-to-engine variation of Method E sensitivities - it is just a result of higher distortion levels in Data Set C compared to Data Set B. One of the limits to the use of Method E is then removed. However, the number of patterns required to define sensitivites has been increased because of the need for a range of pressure defect levels. Further, the distortion levels used in defining sensitivities must encompass those anticipated in the engine installation.

It is now possible to correlate Data Sets B and C as one. This has been done in Figure 66 using both pattern recognition techniques developed herein. This will allow a comparison of this correlation with the previous individual correlations of Data Sets B and C. Again, the comparison is best made with the standard deviations. These are shown in Table VIII where

$\Sigma$ B+C is the summed standard deviations from individual correlations using the number of data points in each data set as weighting factors.

<div align="center">

Table VIII

Comparison of Data Sets B and C
</div>

| Data Set | Pattern Recognition No. 1 | No. 2 | D |
|---|---|---|---|
| B | 0.0309 | 0.0263 | 0.018 |
| C | 0.0344 | 0.0398 | 0.036 |
| $\Sigma$ B+C | 0.0324 | 0.0332 | 0.027 |
| B and C | 0.0295 | 0.0309 | --- |

The standard deviation of the combined data sets shows a better correlation than the summed standard deviation of each data set for both pattern recognition techniques. In the case of pattern recognition technique number 1, the combined data sets have a smaller standard deviation than either of the individual data sets.

Method E can be described as a viable distortion methodology that can be applied to any compression system. The sensitivities in the recommended formulation used here are functions of speed, pattern, and pressure defect level. They are not functions of an individual engine. The number of patterns needed at each speed to define the Method E sensitivities is estimated in Table IX.

<div align="center">

Table IX

Estimated Patterns Needed to Implement Method E
</div>

| Pattern | Pressure Defect Levels | Sensitivity |
|---|---|---|
| 180° one-per-rev | Low, high | |
| 120° one-per-rev | Low | |
| 90° one-per-rev | Low, high | $\theta_{crit}$, $K_C$ |
| 60° one-per-rev | Low | |
| 45° one-per-rev | Low | |
| Hub-radial, 40% extent | Low, medium, high | $K_H$ |
| Hub-radial, 20% extent | Low, high | |
| Tip-radial, 40% extent | Low, medium, high | $K_R$ |
| Tip-radial, 20% extent | Low, high | |

A total of 17 patterns at each speed would be needed to implement Method E. The many radial screens are included so that effects of extent of the radial defect may be observed. Note that one screen can typically produce acceptable patterns over a range of speeds. This does not say that 17 screens are needed at each speed.

34

## CONCLUSIONS

The development of the General Electric distortion methodology, Method D, has been documented. Method D has been applied to steady-state data to show its capability to correlate inlet pressure distortion data to loss of surge pressure ratio. The sensitivities used in Method D that were derived from the steady-state data were used to analyze unsteady data to determine the "critical time" of the J85-13 compressor. The "critical time" is 0.5 rotor revolution, as determined by these data.

It was shown, using Method D equations, that output averaging will produce pressure defects greater than or equal to input averaging. However, due to the nonlinear sensitivities in Method D, it can only be stated that output averaged values of surge pressure ratio loss are not equal to input averaged values of surge pressure ratio loss. The use of output averaged pressure defects to compute surge pressure ratio loss can then lead to highly erroneous values.

Analog and digital analyses of unsteady data have been compared. Analog analysis was shown to agree with digital analysis within $\pm 0.01$ of the Method D pressure defect terms. Within the ground rules established for this comparison, analog analysis is faster and less costly than digital analysis.

Two formulations of the NASA-LeRC distortion methodology, DIDENT, were investigated. One formulation correlated the loss of surge pressure ratio at constant corrected speed. The other correlated the loss of surge airflow at constant corrected speed and combined this with the previous correlation to obtain a correlation of the loss of surge pressure ratio at constant corrected airflow. A methodology that used DIDENT equations to directly correlate the loss of surge pressure ratio at constant corrected airflow was implemented. It was concluded that this last formulation, Method E, provided the most useful results.

The use of DIDENT and Method E requires that some form of pattern recognition be employed to discriminate between hub-radial, tip-radial, and circumferential patterns. Two techniques were developed. Both were based on pressure defect levels and locations in the entrance plane. Resulting correlations showed that neither technique was completely satisfactory. Work at NASA-LeRC on this problem in their work with DIDENT showed that a technique that maximized the computed loss of surge pressure ratio was a more accurate technique.

Method E was applied to an independent data set to verify that the formulation was applicable to data other than that set used to develop it. The pattern recognition technique used was the NASA-LeRC process. The results showed a good correlation of loss of surge pressure ratio. This would indicate that Method E is a viable distortion methodology.

A set of unsteady data were analyzed using analog techniques with the Method E formulation. This analysis was intended to determine the "critical time" of the J85-13. The analysis, instead, showed that the Method E sensi-

tivities are functions of pressure defect level. Because the unsteady data defect levels were typically higher than steady-state data, it was decided not to analyze the unsteady data for "critical time." Such an analysis would require an arbitrary extrapolation of sensitivities to higher defect levels. This effect, however, was used to explain the apparent engine-to-engine variation seen in Method E sensitivities – it is just an effect of pressure defect magnitude.

Method E can then be summarized :

- The Method E formulation is derived from the DIDENT methodology developed by NASA-LeRC. DIDENT utilizes the parallel-compressor model as its basis, Method E, however, is considered to be an empirical formulation not restricted by any parallel compressor model assumptions.

- The correlation capability of Method E was shown to be comparable to Method D. Also, the apparent engine-to-engine variation in the Method E sensitivities has been shown to be nonexistent.

- At this point in its development, Method E requires that the following parameters be defined to implement the methodology:

  - $\theta_{crit}$ – the angle over which the minimum pressure is integrated.

  - $K_C$ – circumferential sensitivity, a function of corrected speed and distortion level.

  - $K_H$ – hub-radial sensitivity, a function of corrected speed, distortion level, and (potentially) of extent of low pressure region.

  - $K_T$ – Tip-radial sensitivity, a function of corrected speed, distortion level, and (potentially) of extent of low pressure region.

The sensitivities would need an estimated 17 patterns at each speed to be defined. Again, it is noted that one screen can produce acceptable patterns over a range of corrected speeds.

36

# APPENDIX I

## DATA SET E

Data Set E consists of 36 surge points whose speeds and $\Delta PRS_{AVAIL}$ values are tabulated in Table I-I. Instrumentation used to define the patterns is shown in Figure 67. Screen patterns are shown in Figures 68 and 69.

## Table I-I

### Data Set E

| SCN | SPD | Build | Stator Schedule | ΔPRS AVAIL | ΔPRS CALC. |
|-----|------|-------|-----------------|------------|------------|
| 100 | 105  | 1     | Nom.            | 0.0941     | 0.0771     |
|     | 100  | 1     | Nom.            | 0.0681     | 0.0615     |
|     | 95   | 1     | Nom.            | 0.0390     | 0.0349     |
| 101 | 95   | 1     | Nom.            | 0.0969     | 0.0988     |
|     | 90   | 1     | Nom.            | 0.0480     | 0.0536     |
|     | 85   | 1     | Nom.            | 0.0317     | 0.0307     |
|     | 75   | 1     | Nom.            | 0.0        | 0.0006     |
| 201 | 105  | 1     | Nom.            | 0.0360     | 0.0360     |
|     | 100  | 1     | Nom.            | 0.0394     | 0.0413     |
|     | 95   | 1     | Nom.            | 0.0575     | 0.0548     |
|     | 90   | 1     | Nom.            | 0.1029     | 0.0842     |
| 202 | 95   | 1     | Nom.            | 0.0965     | 0.0975     |
|     | 85   | 1     | Nom.            | 0.0822     | 0.0822     |
|     | 75   | 1     | Nom.            | -0.0094    | -0.0094    |
| 206 | 105  | 1     | Nom.            | 0.0371     | 0.0371     |
|     | 100  | 1     | Nom.            | 0.0363     | 0.0363     |
|     | 95   | 1     | Nom.            | -0.0517    | -0.0517    |
| 401 | 105  | 1     | Nom.            | 0.0060     | 0.0098     |
|     | 100  | 1     | Nom.            | 0.0        | 0.0147     |
|     | 97.5 | 1     | Nom.            | 0.0024     | 0.0137     |
| 402 | 90   | 1     | Nom.            | 0.0805     | 0.1225     |
|     | 85   | 1     | Nom.            | 0.0632     | 0.0911     |
|     | 75   | 1     | Nom.            | 0.0093     | -0.0036    |
| 100 | 105  | 4     | Nom.            | 0.0667     | 0.0592     |
|     | 105  | 4     | +5°             | 0.0711     | 0.0571     |
|     | 100  | 4     | Nom.            | 0.0689     | 0.0552     |
|     | 100  | 4     | -5°             | 0.0739     | 0.0542     |
|     | 95   | 4     | Nom.            | 0.0453     | 0.0361     |
| 201 | 100  | 4     | Nom.            | 0.0279     | 0.0269     |
|     | 100  | 4     | -5°             | 0.0256     | 0.0270     |
|     | 95   | 4     | Nom.            | 0.0453     | 0.0470     |
| 303 | 105  | 4     | Nom.            | 0.0485     | 0.0235     |
|     | 100  | 4     | Nom.            | 0.0262     | 0.0262     |
|     | 100  | 4     | Nom.            | 0.0221     | 0.0272     |
|     | 95   | 4     | -7°             | 0.0263     | 0.033      |
|     | 95   | 4     | Nom.            | 0.0263     | 0.0294     |

## LIST OF SYMBOLS

### Method A

$P_i$      — total pressures in a ring

$a_n$, $b_n$      — Fourier coefficients

$\theta$      — angular position around inlet

$\omega$      — Fourier coefficient weighting function, empirically determined

$\eta$      — nth Fourier coefficient

$A_n$      — amplitude coefficient

$D_j$      — diameter of jth ring

$\alpha$      — circumferential ring diameter weighting function, empirically determined

$\overline{P}_f$      — face average pressure

$\overline{P}_j$      — jth ring average pressure

$\overline{q}$      — dynamic head

$K_\theta$      — circumferential index

$\beta$      — radial ring diameter weighting function, empirically determined

$b$      — radial speed function, empirically determined

$K_R$      — radial index

$\Delta PRS_{TEST}$      — loss of surge pressure ratio measured from engine/component tests

## Method B

$P_i$ — ith pressure in a ring

$\overline{P}_j$ — jth ring average pressure

$a_n$, $b_n$ — Fourier series coefficients

$\theta$ — angular position around face

$A_j$ — sum of harmonic amplitudes for jth ring

$n$ — nth harmonic of Fourier series

$\omega$ — multi-per-rev weighting function, empirically determined

$W_j$ — empricial ring weighting function for circumferential distortion

$A_c$ — circumferential index, empirical

$K_c$ — circumferential sensitivity, empirical

$\Delta PRS_{TEST}$ — loss of surge pressure ratio measured from engine/component test

$ND_c$ — loss of surge pressure ratio due to circumferential distortion

$\overline{P}_F$ — face average pressure

$W_r$ — empirical ring weighting function for radial distortion

$A_R$ — sum of harmonic amplitudes of radial distortion

$K_R$ — radial distortion sensitivity, empirical

$ND_R$ — loss of surge pressure ratio due to radial distortion

$ND_T$ — loss of surge pressure ratio for generalized pattern

<u>Method C</u>

$\overline{P}_i$         – average pressure in ith ring

$P_{min}$      – minimum pressure in ith ring

$\overline{P}_F$        – face average pressure

n           – number of low pressure regions around each ring

ω          – empirical weighting factor on n

IDC        – circumferential index

$K_c$         – circumferential sensitivity

$\Delta PRS_{circum}$ – loss of surge pressure ratio due to circumferential distortion

Ki         – empirical ring interactor factor

k           – radial extent factor

$IDR_T$      – tip radial index

$IDR_H$      – hub radial index

$K_{R_T}$       – tip sensitivity

$K_{R_H}$       – hub sensitivity

$\Delta PRS_{RAD}$ – loss of surge pressure ratio due to radial distortion

$\Delta PRS_{TOTAL}$ – loss of surge pressure ratio due to general distortion pattern

$\Delta PRS_{TEST}$ – loss of surge pressure ratio measured from engine/component tests

Method D parameters are defined in Figure 5.

DIDENT AND Method E

$\overline{P}_3/\overline{P}_2)_D$ — distorted compressor pressure ratio

$\overline{P}_3/\overline{P}_2)_C$ — undistorted compressor pressure ratio

$(P_{min}, 60°)_{2,r}$ — minimum pressure over 60° sector in plane 2.D (inlet plane), hub ring or tip ring only

$K_i$ — sensitivity, empirically determined. Related to parallel-compressor pressure ratios for DIDENT. Considered to be an empirical coefficient only for Method E

# REFERENCES

1. Burstadt, P.L., and Calogeras, J.E.; "Instantaneous Distortion in a Mach 2.5 40% Internal Contraction Inlet and its Effect on Turbojet Stall Margin, " NASA TMX-3002.

2. Calogeras, J.E., Mehalic, C.M., and Burstadt, P.L.; "Experimental Investigation of the Effect of Screen-Induced Total-Pressure Distortion on Turbojet Stall Margin, " NASA TM X-2239.

3. Calogeras, J.E., Johnsen, R.L., and Burstadt, P.L.; "Effect of Screen-Induced Total-Pressure Distortion on Axial-Flow Compressor Stability, " NASA TM X-3017.

4. Kutschenreuter, P.H., and Younghans, J.L.; "Near Term Distortion Methodology/Task Force Results, " General Electric Report TIS R70AEG410.

5. Calogeras, J.E., and Burstadt, P.L.; "Formulation of a Distortion Index Based on Peak Compressor Pressure Ratios, " NASA TM X-71568.

——— CLEAN

— — — DISTORTED

SURGE LINE

A

C

PR

B

$N/\sqrt{\theta}$ = CONST

$\dfrac{W/\sqrt{\theta}_T}{\delta_T}$
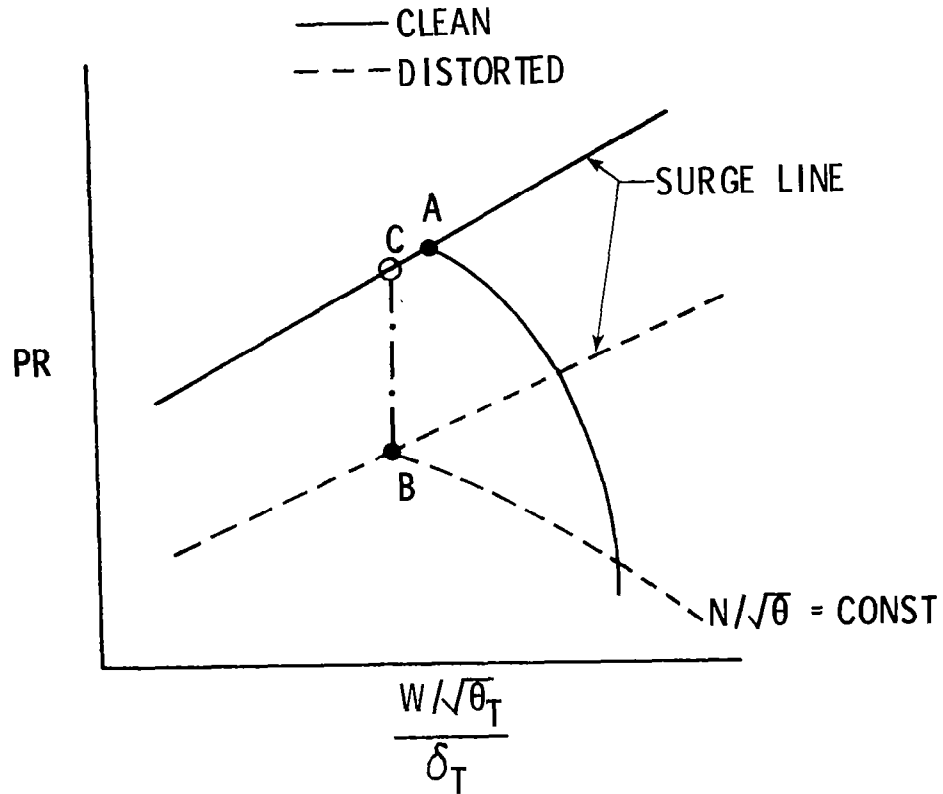
$\triangle PRSN = \dfrac{PR_A - PR_B}{PR_A}$

$\triangle PRSW = \dfrac{PR_C - PR_B}{PR_C}$

$\triangle WS \quad = \dfrac{\left(\dfrac{W/\sqrt{\theta}_T}{\delta_T}\right)_A - \left(\dfrac{W/\sqrt{\theta}_T}{\delta_T}\right)_A}{\left(\dfrac{W/\sqrt{\theta}_T}{\delta_T}\right)_A}$

FIGURE 1 — DEFINITION OF LOSS OF SURGE PRESSURE RATIO AND LOSS OF SURGE AIRFLOW

# PROCEDURE FOR CIRCUMFERENTIAL CONTRIBUTION
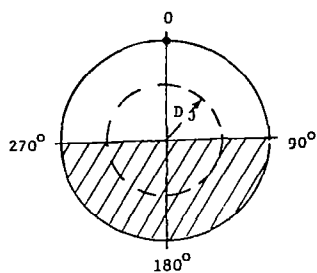


INTERFACE PLANE
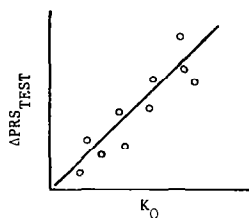


- FOURIER SERIES APPLIED TO EACH RING PRESSURE VARIATION

$$P_i = 1 + \bar{P}_F \sum_{i=1}^{N} \left[ a_n \cos n\,\Theta + b_n \sin n\,\Theta \right]$$

- SELECT LARGEST HARMONIC AMPLITUDES FOR EACH RING

$$\frac{A_n}{n^\omega} = \frac{\sqrt{a_n^2 + b_n^2}}{n^\omega}$$

- WEIGHT EACH RING CONTRIBUTION INVERSELY TO RING DIAMETER

$$\left( \frac{1}{D_j} \right)^\alpha$$

- DEFINE CIRCUMFERENTIAL INDEX

$$K_\Theta \equiv \frac{\sum_{J=1}^{M} \left[ \left( \frac{A_n}{n^\omega} \right)_{MAX} \right]_j \quad * \quad \frac{\bar{P}_F}{\bar{q}} * \left( \frac{1}{D_j} \right)^\alpha}{\sum_{J=1}^{M} \left( \frac{1}{D_j} \right)^\alpha}$$

- CORRELATE $\Delta PRS_{TEST}$ VS. $K_\Theta$ AT   ALL SPEEDS
  ALL LEVELS
  ALL EXTENTS
  $(1/n)^\omega$ MULTI/REVS

j is ring subscript

# PROCEDURE FOR RADIAL CONTRIBUTION
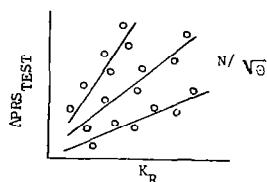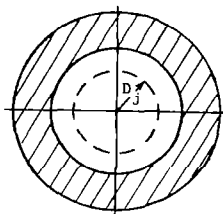




- DEFINE LEVEL PARAMETER FOR EACH RING

$$\frac{\bar{P}_F - \bar{P}_j}{\bar{q}}$$

- WEIGHT EACH RING LEVEL INVERSELY TO DIAMETER

$$\left( \frac{1}{D_j} \right)^\beta$$

- DEFINE RADIAL INDEX AND CORRELATE $\Delta PRS_{TEST}$

$$K_R \equiv \frac{\sum_{J=1}^{M} \left[ \frac{\bar{P}_F - \bar{P}_j}{\bar{q}} \quad * \left( \frac{1}{D_j} \right)^\beta \right]}{\sum_{J=1}^{M} \left( \frac{1}{D_j} \right)^\beta}$$

- COLLAPSE SPEED EFFECTS WITH b FACTOR

$$b = f(N/\sqrt{\theta})$$

$$b * K_R = K_{RA}$$

PROCEDURE FOR COMBINED PATTERNS

- $K_A = K_\Theta \cdot b K_R$
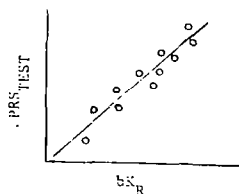


FIGURE 2 — METHOD A PROCEDURE

# PROCEDURE FOR CIRCUMFERENTIAL CONTRIBUTION
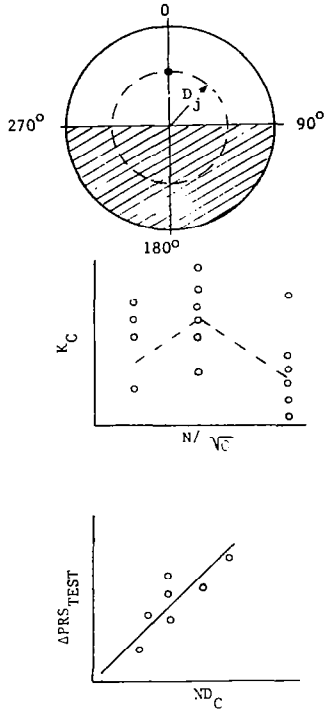


- FOURIER SERIES APPLIED TO EACH RING PRESSURE VARIATION

$$P_i = P_j + \sum_{n=1}^{N} \left[ a_n \cos n\theta + b_n \sin n\theta \right]$$

$$P_i = P/P_{Face\ avg}$$

- SUM AND WEIGHT 4 HARMONIC AMPLITITUDES FOR EACH RING

$$A_j = \frac{1}{\bar{P}_j} \sum_{n=1}^{4} \sqrt{a_n^2 + b_n^2} \; \star \; \left(\frac{1}{n}\right)^{\omega}$$

- WEIGHT EACH RING SEPARATELY

$$W_j = f(D_j)$$

- DEFINE CIRCUMFERENTIAL INDEX COEFFICIENT

$$A_C \equiv \frac{\sum_{J=1}^{M} A_j \star W_j}{\sum_{J=1}^{M} W_j}$$

- DEFINE DISTORTION SENSITIVITY

$$K_C \equiv \Delta PRS_{TEST} / A_C$$

- CORRELATE DATA WITH PARAMETER

$$ND_C = K_C \star A_C$$

# PROCEDURE FOR RADIAL CONTRIBUTION
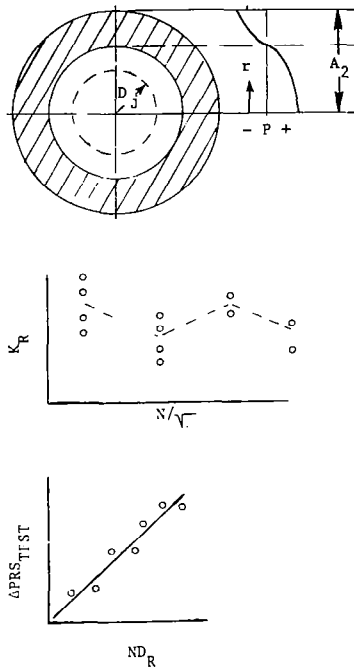


- FOURIER SERIES APPLIED TO AVERAGED RING PRESSURES

$$\bar{P}_j = \bar{P}_F + \sum_{n=1}^{2} a_n \cos \frac{n\pi A}{A_{FACE}}$$

- RING WEIGHTING FUNCTION OF DISTORTION TYPE

$$W_r = g(D_j)$$

- DEFINE RADIAL COEFFICIENT

$$A_R = \frac{1}{\bar{P}_F} \sum_{n=1}^{2} \left| a_n \right| \star W_r$$

- DEFINE RADIAL DISTORTION SENSITIVITY

$$K_R \equiv \Delta PRS_{TEST} / A_R$$

- CORRELATE DATA WITH PARAMETER

$$ND_R = K_R \star A_R$$

PROCEDURE FOR COMBINED PATTERNS

- $ND_T = ND_C + ND_R$

## FIGURE 3 — METHOD B PROCEDURE

## PROCEDURE FOR CIRCUMFERENTIAL CONTRIBUTION
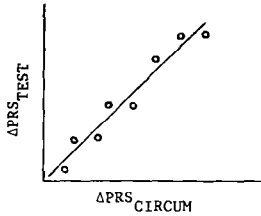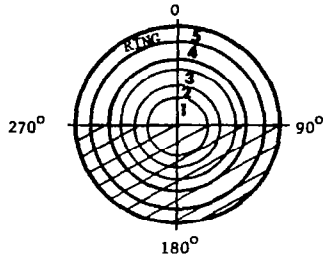


- FOR EACH RING DETERMINE LARGEST LEVEL FACTOR

$$IDC \equiv \left(\frac{1}{n}\right)^{\omega} * \left(\frac{\overline{P}_i - P_{MIN}}{\overline{P}_F}\right) * (\text{EXTENT FACTOR}) * (\text{SHAPE FACTOR})$$

- FOR <u>BASIC</u> CIRCUMFERENTIAL $\Delta PRS_{TEST}$ DETERMINE SENSITIVITY



$$KC \equiv \frac{\Delta PRS_{TEST}}{IDC}$$
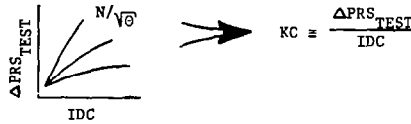
- WEIGHT EACH RING WITH <u>EXPLICITLY</u> FORMULATED INTERACTOR FACTORS

$$K_i \equiv f(KC, KR, SHAPE)$$

- DEFINE CIRCUMFERENTIAL INDEX

$$\Delta PRS_{CIRCUM} \equiv \frac{\sum_{i=1}^{5} K_i * KC_i * IDC_i}{\sum_{i=1}^{5} K_i}$$

$$i = ring$$

## PROCEDURE FOR RADIAL CONTRIBUTION
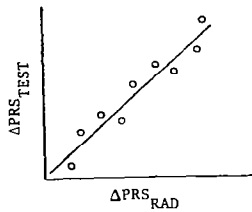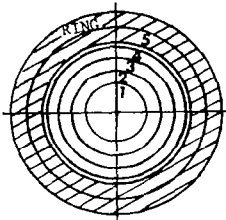


- FOR EACH RING DETERMINE LEVEL FACTORS

$$IDR \equiv \frac{\overline{P}_F - \overline{P}_i}{\overline{P}_F}$$

- DEFINE TIP AND HUB LEVEL FACTORS

$$IDRT \equiv \ell\, IDR_{i=5} + IDR_{i=4}$$

$$IDRH \equiv \ell\, IDR_{i=1} + IDR_{i=2}$$

$$\ell \equiv f(\text{radial extent}, N/\sqrt{\theta})$$

- FOR <u>BASIC</u> RADIAL $\Delta PRS_{TEST}$ DETERMINE SENSITIVITY



$$KRT \equiv \frac{\Delta PRS_{TEST}}{IDR_T}$$

$$KRH \equiv \frac{\Delta PRS_{TEST}}{IDR_H}$$
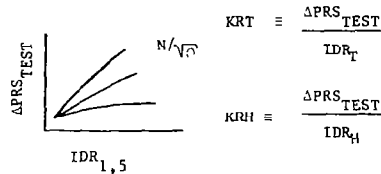
- DEFINE RADIAL INDEX

$$\Delta PRS_{RAD} \equiv KRT * IDRT + KRH * IDRH$$

PROCEDURE FOR COMBINED PATTERNS

- $\Delta PRS_{TOTAL} = \Delta PRS_{CIRCUM} + \Delta PRS_{RAD}$

## FIGURE 4 — METHOD C PROCEDURE

FOR EACH RING:

$$(\Delta PRS)_{CIRCUM_i} = \left(\frac{\Delta P}{P}\right)_i \cdot \left[(MR) \cdot (SF) \cdot (EF)\right] \cdot K_C \quad \text{SENSITIVITY COEFFICIENT}$$

→ EXTENT FACTOR

→ SHAPE FACTOR

→ MULTIPLE PER REV FACTOR

→ LEVEL PARAMETER

1/REV DATA

$\Delta N/\sqrt{\theta}$

$\Delta PRS_{TEST}$

$$K_C \equiv \left[\frac{\Delta PRS}{1/5 \Sigma \left(\frac{\Delta P}{P}\right)_i}\right] = f\left(N/\sqrt{\theta}, \frac{\Delta P}{P}\right)$$

- sq WAVE
- 180° EXTENT

$1/5 \Sigma \left(\frac{\Delta P}{P}\right)_i$

NOTE: $\left(\frac{\Delta P}{P}\right)_i \equiv \dfrac{RING\ AVG - RING\ MIN}{FACE\ AVG}$
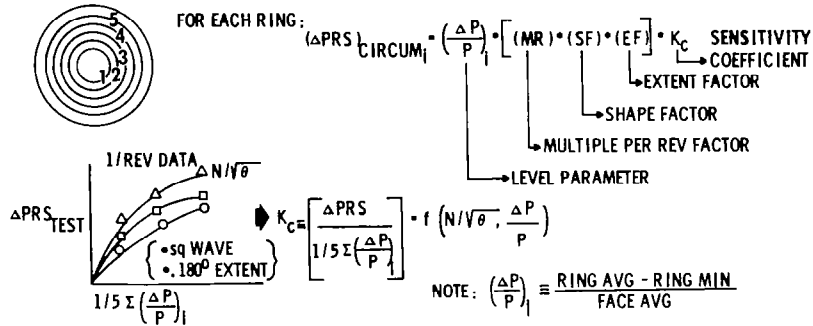
$(\Delta PRS)_{CIRCUM} \equiv 1/2 \ (\Delta PRS_1 + \Delta PRS_2)$   HUB

$(\Delta PRS)_{CIRCUM} \equiv 1/2 \ (\Delta PRS_4 + \Delta PRS_5)$   TIP

SELECT LARGEST AS $(\Delta PRS)_{CIRCUM}$

EXTENT FACTOR

$\Delta PRS_{TEST}$

$\Delta\theta = 180°$

$\Delta\theta$

$N/\sqrt{\theta} = CONST$

$1/5 \sum \left(\frac{\Delta P}{P}\right)_i$

$\Delta\theta$ IS REGION OF P < P_AVG

$$EF \equiv \frac{\left[\Delta PRS / 1/5 \sum \left(\frac{\Delta P}{P}\right)_i\right]_{\Delta\theta}}{\left[\Delta PRS / 1/5 \sum \left(\frac{\Delta P}{P}\right)_i\right]_{180}} \equiv \frac{K_{C_\theta}}{K_{C_{180}}}$$

MULTIPLE/REV FACTOR

$\Sigma \Delta\theta = CONST$

$\Delta PRS_{TEST}$

$\Delta\theta = 180°$

$N = 2$

$N = 4$

$N/\sqrt{\theta} = CONST$

$1/5 \sum \left(\frac{\Delta P}{P}\right)_i$

$$MR \equiv \frac{\left[\Delta PRS / 1/5 \sum \left(\frac{\Delta P}{P}\right)_i\right]_{N/REV}}{\left[\Delta PRS / 1/5 \sum \left(\frac{\Delta P}{P}\right)_i\right]_{1/REV}} \equiv \left(\frac{1}{N}\right)^\omega$$

N IS THE NUMBER OF LOW PRESSURE REGIONS

SHAPE FACTOR

$[\Delta PRS]_{SQ}$

SAME LEVEL AND EXTENT

$[\Delta PRS]_{SINE}$

$$SF \equiv \frac{\left[\Delta PRS / 1/5 \sum \left(\frac{\Delta P}{P}\right)_i\right]}{\left[\Delta PRS / 1/5 \sum \left(\frac{\Delta P}{P}\right)_i\right]_{SQ}} \equiv \left\{\frac{\left[\int_{\Delta\theta} P d\theta\right]}{\left[\int_{\Delta\theta} P d\theta\right]_{SQ}}\right\}^\infty$$

( $\Delta\theta$ IS REGION OF P < P_AVG )
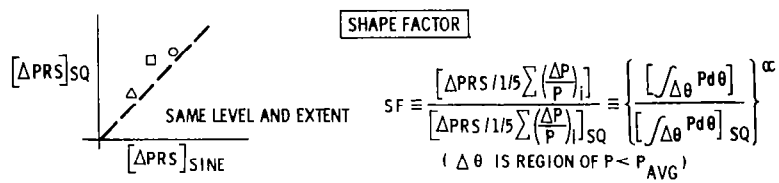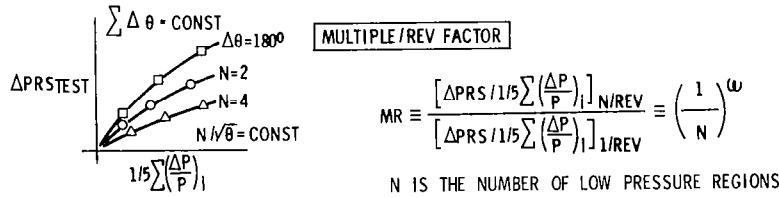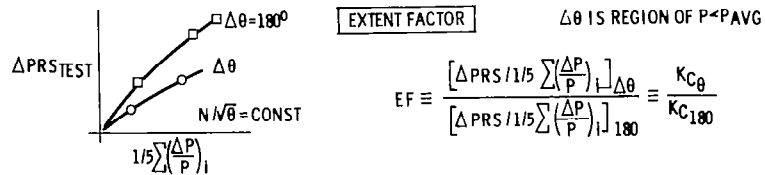
METHOD D CIRCUMFERENTIAL DISTORTION

IN HUB REGION

LEAST SQUARES DATA FIT THRU ORIGIN

$\Delta PRS_{TEST}$

$N/\sqrt{\theta}$

$K_H$

$1$

$$(\Delta PRS)_{HR} \equiv \left[\left(\frac{\Delta P}{P}\right)_1 + \alpha_H\left(\frac{\Delta P}{P}\right)_2\right] K_H \quad \text{SENSITIVITY COEFFICIENT}$$

→ EXTENT COEFFICIENT

$\left(\frac{\Delta P}{P}\right)_1 + \alpha_H \left(\frac{\Delta P}{P}\right)_2$

$$\frac{\Delta P}{P} \equiv \frac{FACE\ AVG - RING\ AVG}{FACE\ AVG}$$

IN TIP REGION

$\Delta PRS_{TEST}$

$N/\sqrt{\theta}$

$K_T$

$1$

$$(\Delta PRS)_{TR} \equiv \left[\left(\frac{\Delta P}{P}\right)_5 + \alpha_T\left(\frac{\Delta P}{P}\right)_4\right] K_T$$

$\left(\frac{\Delta P}{P}\right)_5 + \alpha_T \left(\frac{\Delta P}{P}\right)_4$
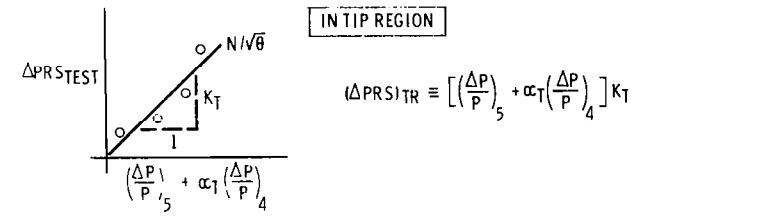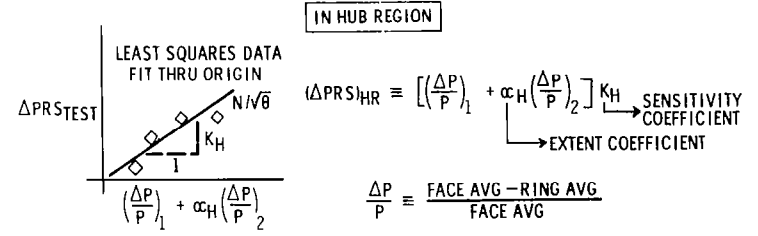
SELECT LARGEST AS $(\Delta PRS)_{RAD}$

METHOD D RADIAL DISTORTION

EVALUATE:

$(\Delta PRS)CIRCUM$

$(\Delta PRS)RAD$

→ $(\Delta PRS)_{COMB}$

$\equiv b \cdot (\Delta PRS)CIRCUM + (\Delta PRS)RAD$

(MAX)   (MAX)

→ SUPERPOSITION FACTOR

COMBINED DATA

$1.0$

$b$

$0$
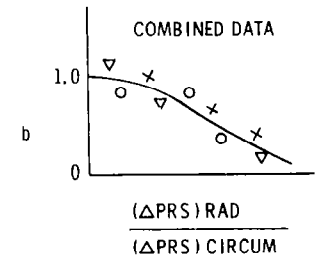
$\dfrac{(\Delta PRS)RAD}{(\Delta PRS)CIRCUM}$

$$b \equiv \frac{(\Delta PRS)TEST - (\Delta PRS)RAD}{(\Delta PRS)CIRCUM}$$

METHOD D COMBINED DISTORTION

FIGURE 5 – METHOD D PROCEDURE
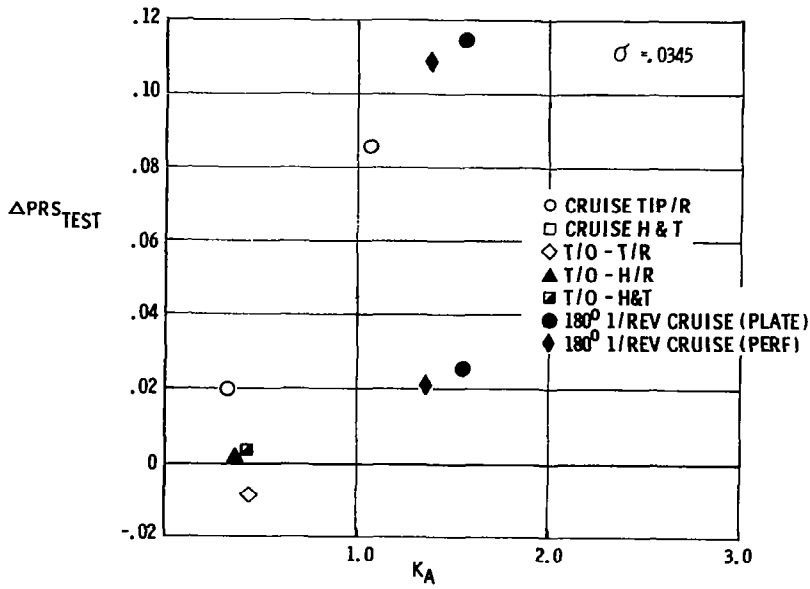
FIGURE 6 — METHOD A — GE4 (72T,85T)
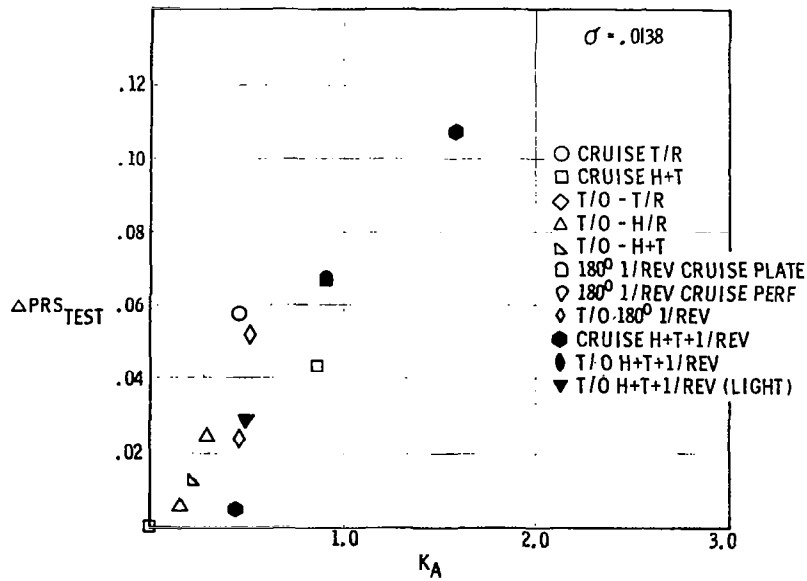


FIGURE 7 — METHOD A — GE4 (72P, 85W, V95)
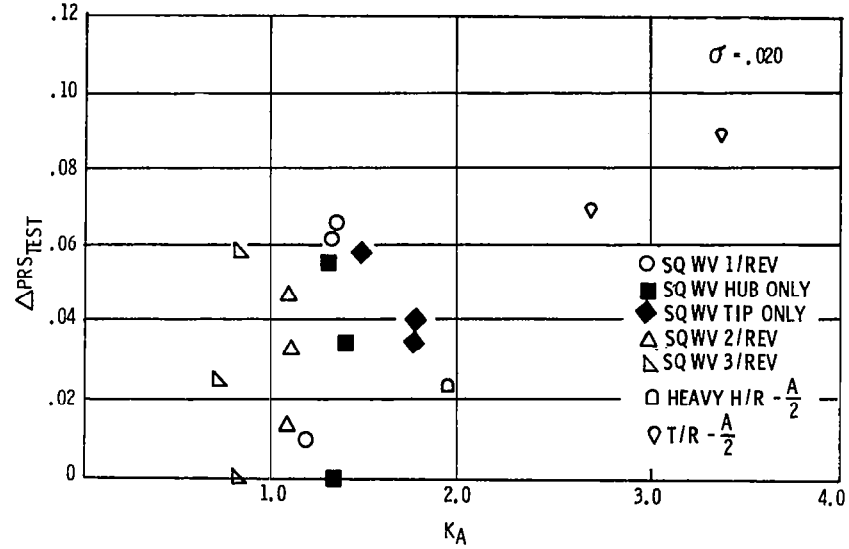
FIGURE 8 — METHOD A — GE-F100 BU/7 & IGV'S & O.S.
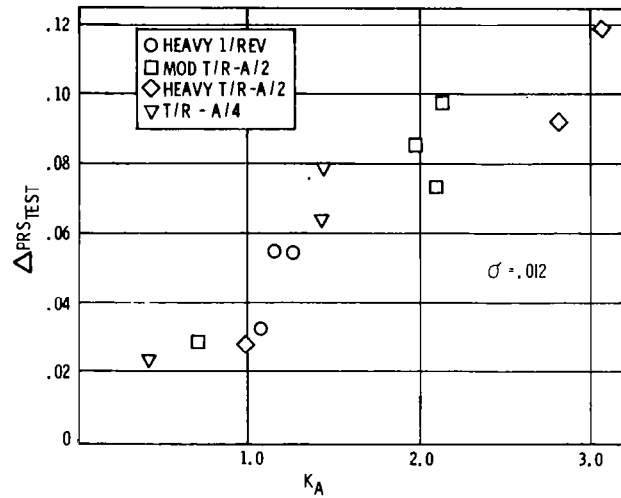


FIGURE 9 — METHOD A — GE-F100 BU/7 & IGV'S
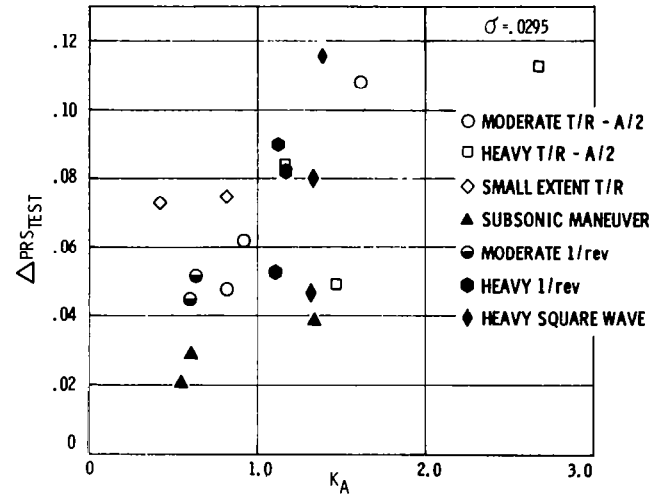
FIGURE 10 — METHOD A — GE-F100 BU/6
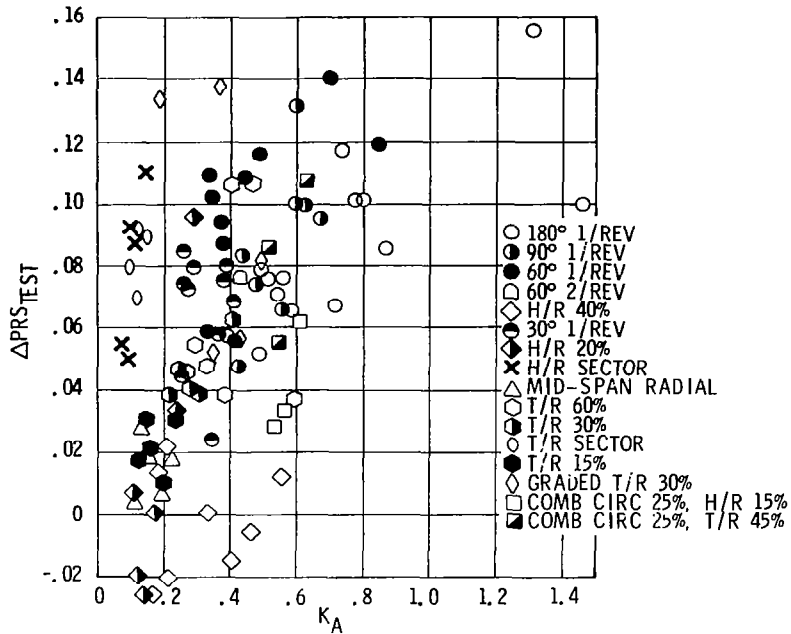
FIGURE 11 — METHOD A NASA — LeRC DATA SET B
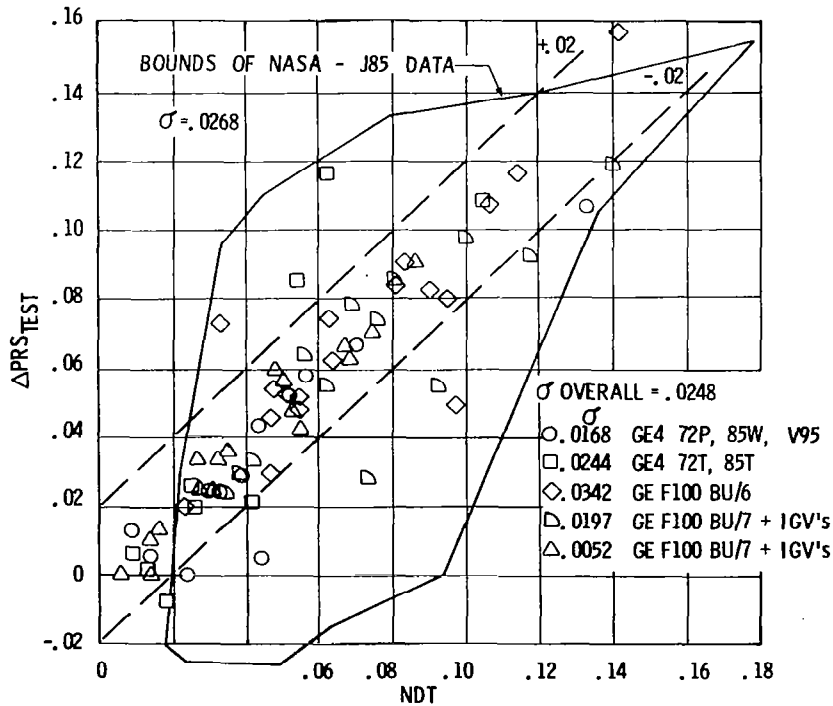


FIGURE 12 — METHOD B CORRELATION
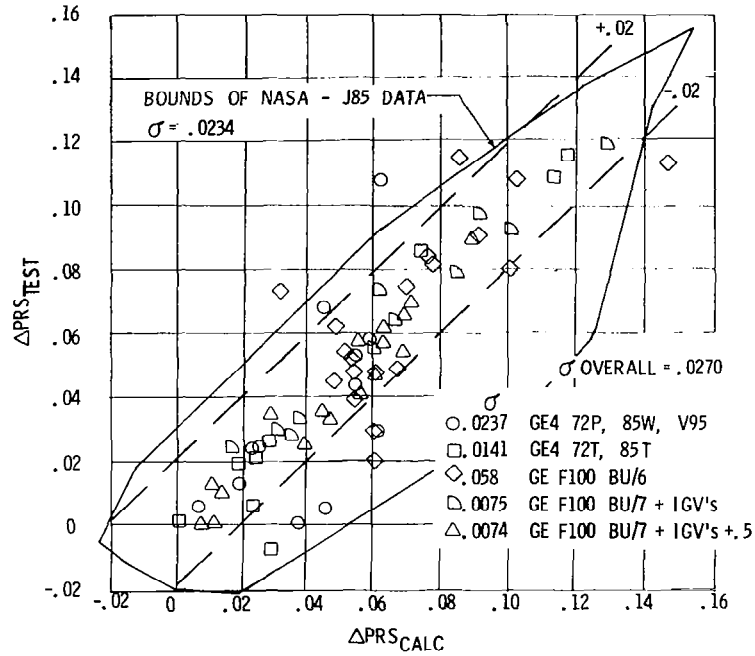
FIGURE 13 — METHOD C CORRELATION
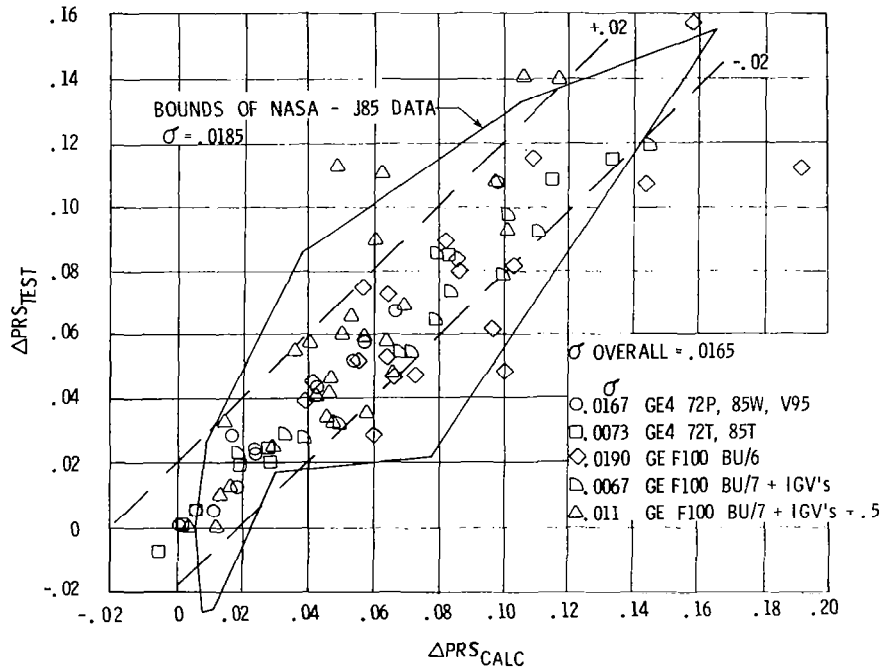
FIGURE 14 — METHOD D CORRELATION

**Figure 13 (top plot):**

Y-axis: $\Delta PRS_{TEST}$ (values .16, .14, .12, .10, .08, .06, .04, .02, 0, -.02)

X-axis: $\Delta PRS_{CALC}$ (values -.02, 0, .02, .04, .06, .08, .10, .12, .14, .16)

+.02
-.02

BOUNDS OF NASA – J85 DATA
$\sigma = .0234$

$\sigma$ OVERALL = .0270

| $\sigma$ | |
|---|---|
| O .0237 | GE4 72P, 85W, V95 |
| □ .0141 | GE4 72T, 85T |
| ◇ .058 | GE F100 BU/6 |
| ◻ .0075 | GE F100 BU/7 + IGV's |
| △ .0074 | GE F100 BU/7 + IGV's +.5 |

**Figure 14 (bottom plot):**

Y-axis: $\Delta PRS_{TEST}$ (values .16, .14, .12, .10, .08, .06, .04, .02, 0, -.02)

X-axis: $\Delta PRS_{CALC}$ (values -.02, 0, .02, .04, .06, .08, .10, .12, .14, .16, .18, .20)

+.02
-.02

BOUNDS OF NASA – J85 DATA
$\sigma = .0185$

$\sigma$ OVERALL = .0165

| $\sigma$ | |
|---|---|
| O .0167 | GE4 72P, 85W, V95 |
| □ .0073 | GE4 72T, 85T |
| ◇ .0190 | GE F100 BU/6 |
| ◻ .0067 | GE F100 BU/7 + IGV's |
| △ .011 | GE F100 BU/7 + IGV's + .5 |

FIGURE 15 – DATA SET B CIRCUMFERENTIAL SENSITIVITIES, METHOD D
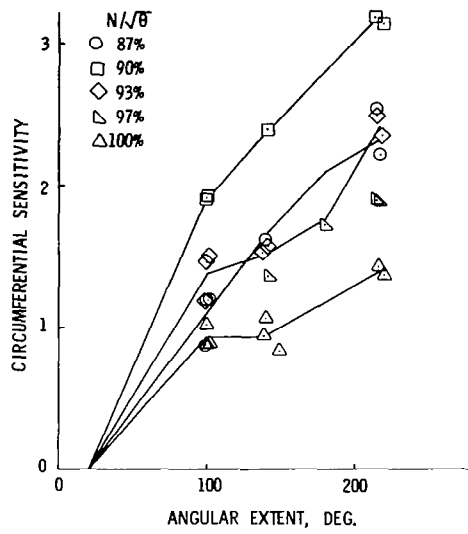
FIGURE 16 – DATA SET B CIRCUMFERENTIAL
SENSITIVITY VS ANGULAR
EXTENT
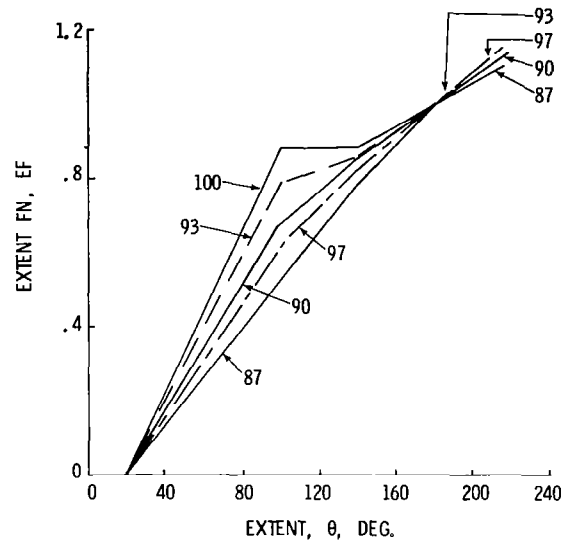
FIGURE 17 – DATA SET B EXTENT FUNC-
TION VS ANGULAR EXTENT
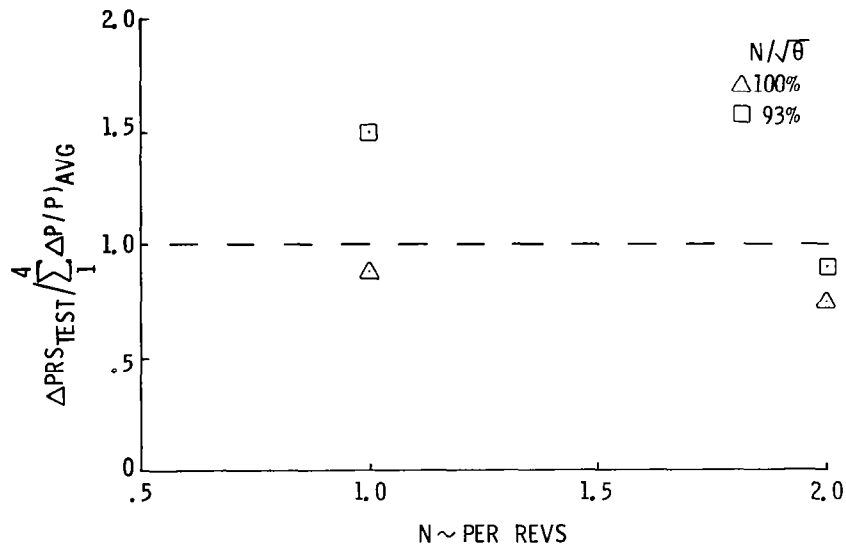


FIGURE 18 – MULTI–PER REV FUNCTION VS NUMBER OF LOW PRESSURE ZONES

NOTE : FOR $N/\sqrt{\theta} = 100$

$$10[(\Delta P/P)_{R_1} + \alpha_H(\Delta P/P)_{R_2}]$$

IS PLOTTED
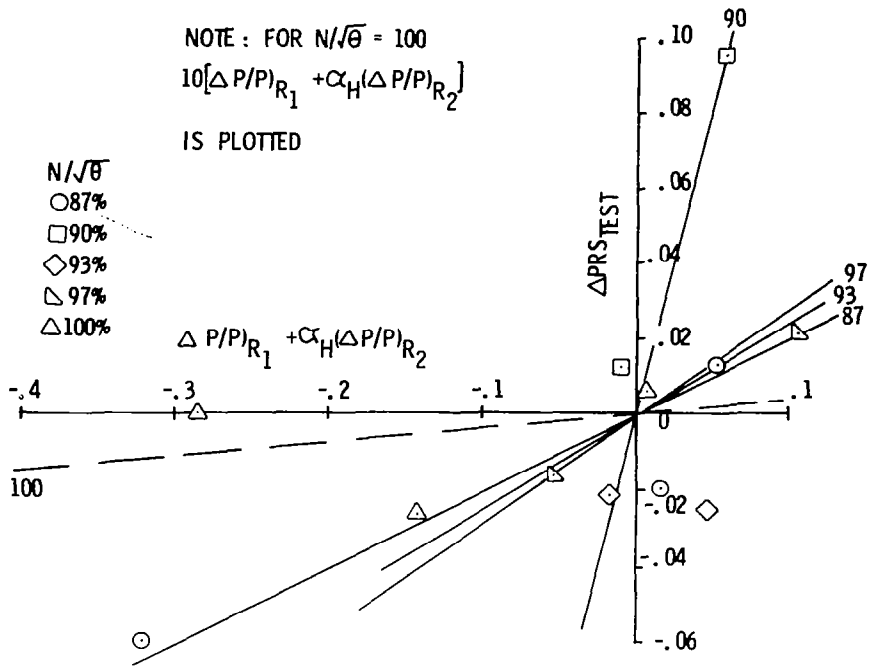
FIGURE 19 — DATA SET B HUB RADIAL SENSITIVITY
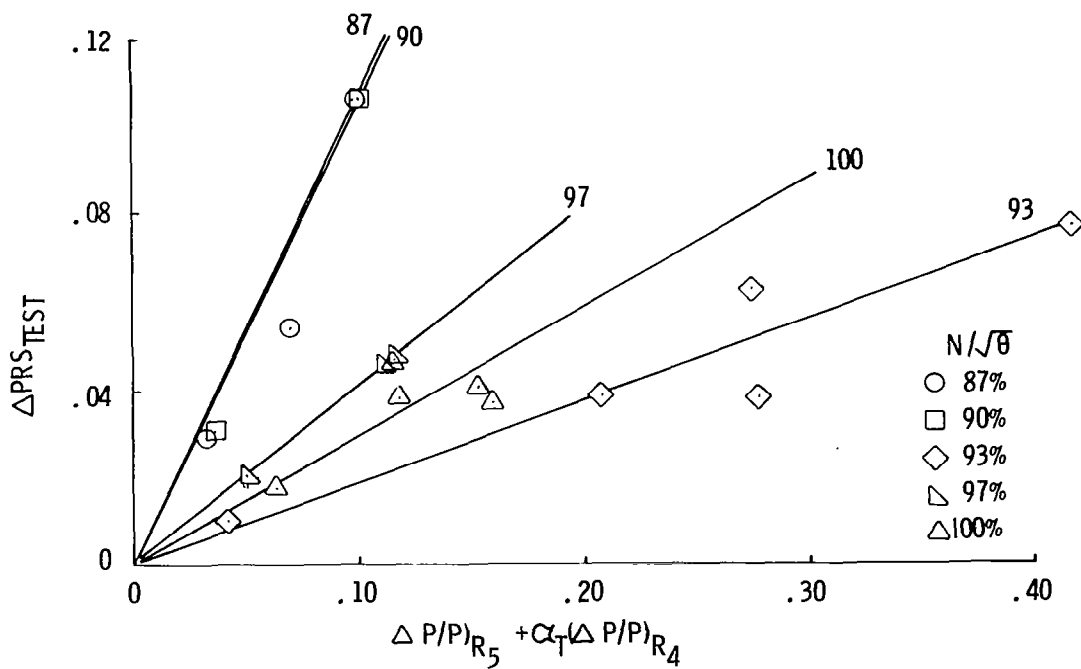


FIGURE 20 — DATA SET B TIP RADIAL SENSITIVITY
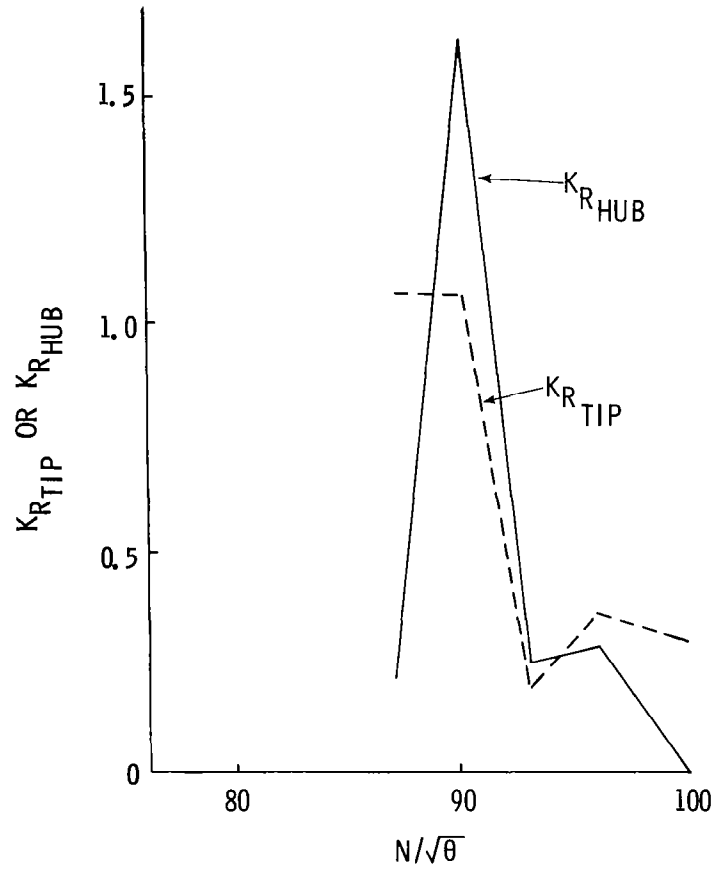
FIGURE 21 – DATA SET B RADIAL SENSITIVITIES VS
CORRECTED SPEED
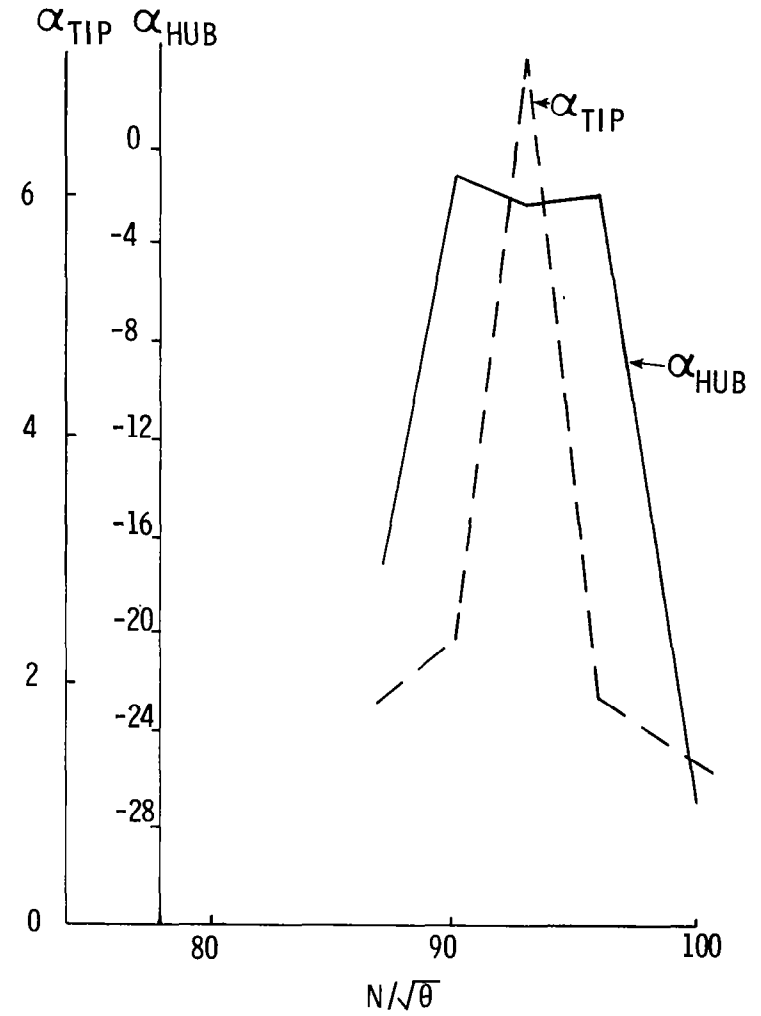


FIGURE 22 – DATA SET B RADIAL EXTENT FUNCTIONS
VS CORRECTED SPEEDS

$N/\sqrt{\theta}$

○ 87%

□ 90%

◇ 93%

◁ 97%

△ 100%

1.2

0.8

b - FACTOR

0.4

0

0        0.4        0.8        1.2
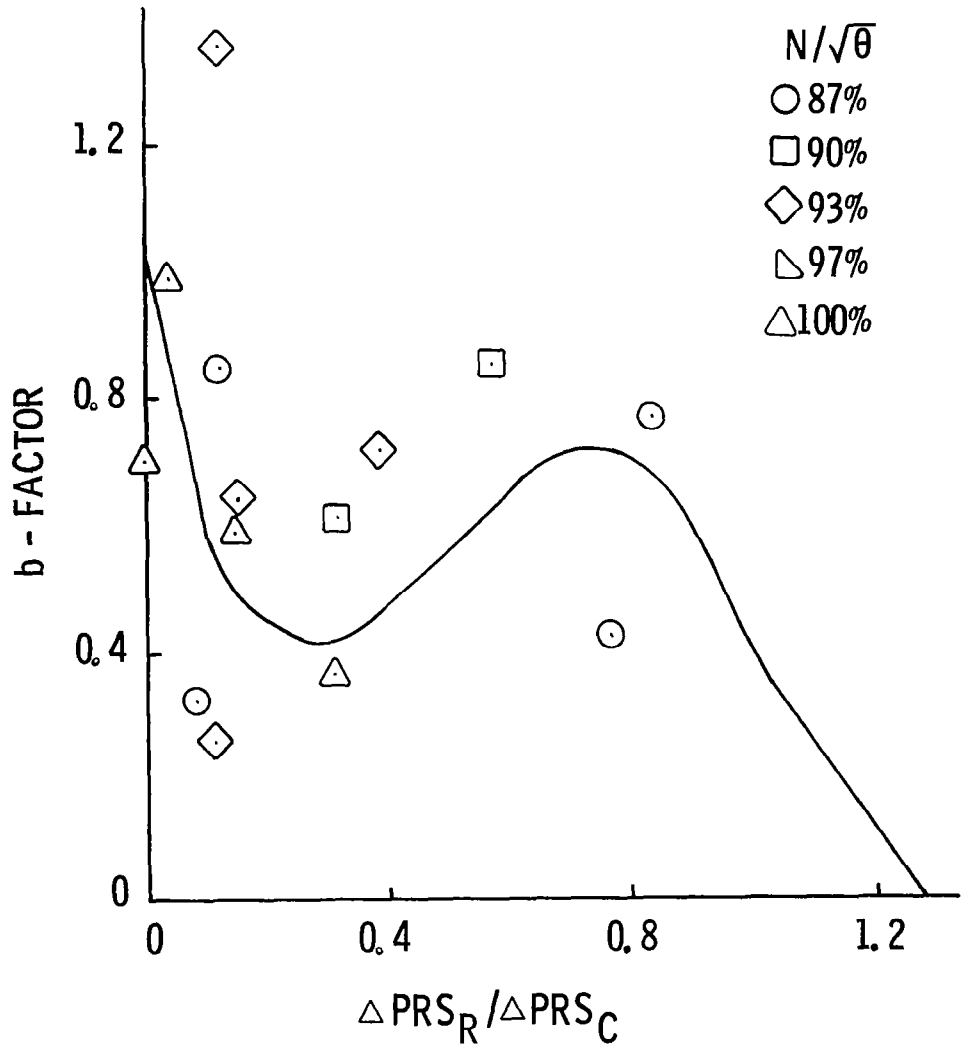
$\triangle PRS_R/\triangle PRS_C$

FIGURE 23 - J-85 DATA SET B SUPERPOSITION FACTOR VS. $\triangle PRS_R/\triangle PRS_C$
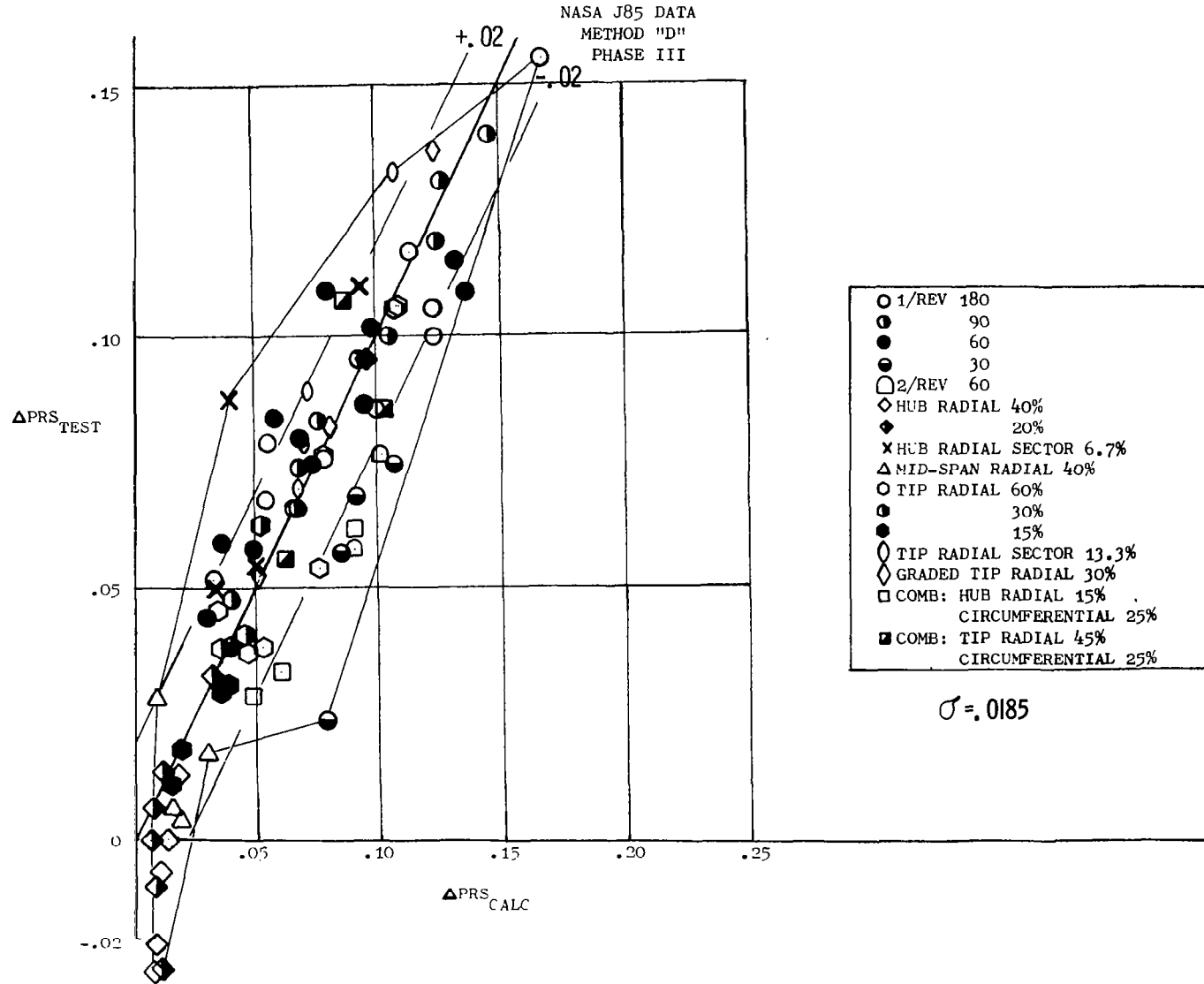
FIGURE 24 — J-85 DATA SET B CORRELATION

$$CEF = \frac{SLOPE)_{CE}}{SLOPE)_{180°}}$$
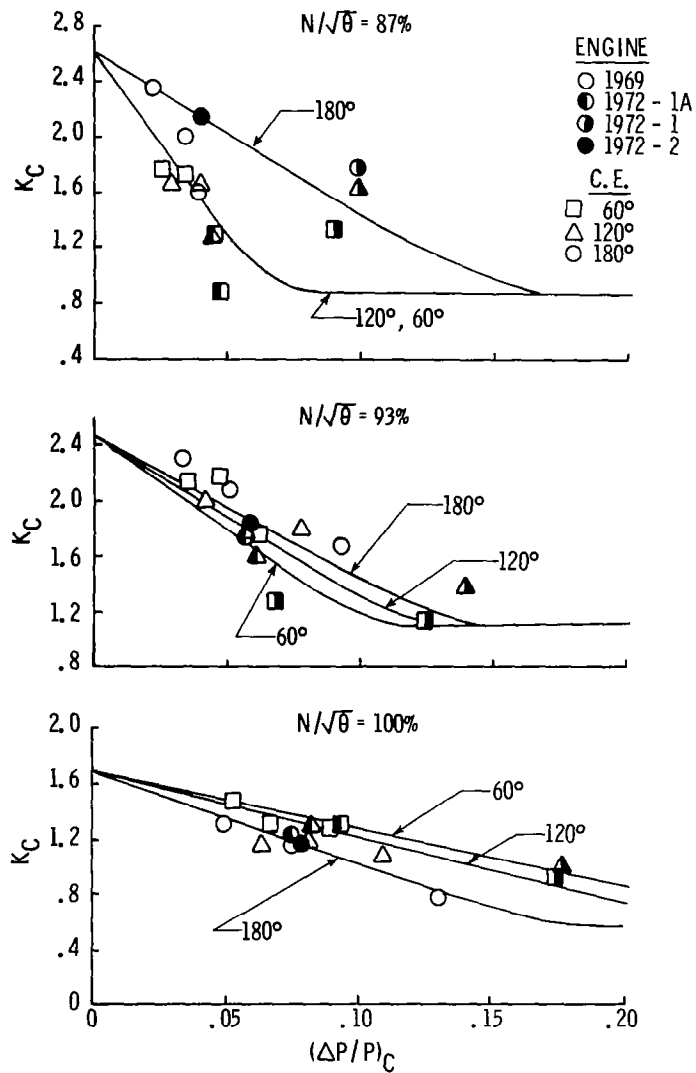
FIGURE 25 – CIRCUMFERENTIAL SENSITIVITY AS A
FUNCTION OF CIRCUMFERENTIAL DIS-
TORTION FOR VARIOUS ANGULAR EXTENTS
(METHOD D+)
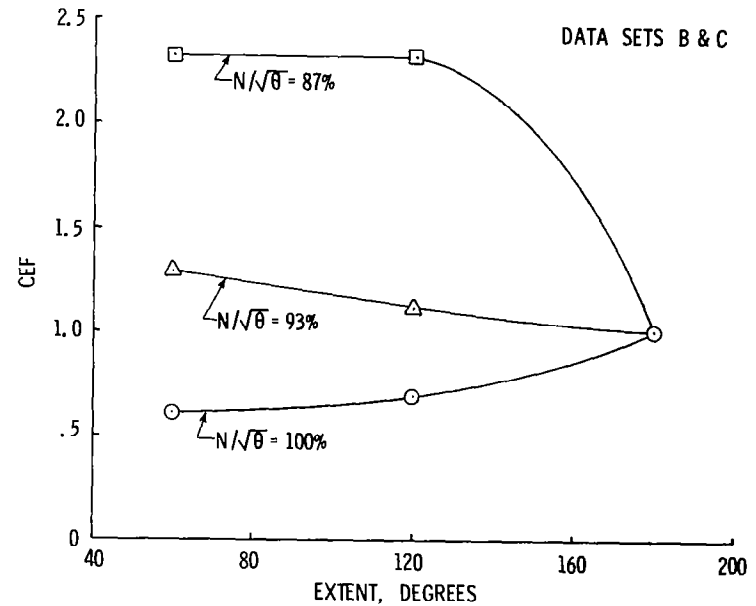
FIGURE 26 – CIRCUMFERENTIAL EXTENT FUNCTION
VERSUS ANGULAR EXTENT (METHOD D+)
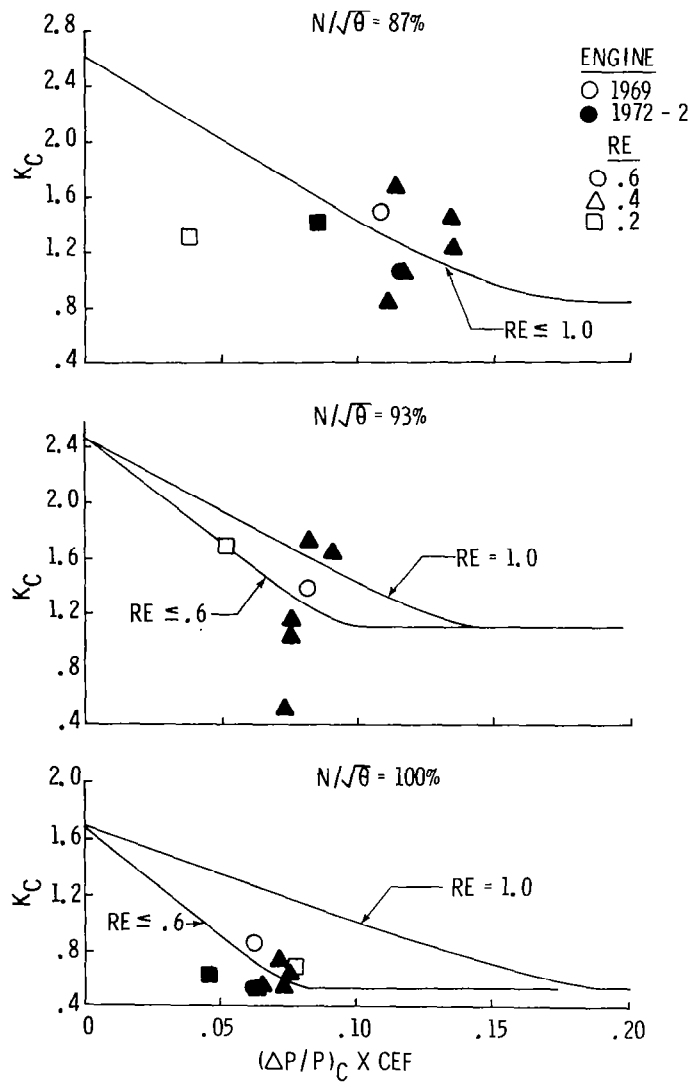
FIGURE 27 – CIRCUMFERENTIAL SENSITIVITY AS A
FUNCTION OF 180° – NORMALIZED
CIRCUMFERENTIAL DISTORTION FOR
VARIOUS RADIAL EXTENTS (METHOD D+)
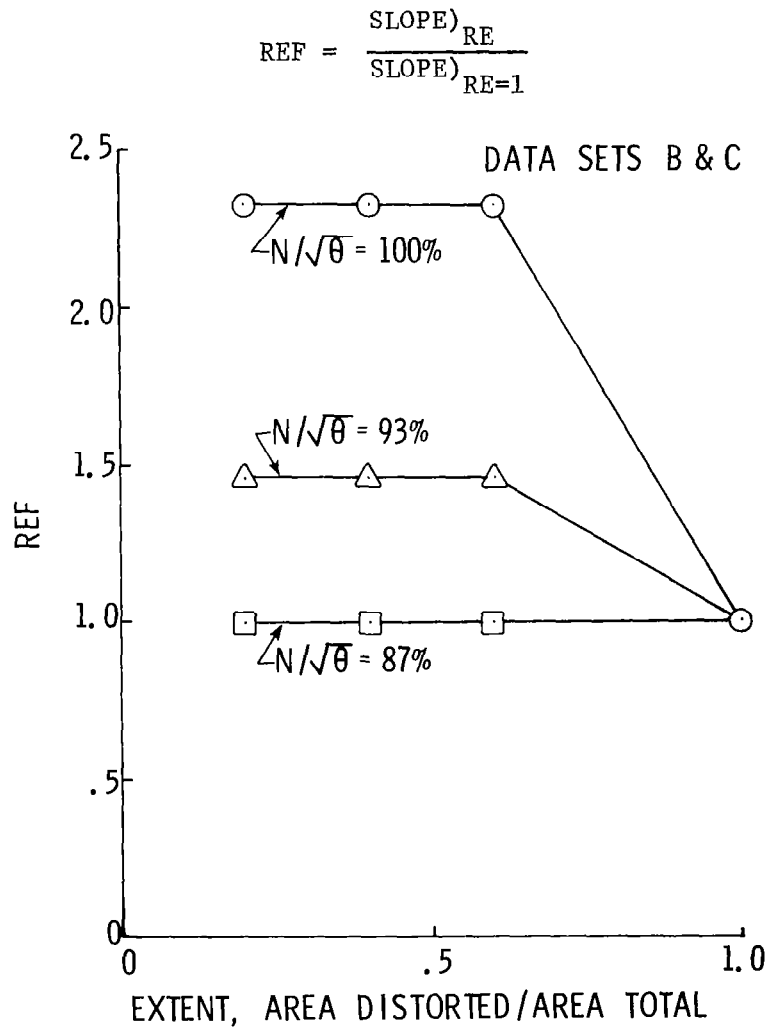


FIGURE 28 – RADIAL EXTENT FACTOR VERSUS RADIAL
EXTENT (METHOD D+)
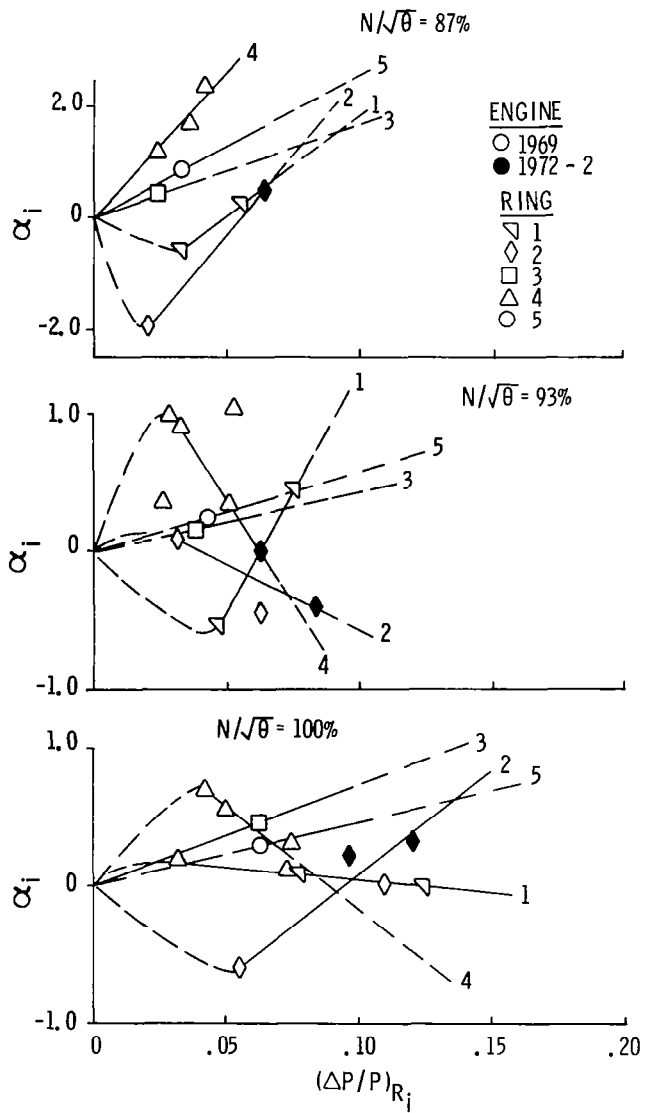
FIGURE 29 – RADIAL SENSITIVITY AS A FUNCTION
OF RADIAL DISTORTION (METHOD D+)
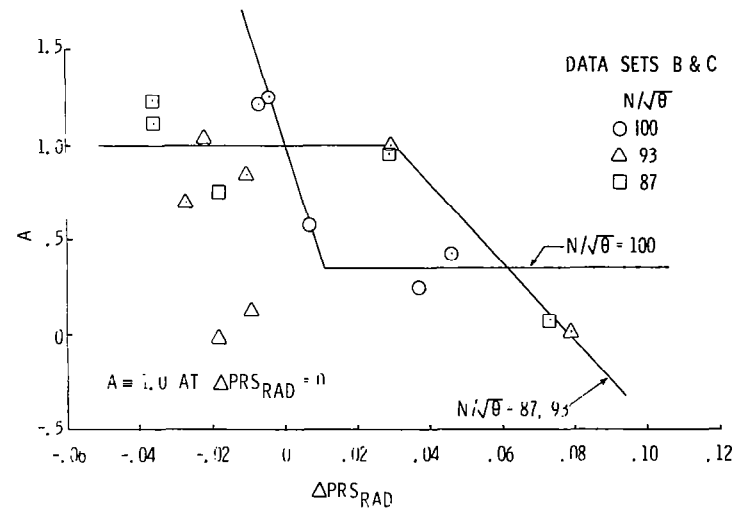
FIGURE 30 – SUPERPOSITION FUNCTION VERSUS RADIAL
LOSS IN SURGE PRESSURE RATIO
(METHOD D+)

FIGURE 31 - METHOD D+ CORRELATION, DATA SETS B AND C.
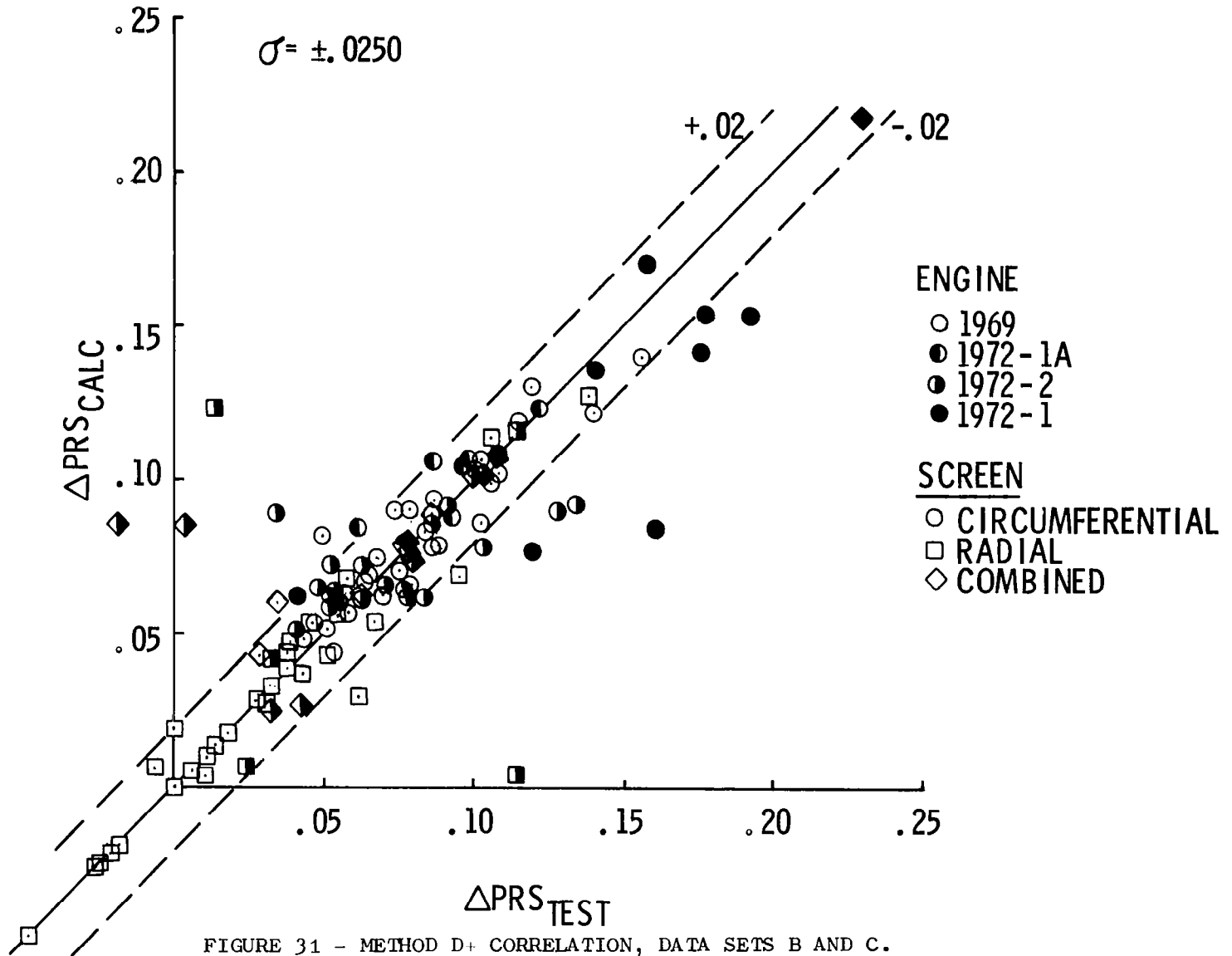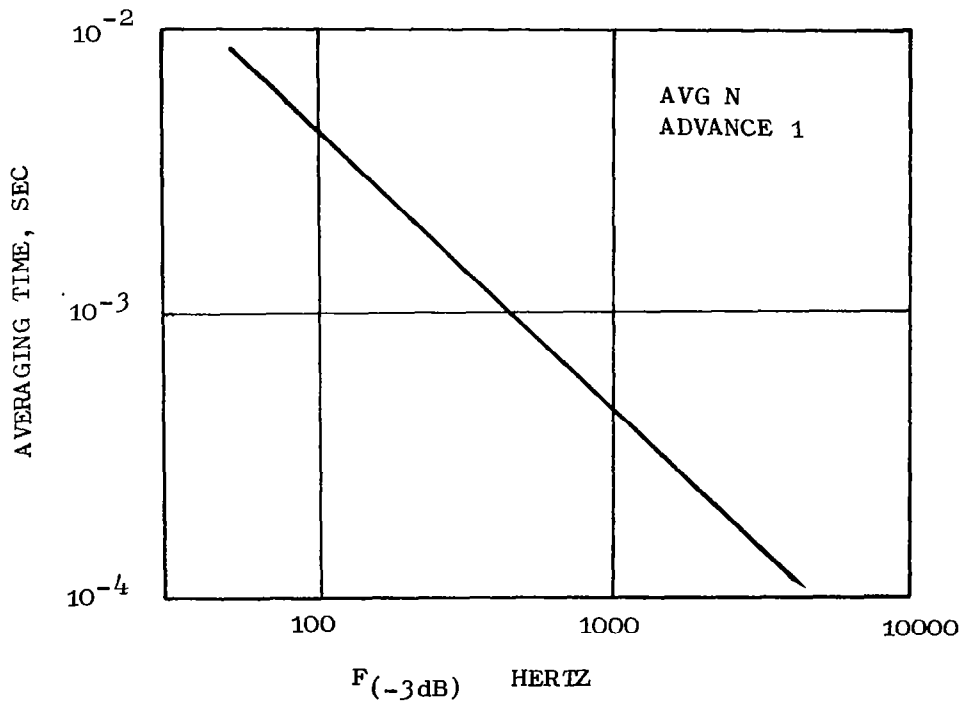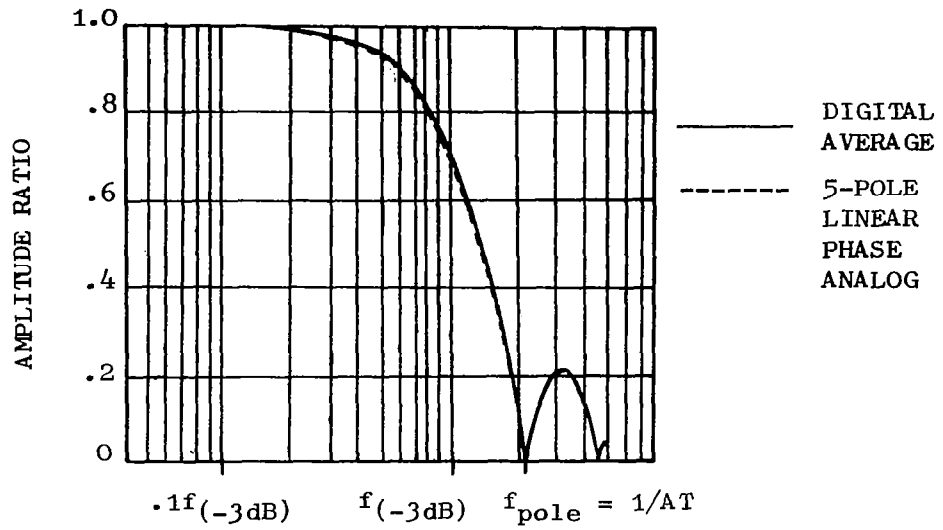
FIGURE 32 — CHARACTERISTICS OF DIGITAL FILTER USED IN D-DAP

63
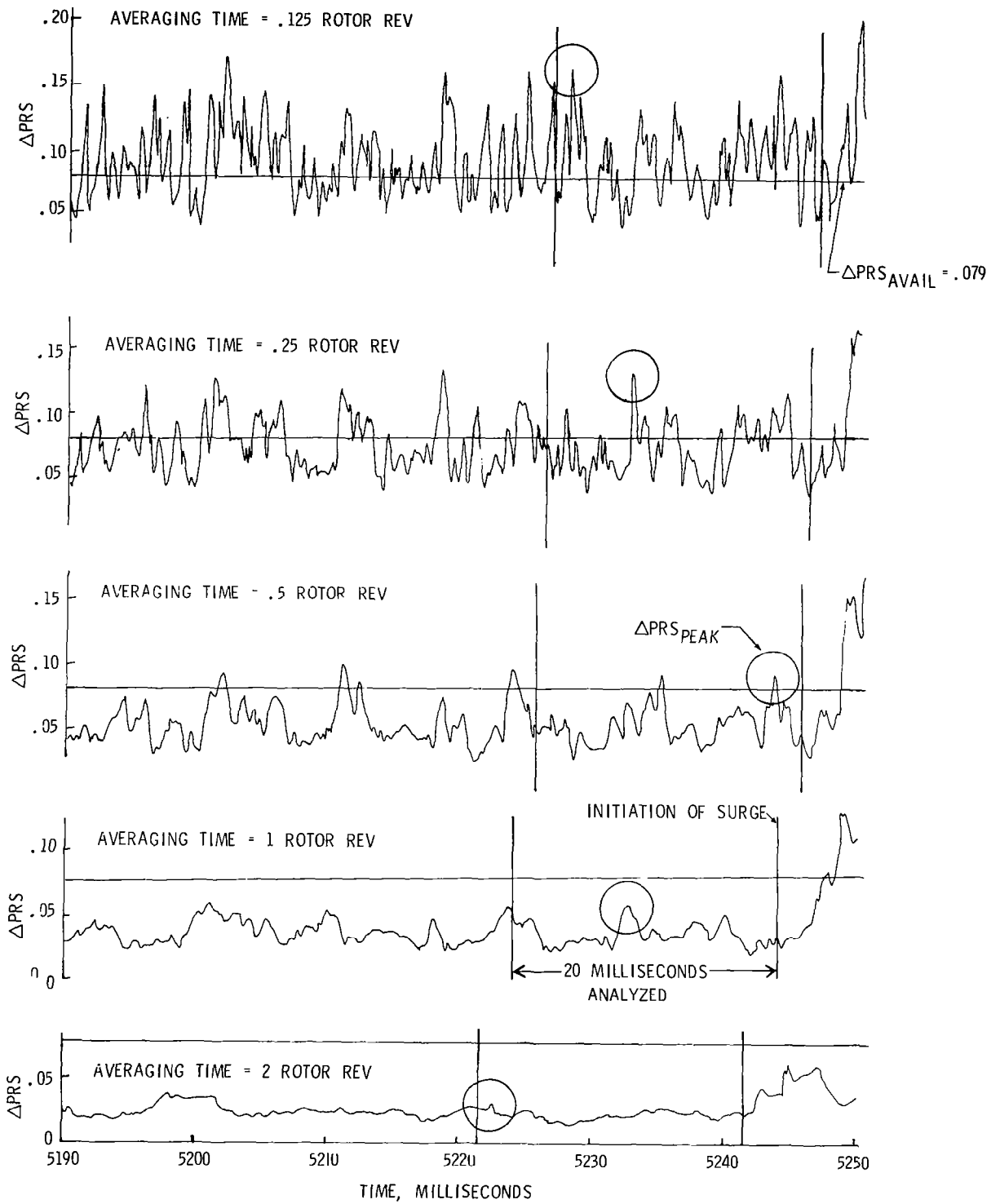
FIGURE 33 — SURGE NO. 141, DATA SET A
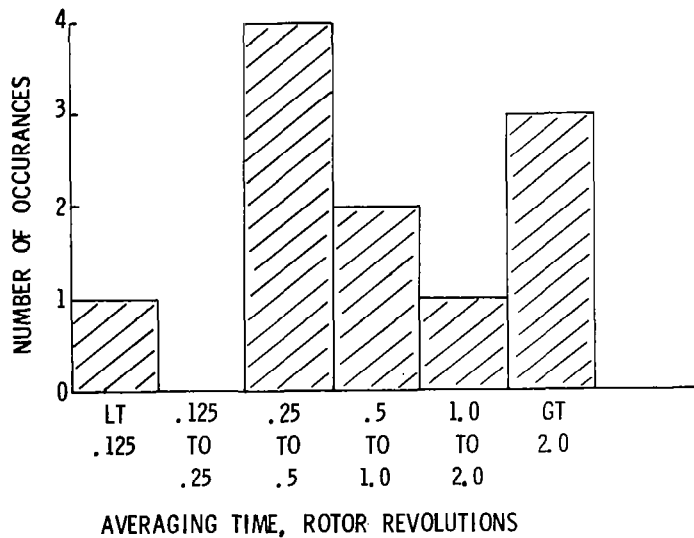
FIGURE 34 — HISTOGRAM OF AVERAGING TIME,
METHOD D, DATA SET A
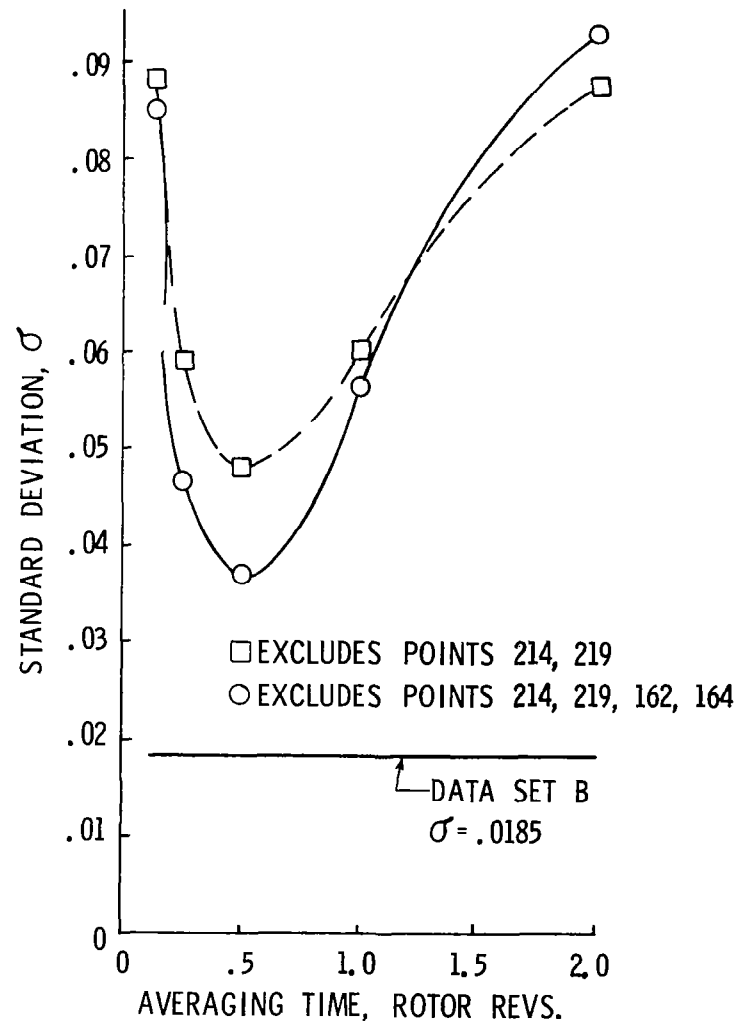


FIGURE 35 — STANDARD DEVIATION VERSUS AVERAGING
TIME, METHOD D, DATA SET A
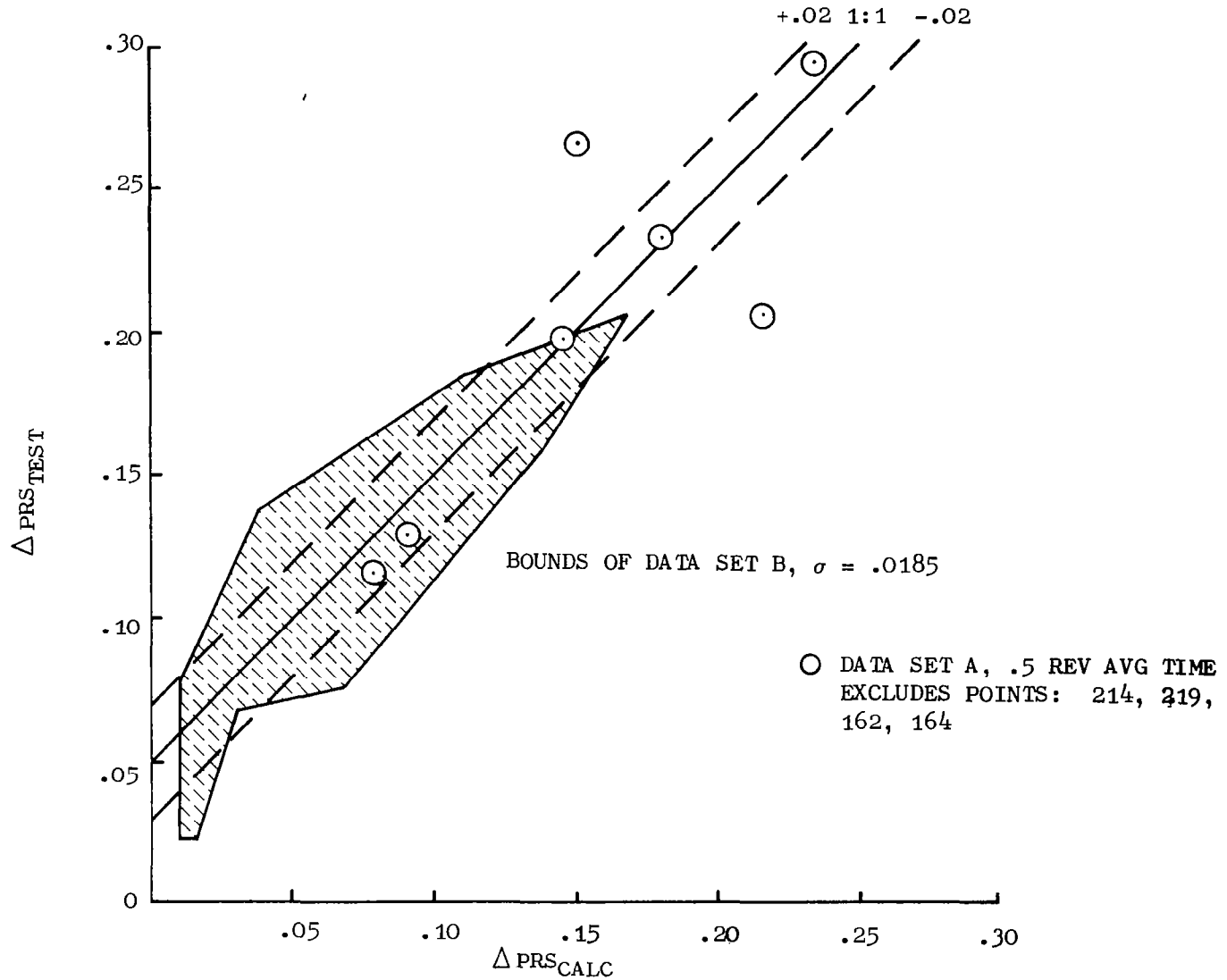
FIGURE 36 – MEASURED VS CALCULATED SURGE PRESSURE RATIO LOSS FOR DATA SETS A AND B – SET A
AVERAGING TIME AT 0.5 ROTOR REVOLUTION

ANALOG
COMPUTERS

CHART RECORDER

TAPE PLAY BACK
1 INCH 14 TRACK

OUTPUT
FILTERS

TIME CODE
IRIG "A" OR "B"

DISCRIMINATORS WITH CBW
OR CHANNEL/TRACK PLUG-INS
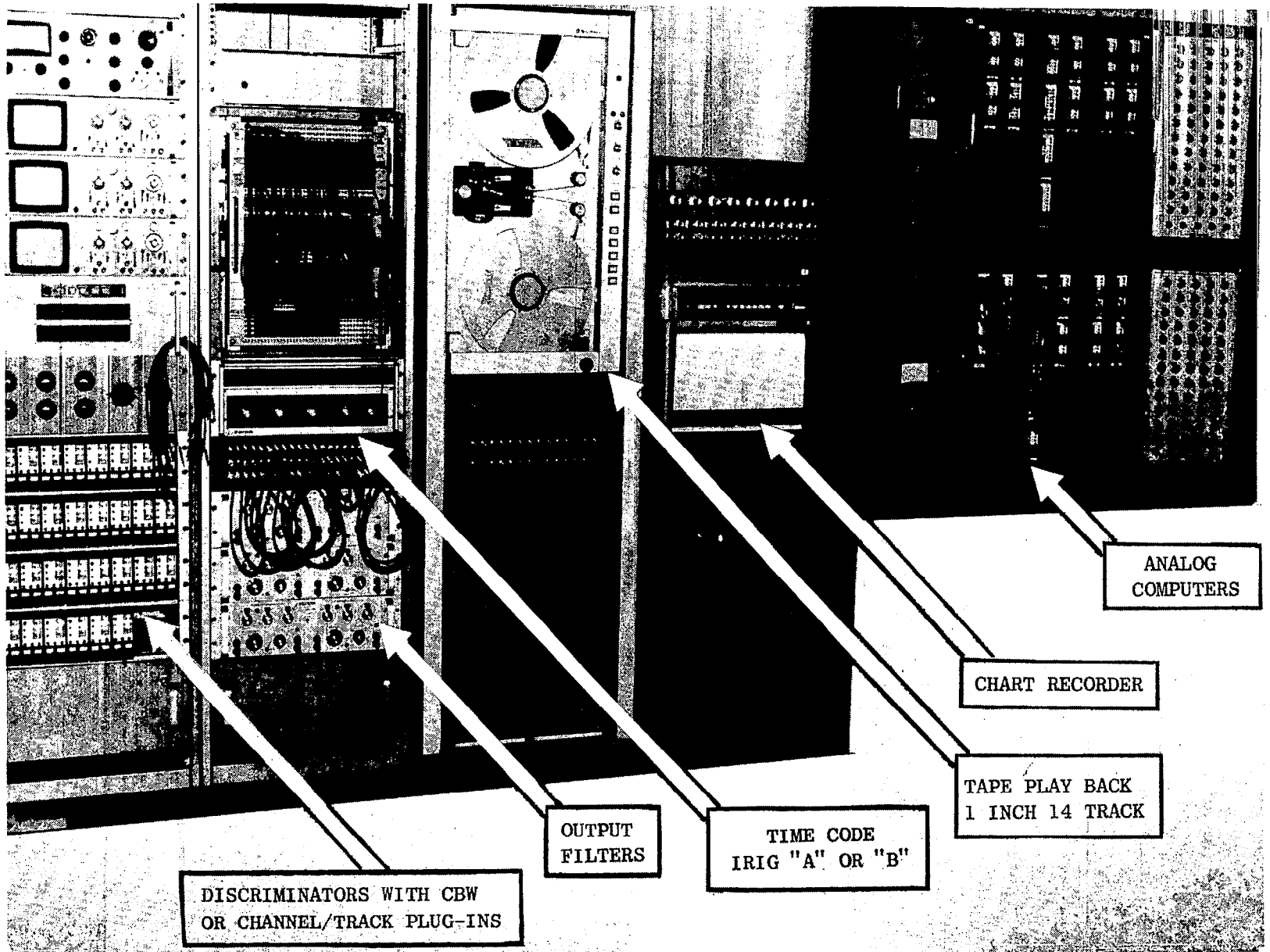
FIGURE 37 - STABILITY MEASUREMENTS ANALYSIS LABORATORY
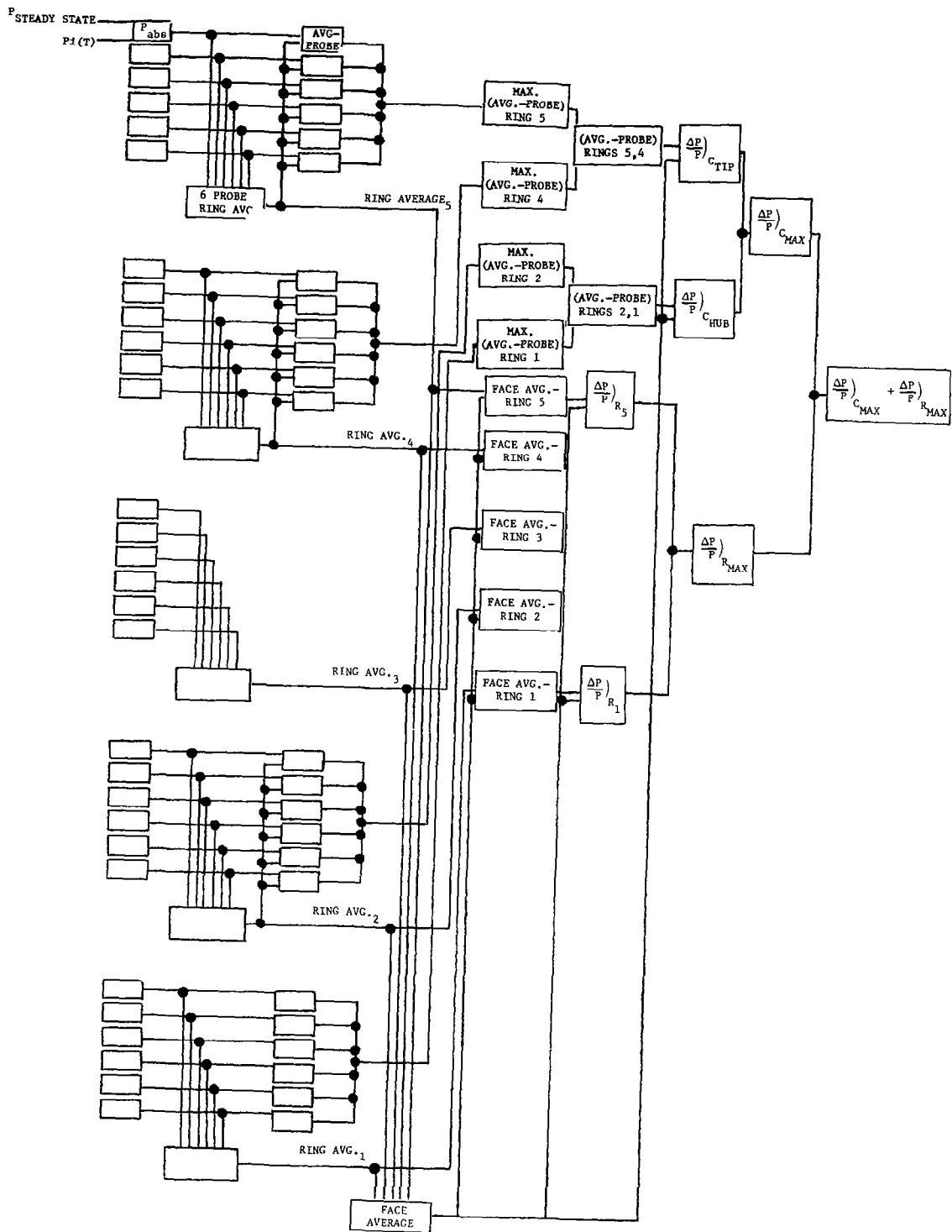
FIGURE 38 — DATA SET A ANALOG ANALYSIS BLOCK DIAGRAM

ΔP/P)$_{R_{MAX}}$

DIGITAL VS ANALOG COMPUTATION

TOP – DIGITAL @ 2.25 X $10^{-3}$ AVG TIME

BOTTOM – ANALOG @ ~200 HZ FILTER

ΔP/P)$_{C_{MAX}}$

ΔP/P)$_{C_{MAX}}$ + ΔP/P)$_{R_{MAX}}$

250 MILLISECONDS

250 MILLISECONDS
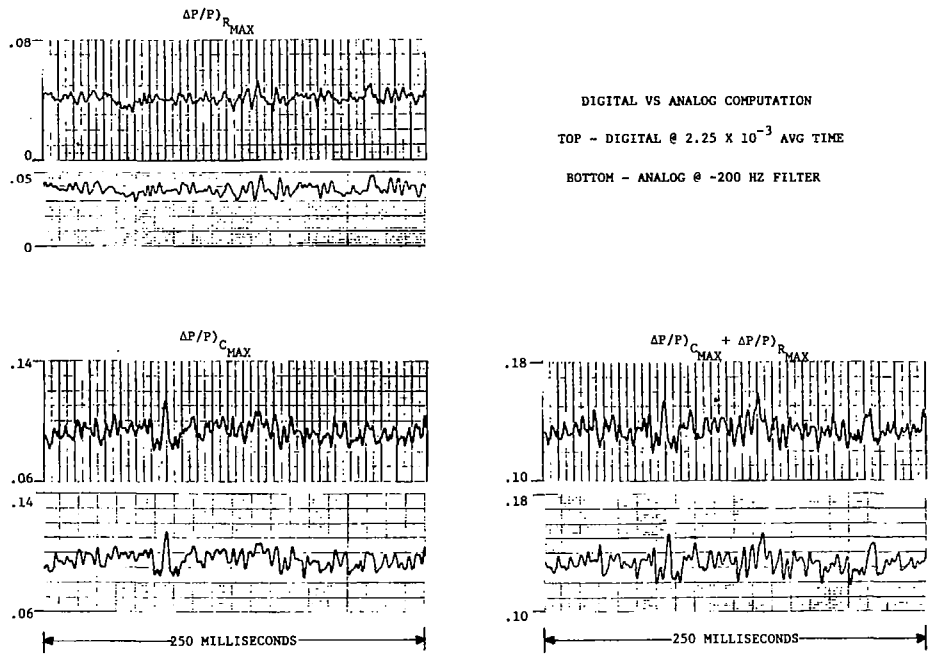
FIGURE 39 – DATA SET A, POINT 82
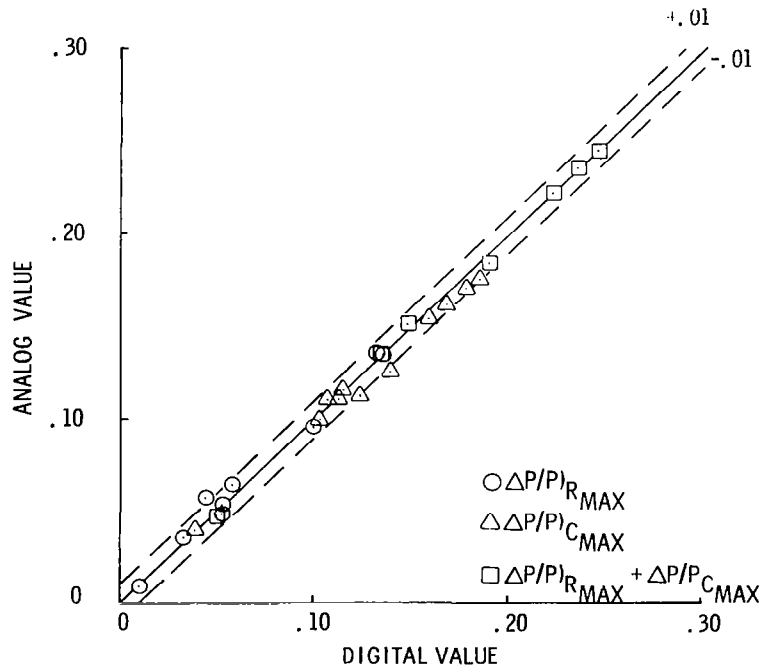


FIGURE 40 – COMPARISON OF DIGITAL AND ANALOG ANALYSES    DATA SET A
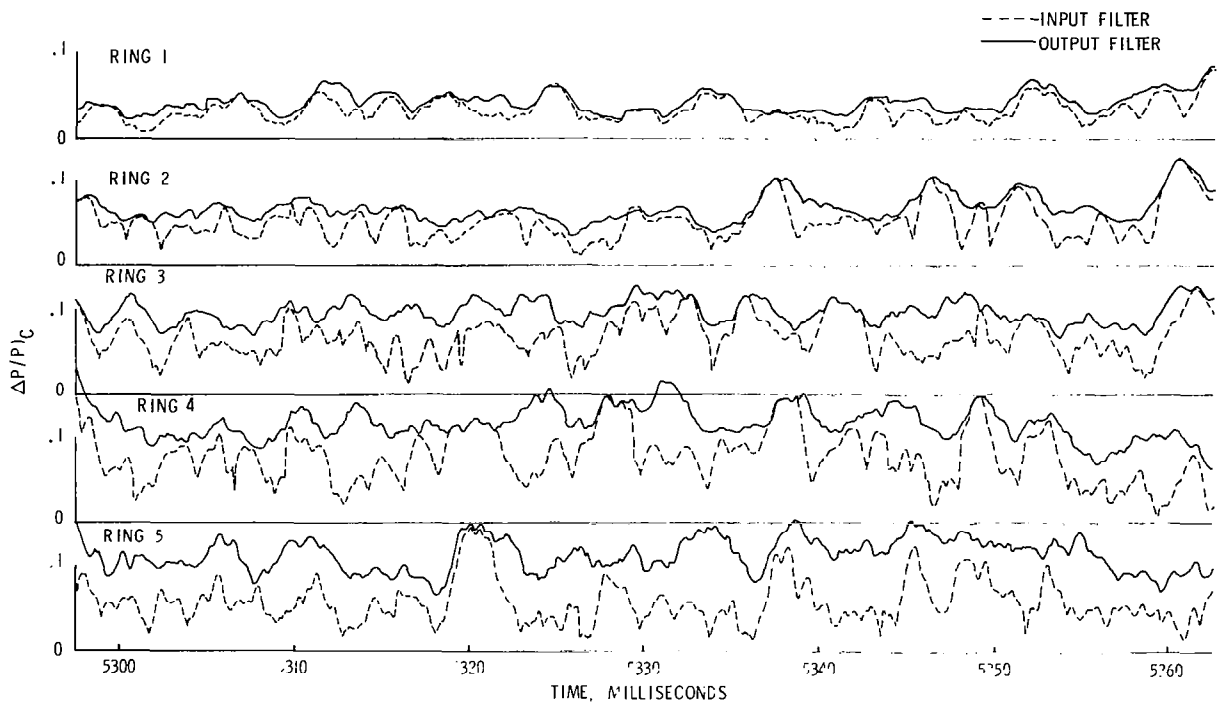
FIGURE 41 — COMPARISON OF INPUT VERSUS OUTPUT FILTERING OF $\Delta P/P)_C$. POINT 148, DATA SET A
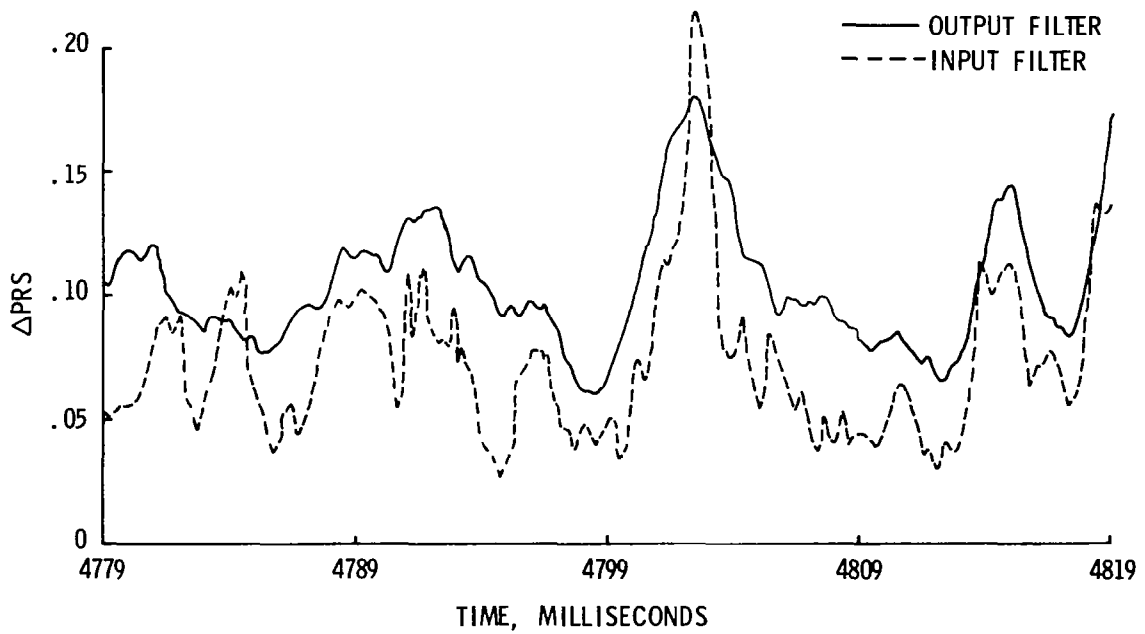


FIGURE 42 — COMPARISON OF INPUT VERSUS OUTPUT FILTERING OF $\Delta PRS_{CALC}$. POINT 148, DATA SET A
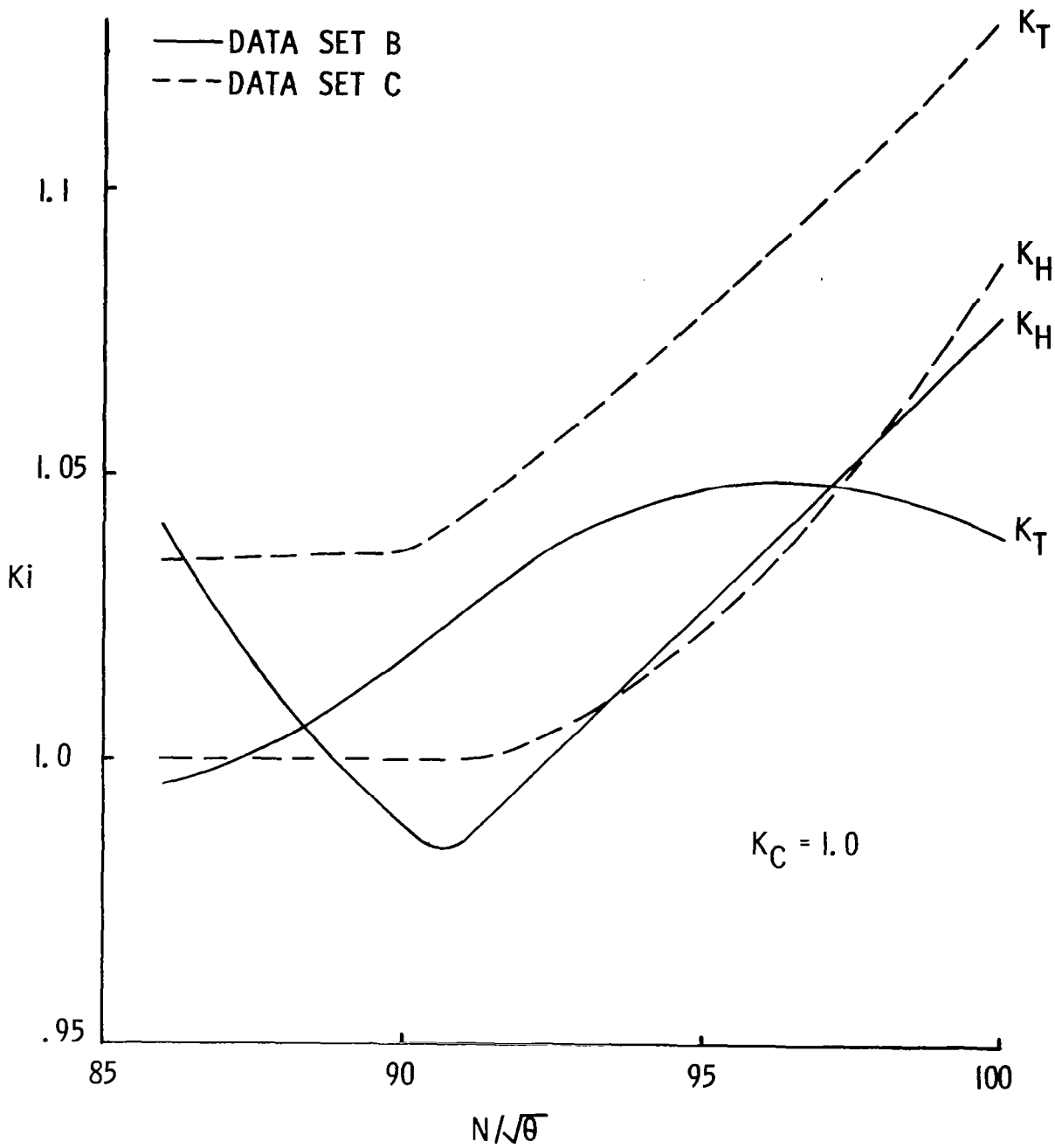
FIGURE 43 – DIDENT SENSITIVITIES FOR LOSS OF SURGE PRESSURE RATIO AT CONSTANT CORRECTED SPEED CORRELATION, DATA SETS B AND C.
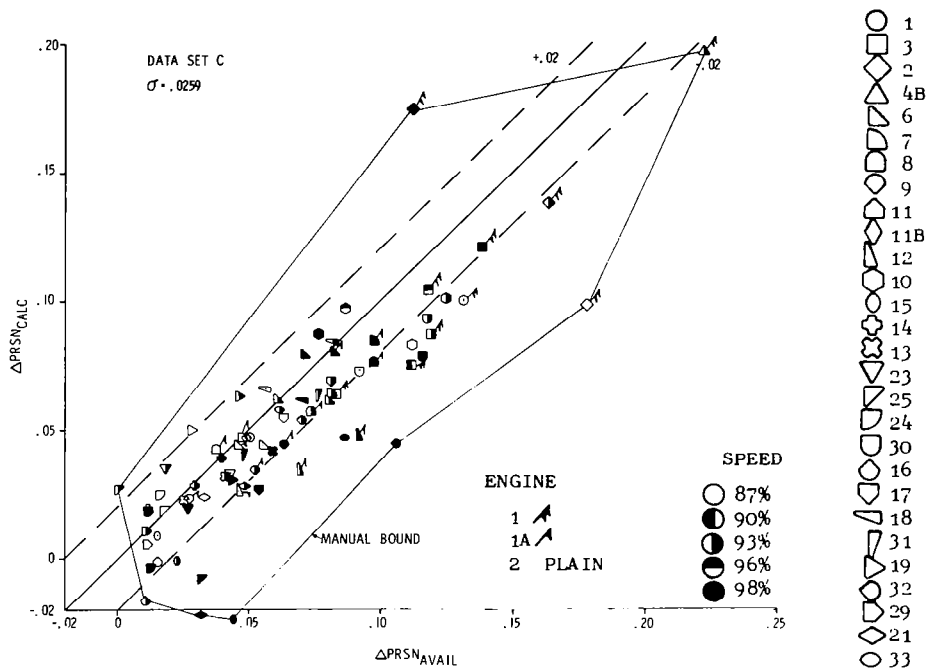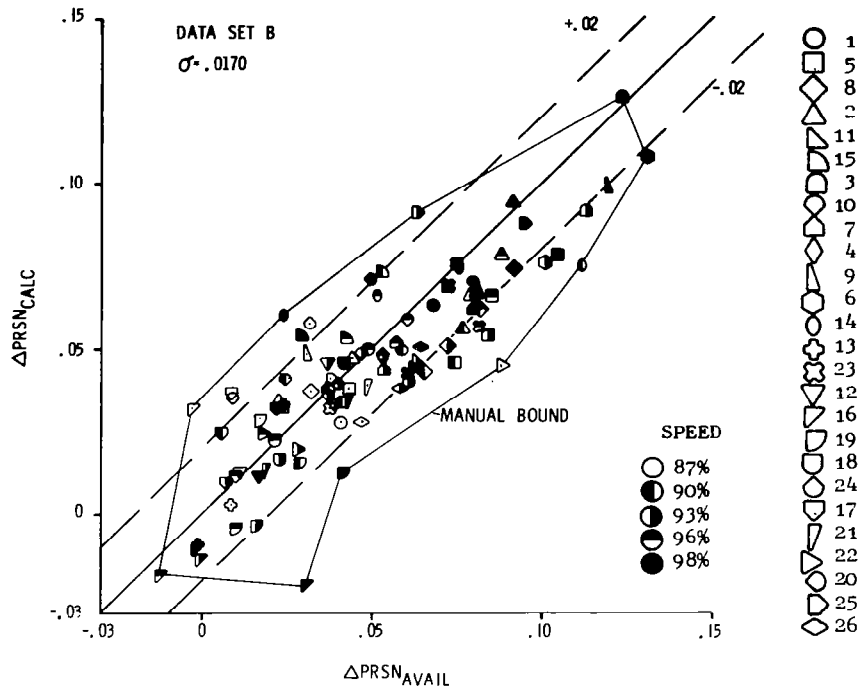
FIGURE 44 – CORRELATIONS OF DATA SETS B AND C WITH
MANUAL PATTERN RECOGNITION
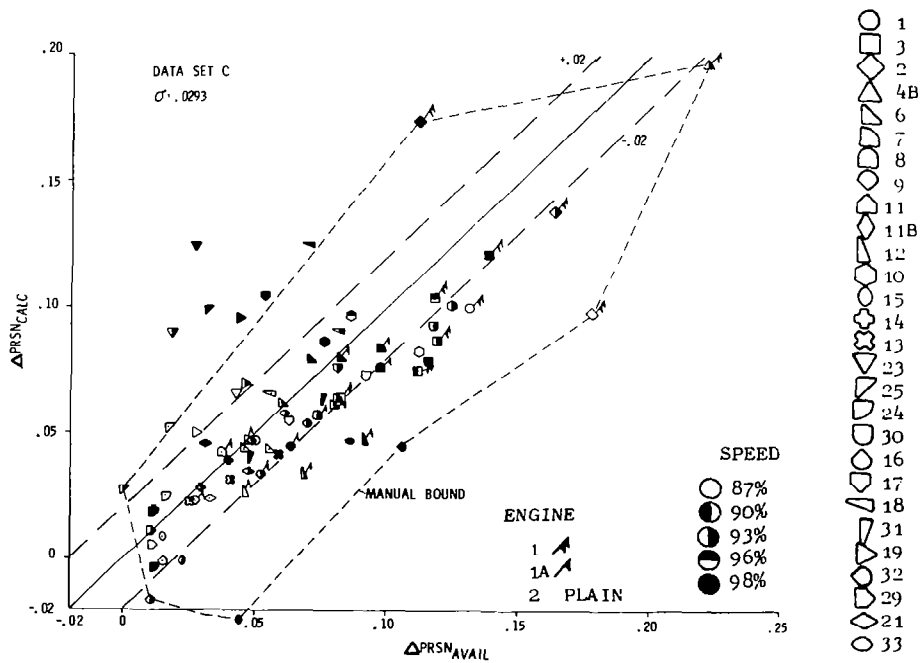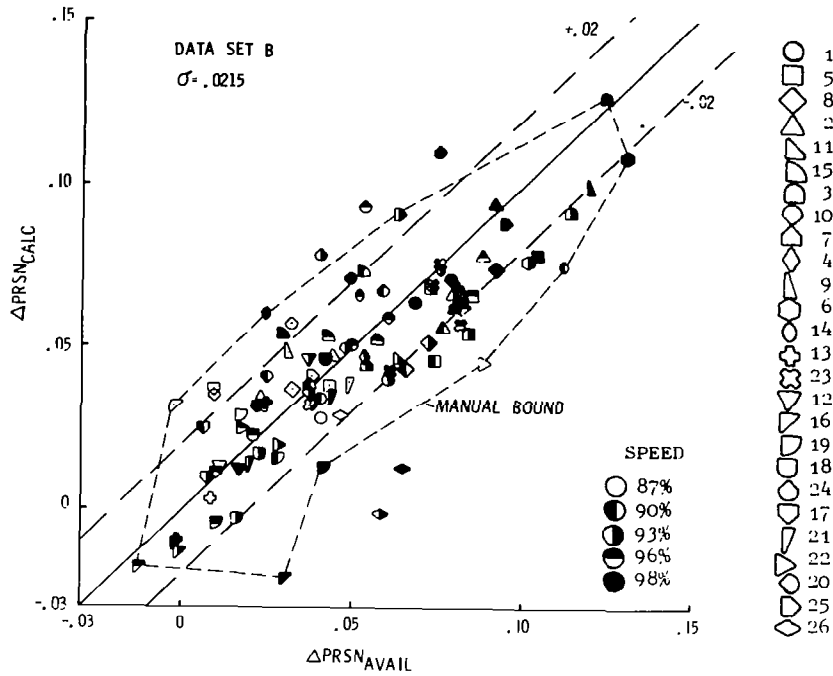
FIGURE 45 – CONSTANT CORRECTED SPEED CORRELATION OF DATA SETS B AND
C USING PATTERN RECOGNITION TECHNIQUE NO. 1
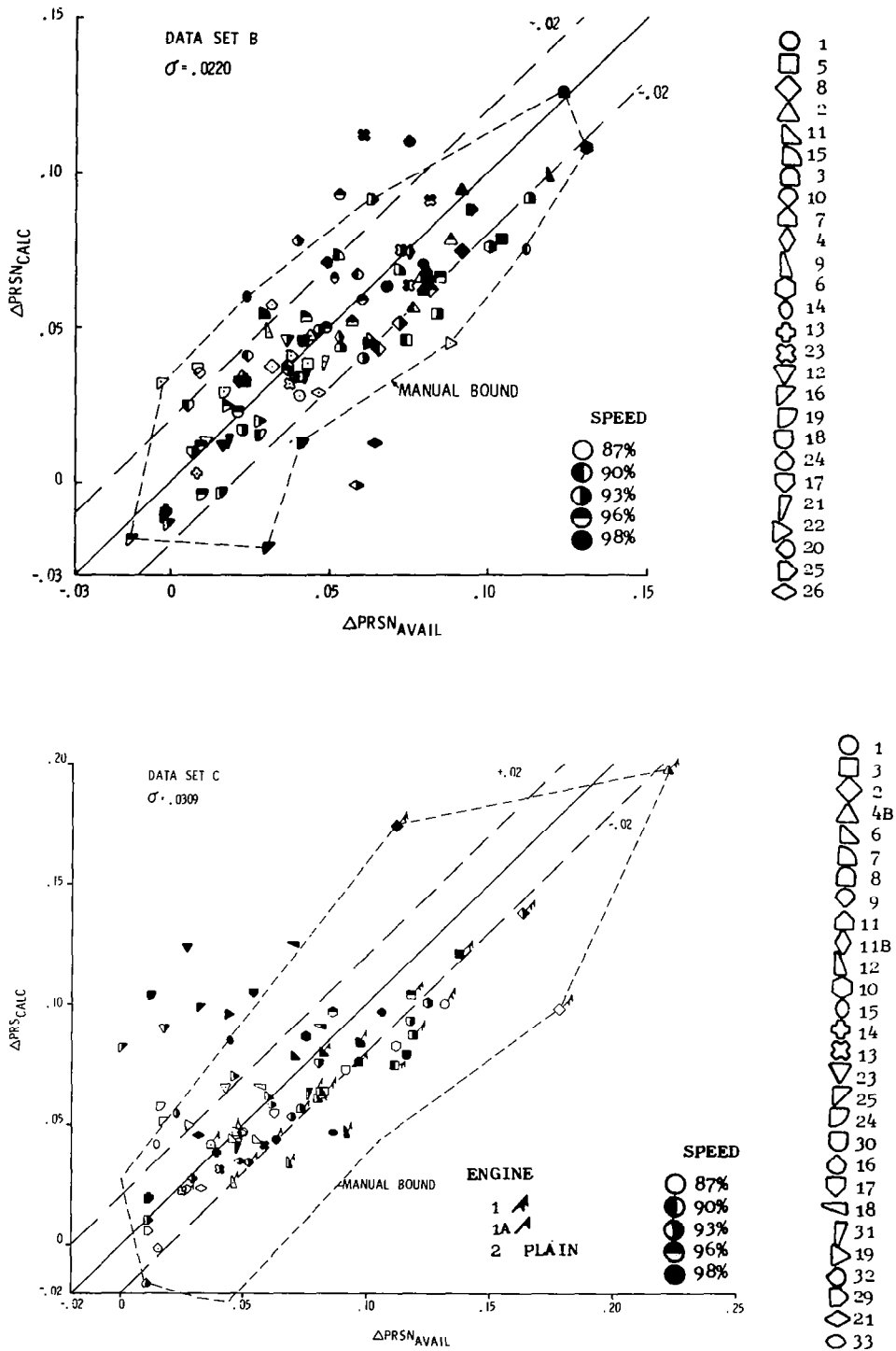
FIGURE 46 – CONSTANT CORRECTED SPEED CORRELATION OF DATA SETS B AND C USING PATTERN RECOGNITION TECHNIQUE NO. 2

CLEAN
DISTORTED
SURGE LINE

P.R.

ERROR IN
SURGE
AIRFLOW

$N/\sqrt{\theta}$ = CONSTANT

CORRECTED AIRFLOW
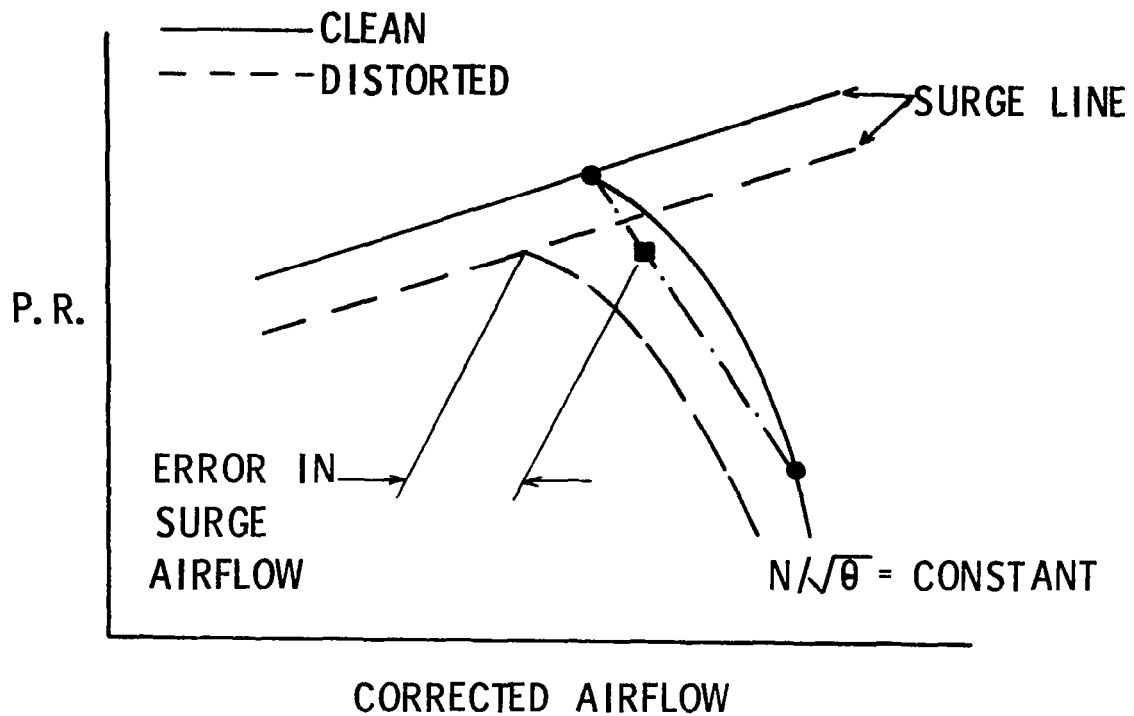
● PARALLEL - COMPRESSOR SECTORS
■ PREDICTED SURGE POINT

FIGURE 47 - PREDICTION OF SURGE AIRFLOW USING A
PARALLEL - COMPRESSOR MODEL

# CIRCUMFERENTIAL FLOW LOSS SENSITIVITY



DATA SET B

DATA SET C

%SPEED

87
90
93
96
98

$1 - (P_{MIN, 60°})_{2, r} / \overline{P_2}$

$1 - (P_{MIN, 60°})_{2, r} / \overline{P_2}$
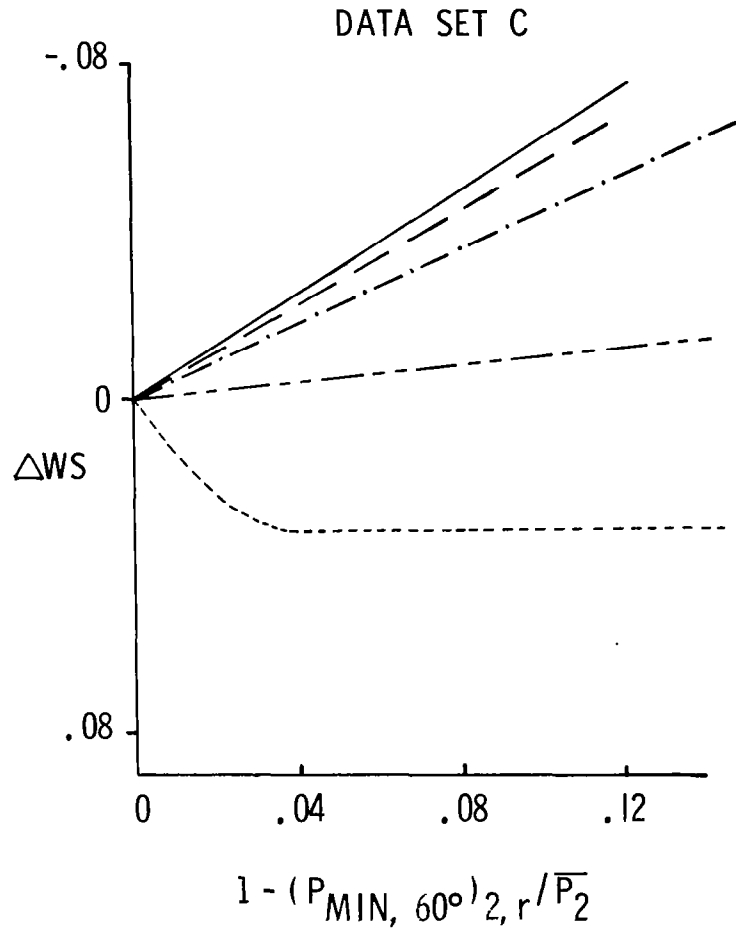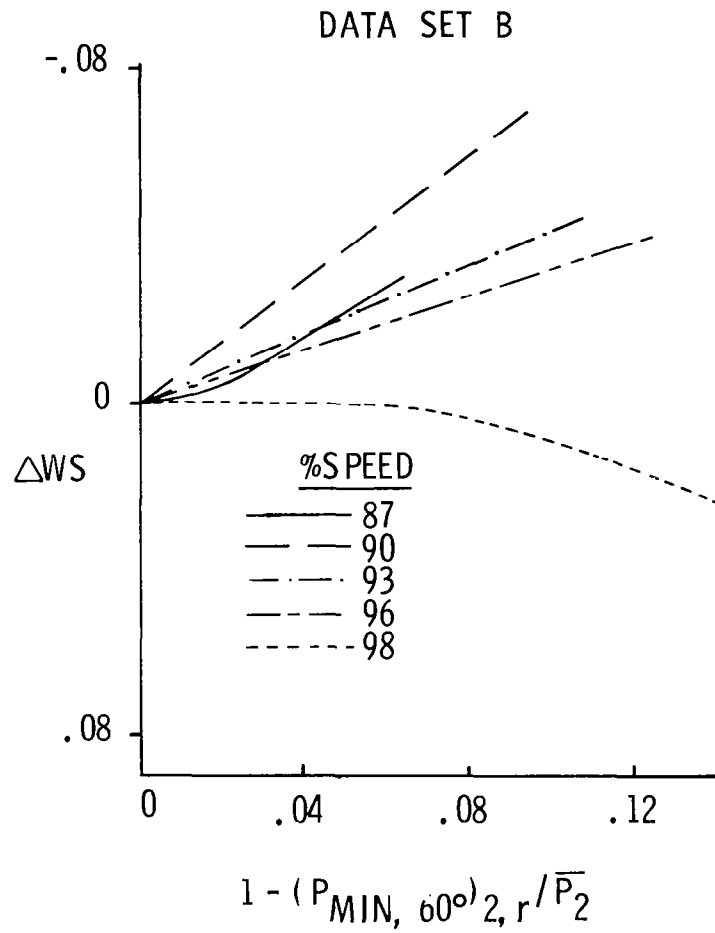
# TIP RADIAL FLOW LOSS SENSITIVITY
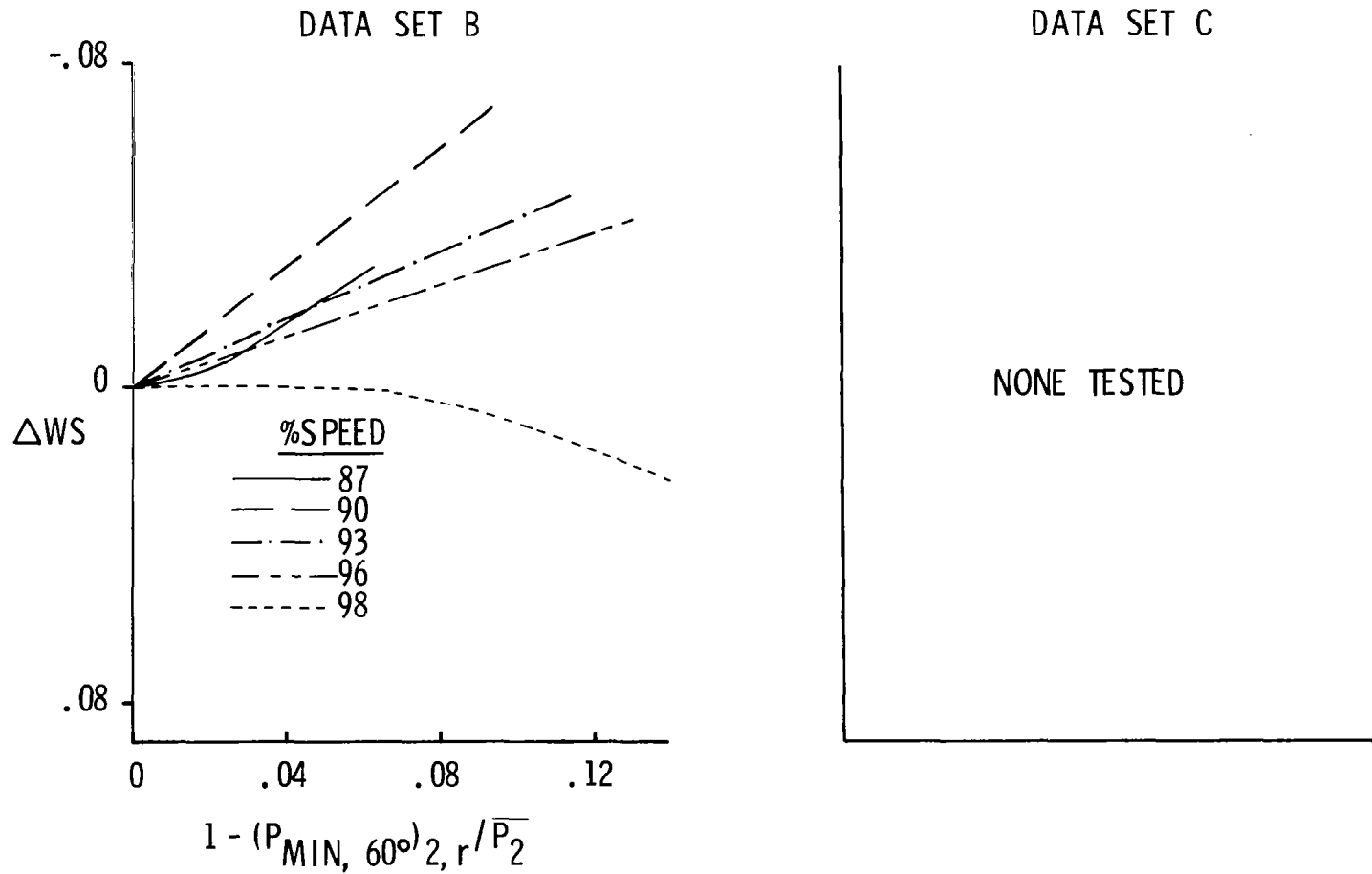


FIGURE 49 – CORRELATION OF $\triangle$WS WITH PRESSURE DEFECT FOR TIP-RADIAL PATTERNS

# HUB RADIAL FLOW LOSS SENSITIVITY
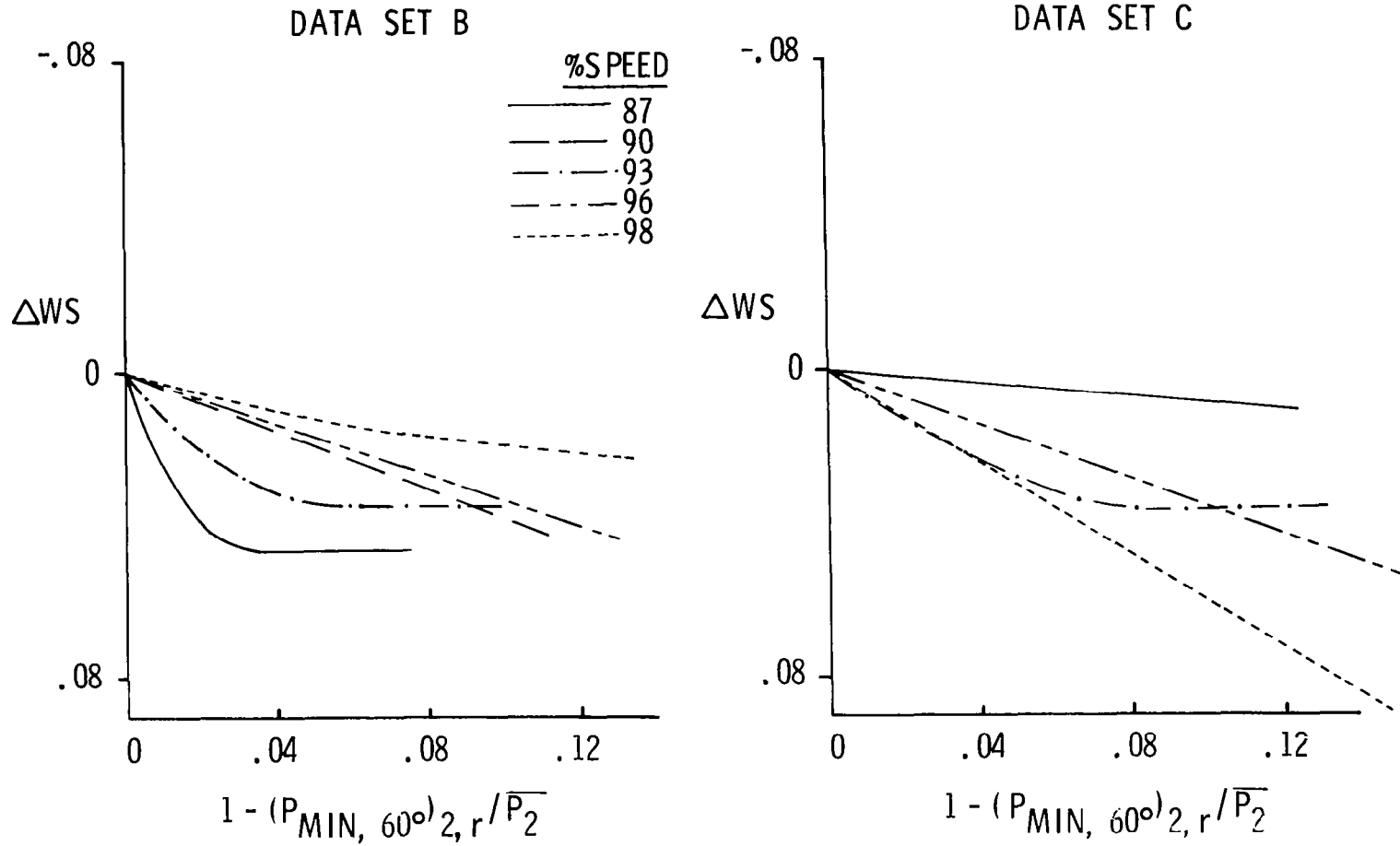


FIGURE 50 – CORRELATION OF $\triangle$WS WITH PRESSURE DEFECT FOR HUB-RADIAL PATTERNS
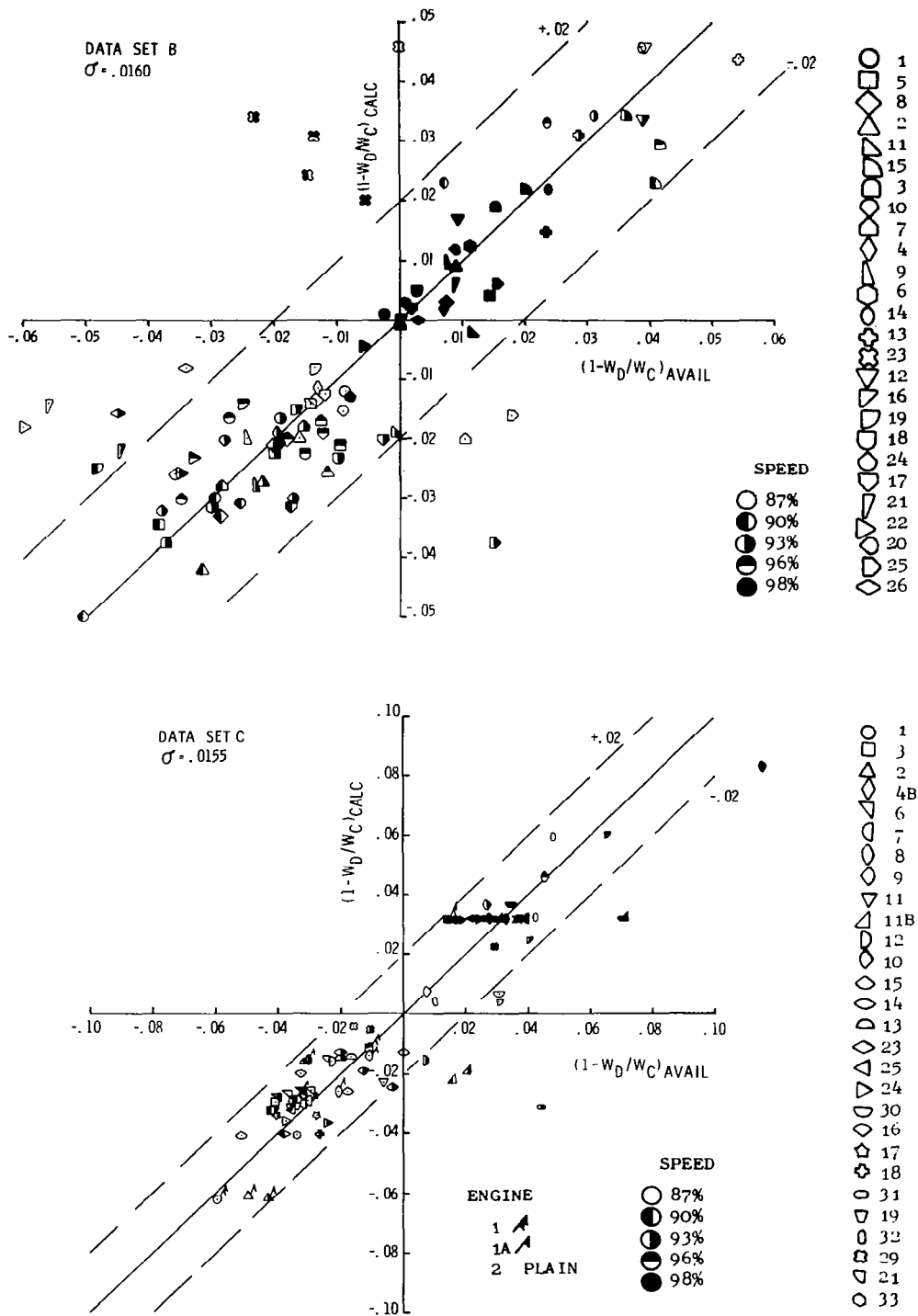
FIGURE 51 – LOSS OF SURGE AIRFLOW CORRELATION USING PATTERN
RECOGNITION TECHNIQUE NO. 1
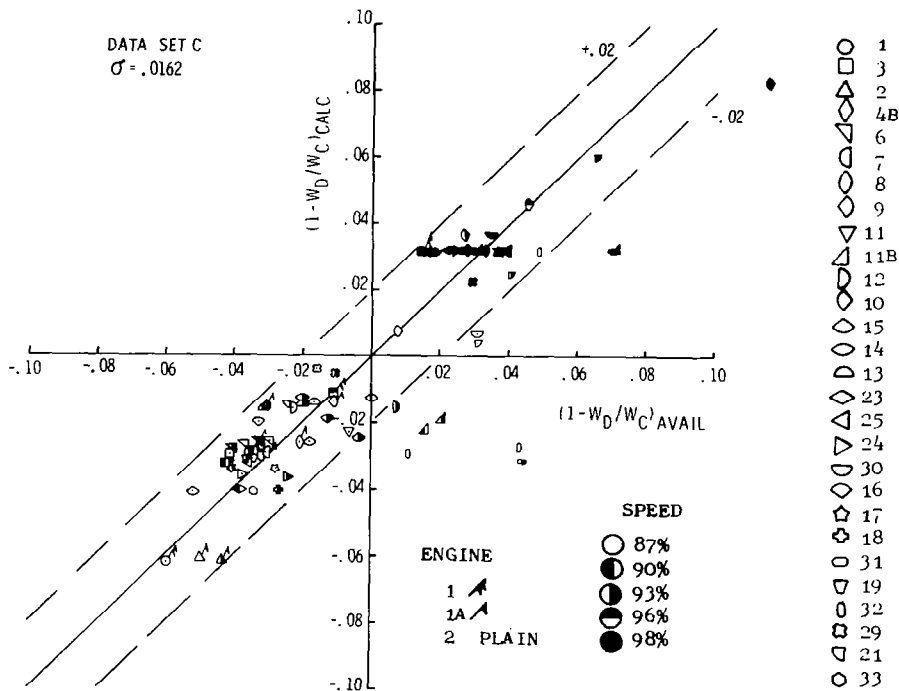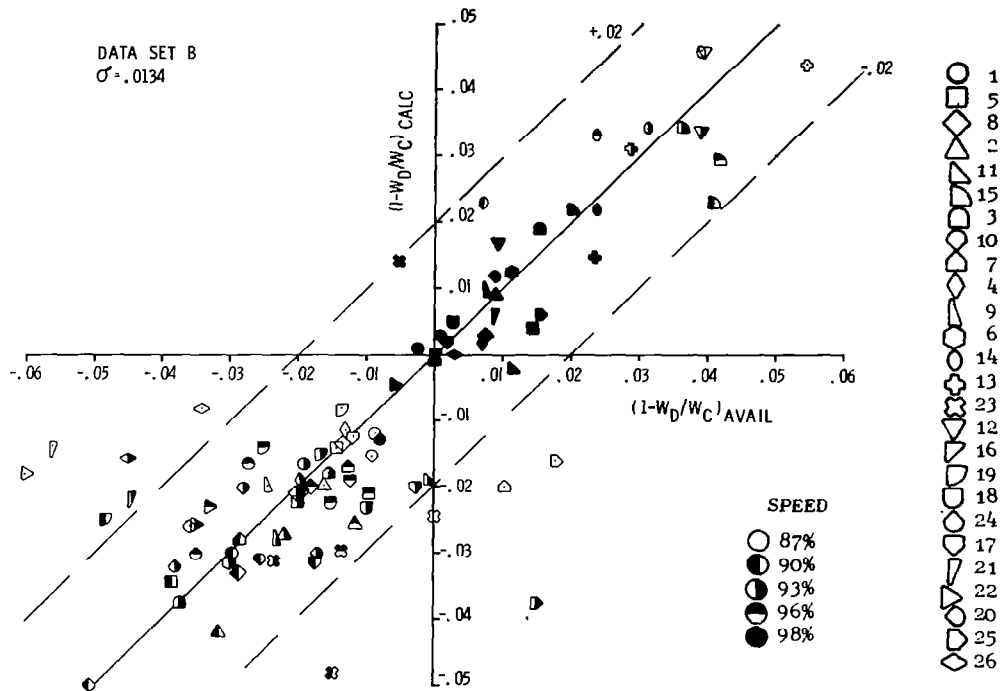
FIGURE 52 – LOSS OF SURGE AIRFLOW CORRELATION USING PATTERN RECOGNITION
TECHNIQUE NO. 2
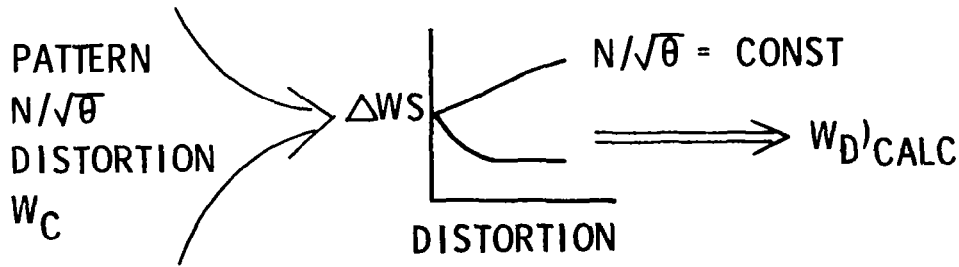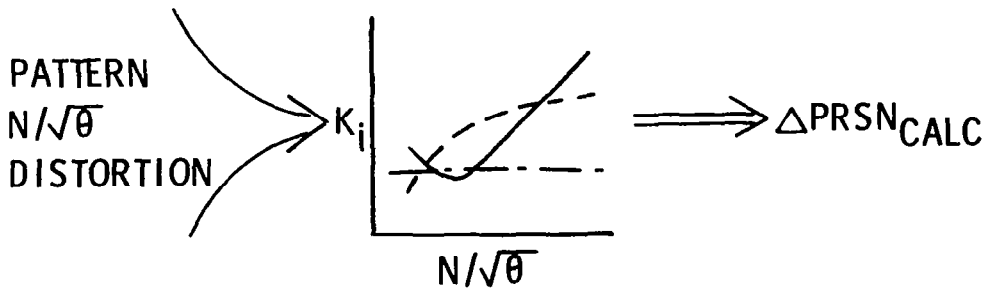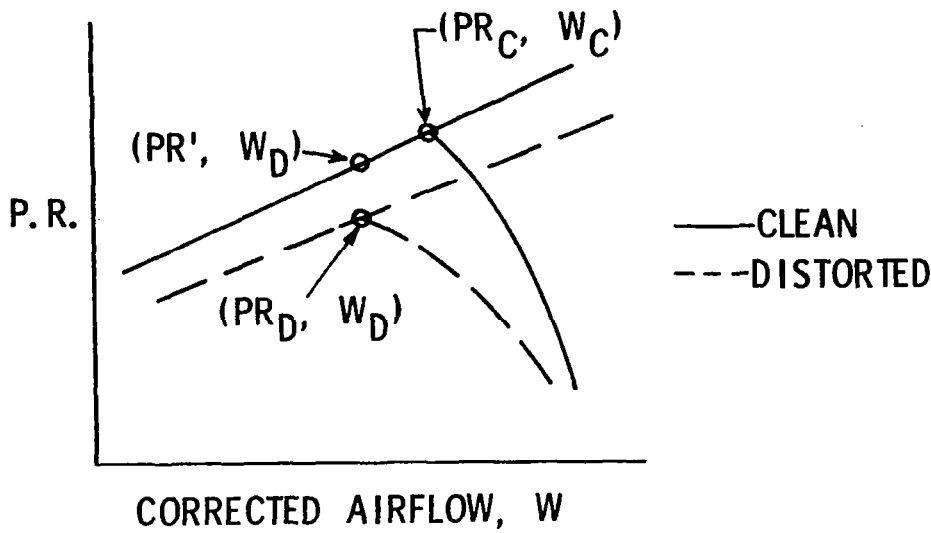
$PR_C = f(N/\sqrt{\theta})$ AND $N/\sqrt{\theta} \Longrightarrow PR_C$

$PR_C = g(W)$ AND $W_D)_{CALC} \Longrightarrow PR')_{CALC}$

$\Delta PRSW_{CALC} = 1 - (1 - \Delta PRSN_{CALC}) \, PR_C / PR')_{CALC}$

FIGURE 53 — SUMMATION OF $\Delta PRSN$ AND $\Delta WS$ INTO $\Delta PRSW$
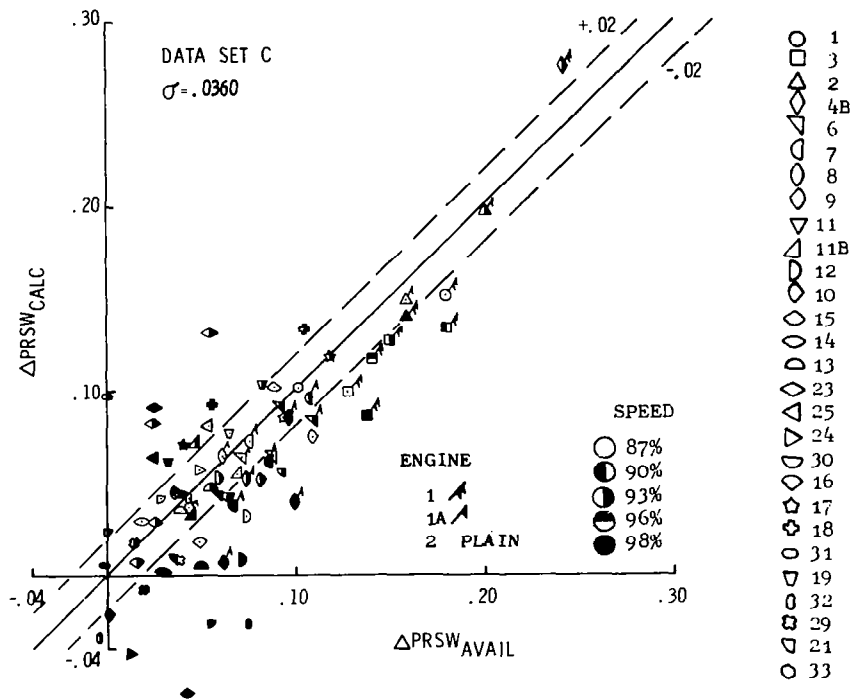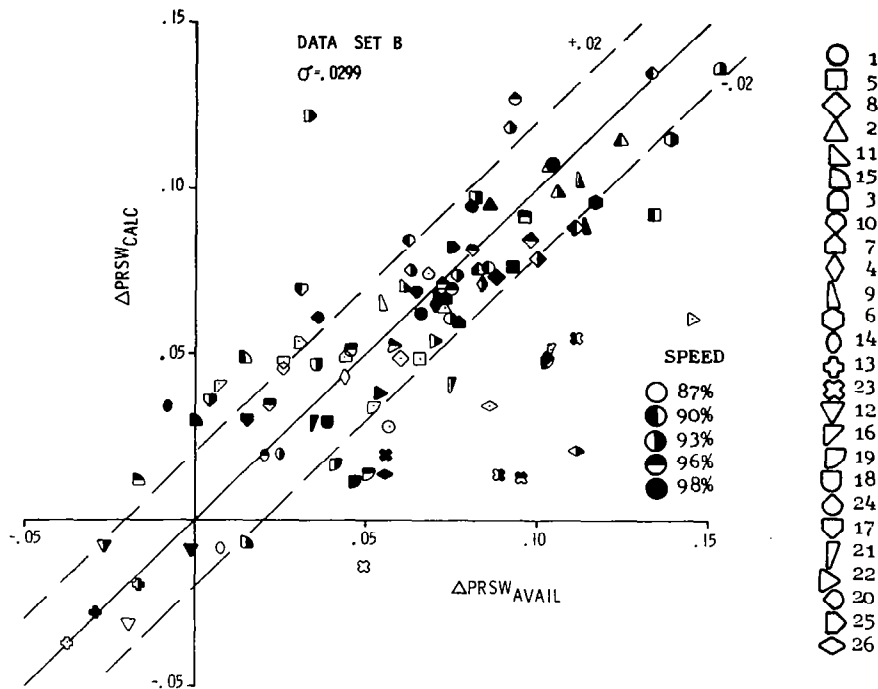
FIGURE 54 – CORRELATION OF $\Delta$PRSN AND $\Delta$WS INTO $\Delta$PRSW, PATTERN RECOGNITION TECHNIQUE NO. 1
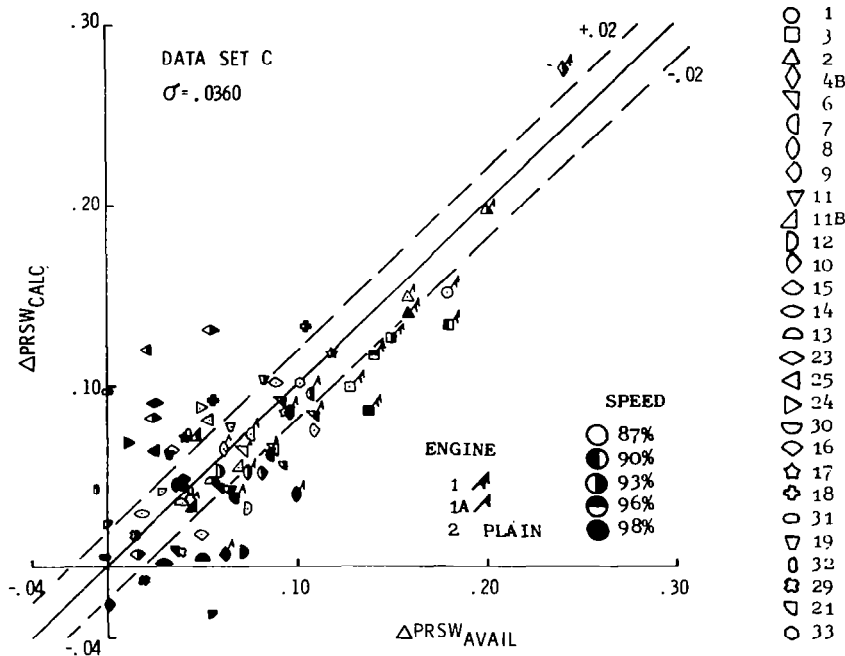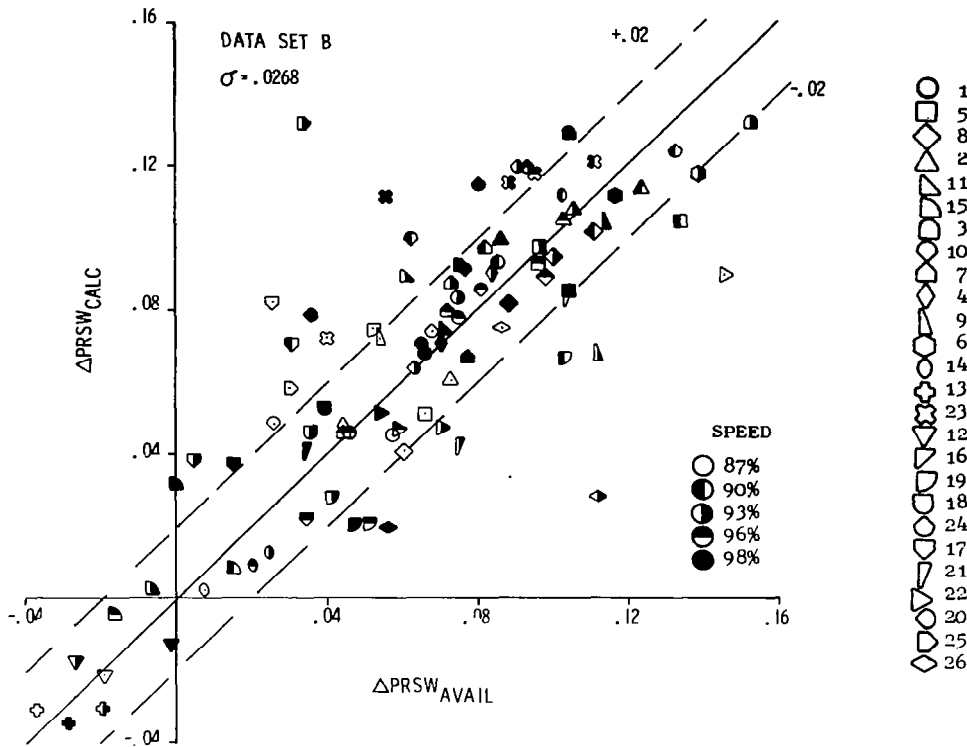
FIGURE 55 – CORRELATION OF $\triangle$PRSN AND $\triangle$WS INTO $\triangle$PRSW, PATTERN RECOGNITION TECHNIQUE NO. 2
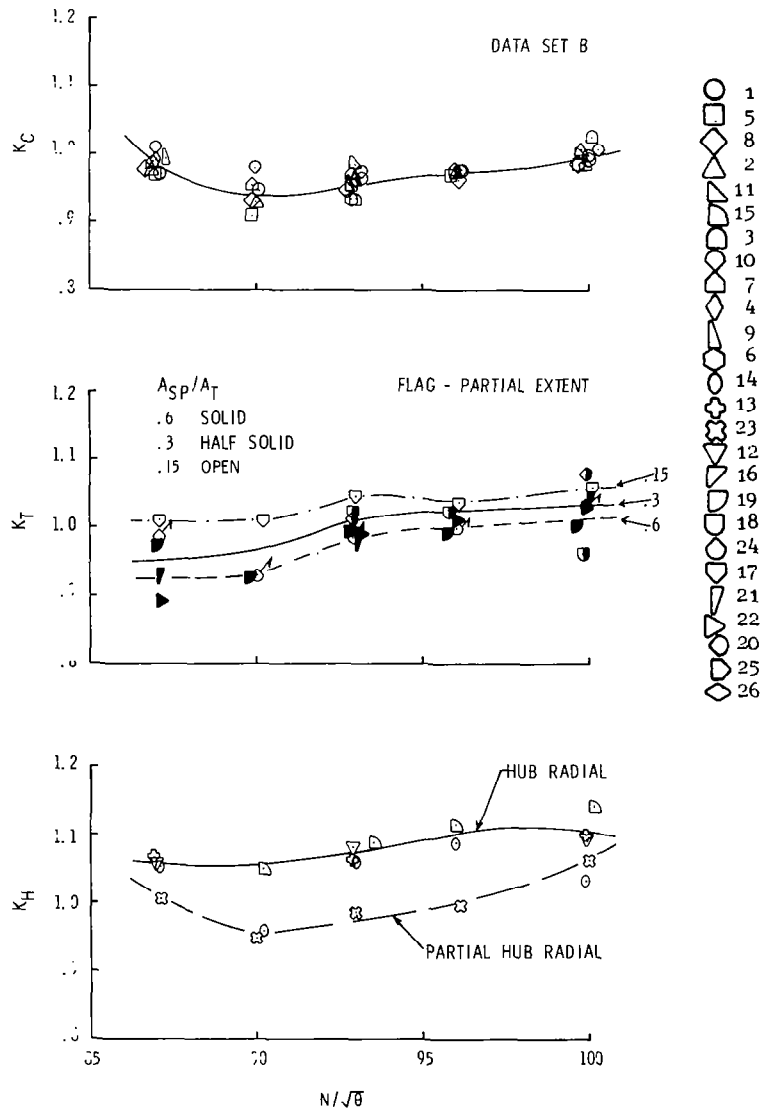
FIGURE 56 – METHOD E DENSITIVITIES FOR LOSS OF
SURGE PRESSURE RATIO AT CONSTANT
AIRFLOW CORRELATION, DATA SET B
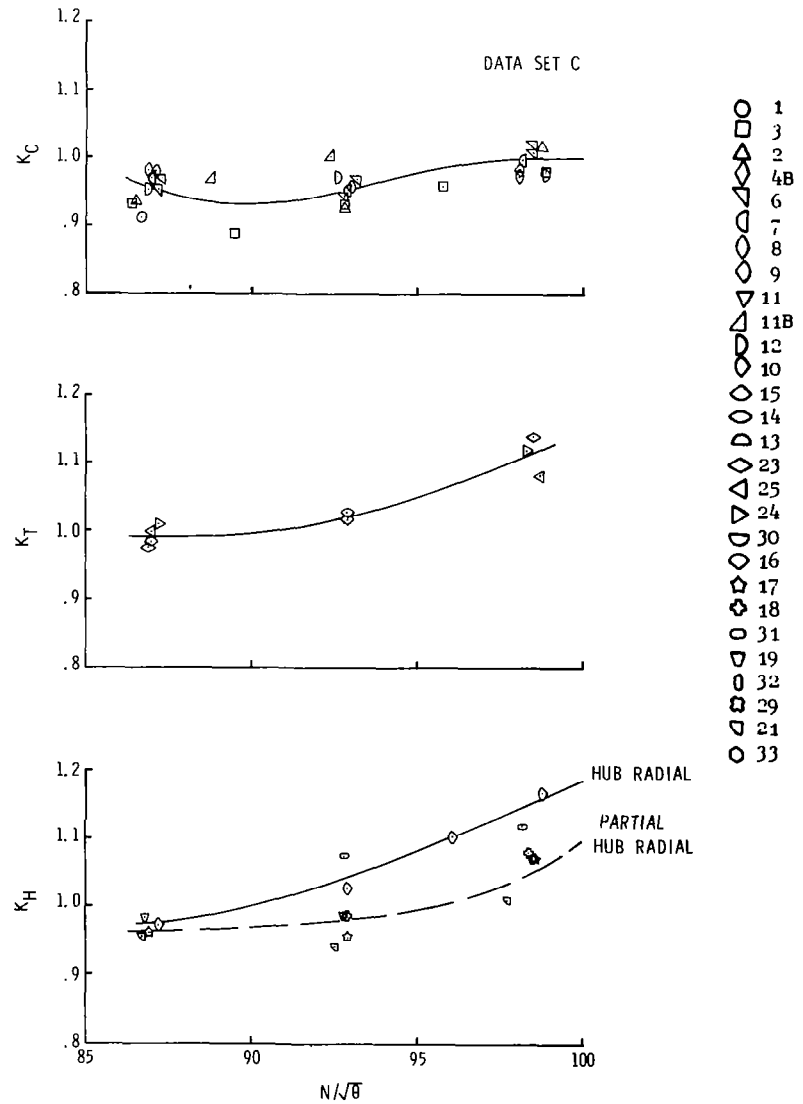
FIGURE 57 – METHOD E SENSITIVITIES FOR LOSS OF
SURGE PRESSURE RATIO AT CONSTANT
AIRFLOW CORRELATION, DATA SET C
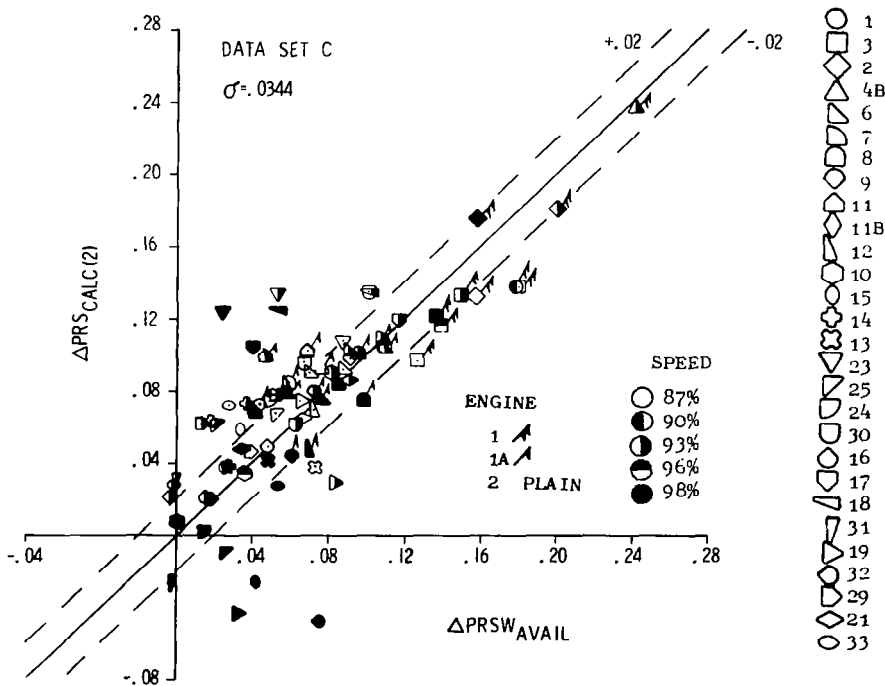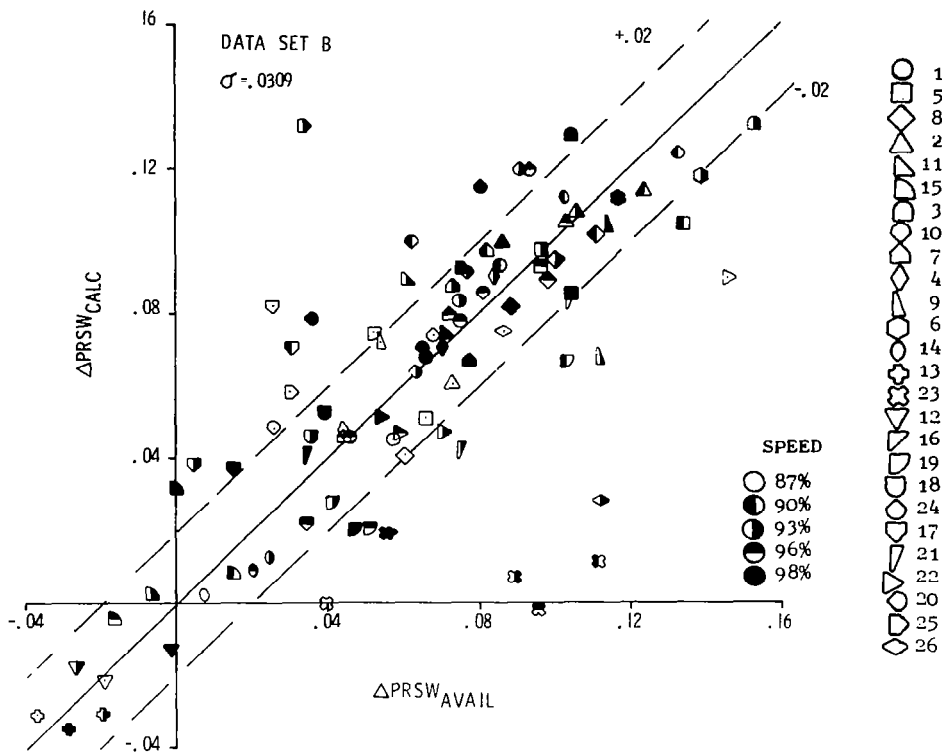
FIGURE 58 – CORRELATION OF △PRSW, PATTERN RECOGNITION TECHNIQUE NO. 1

85
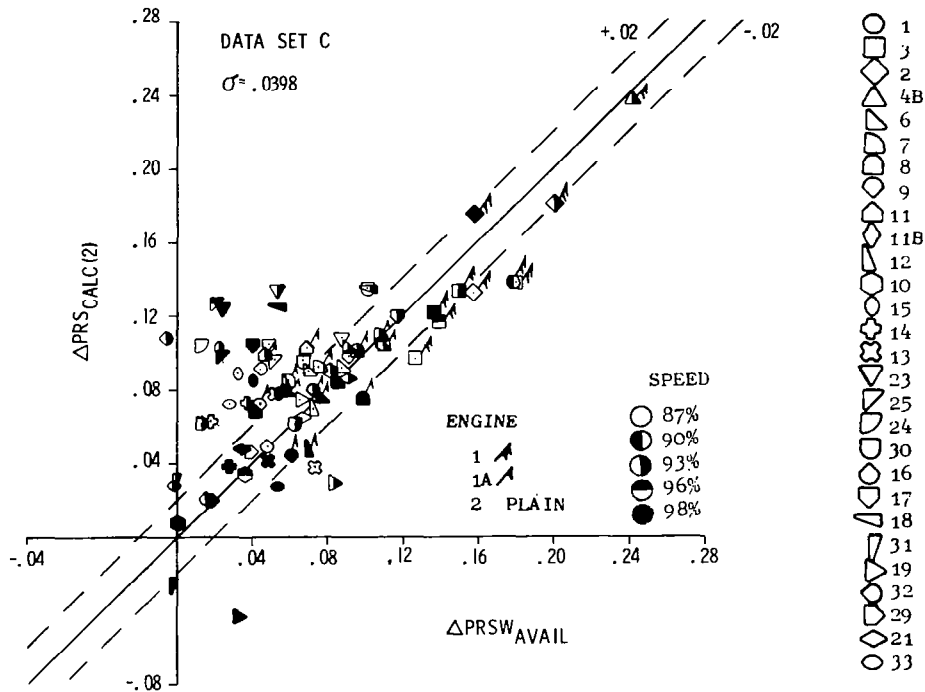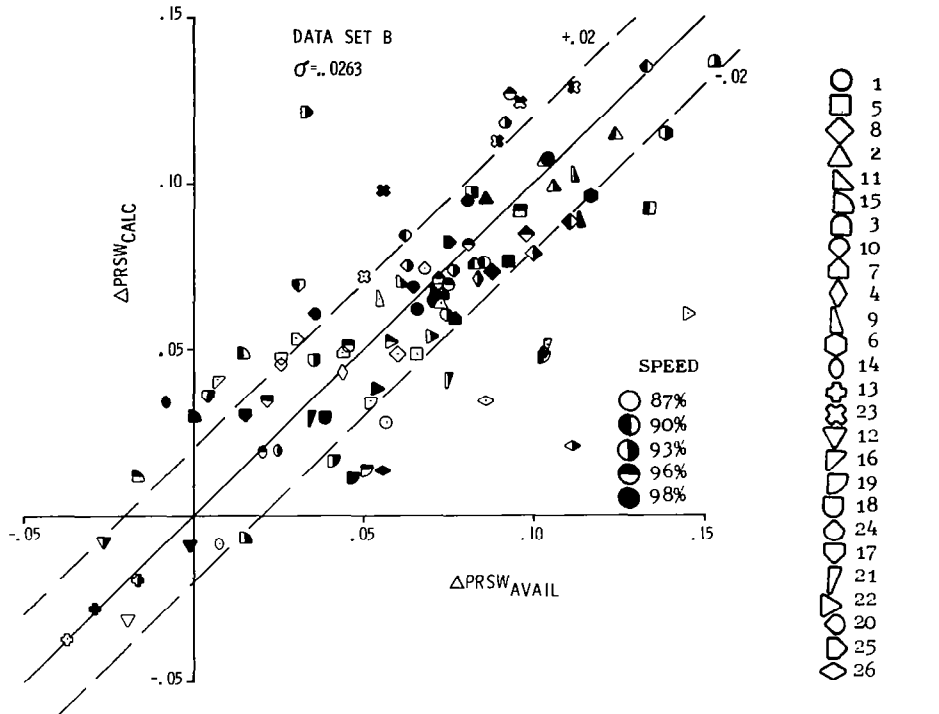
FIGURE 59 — CORRELATION OF △PRSW, PATTERN RECOGNITION TECHNIQUE NO. 2
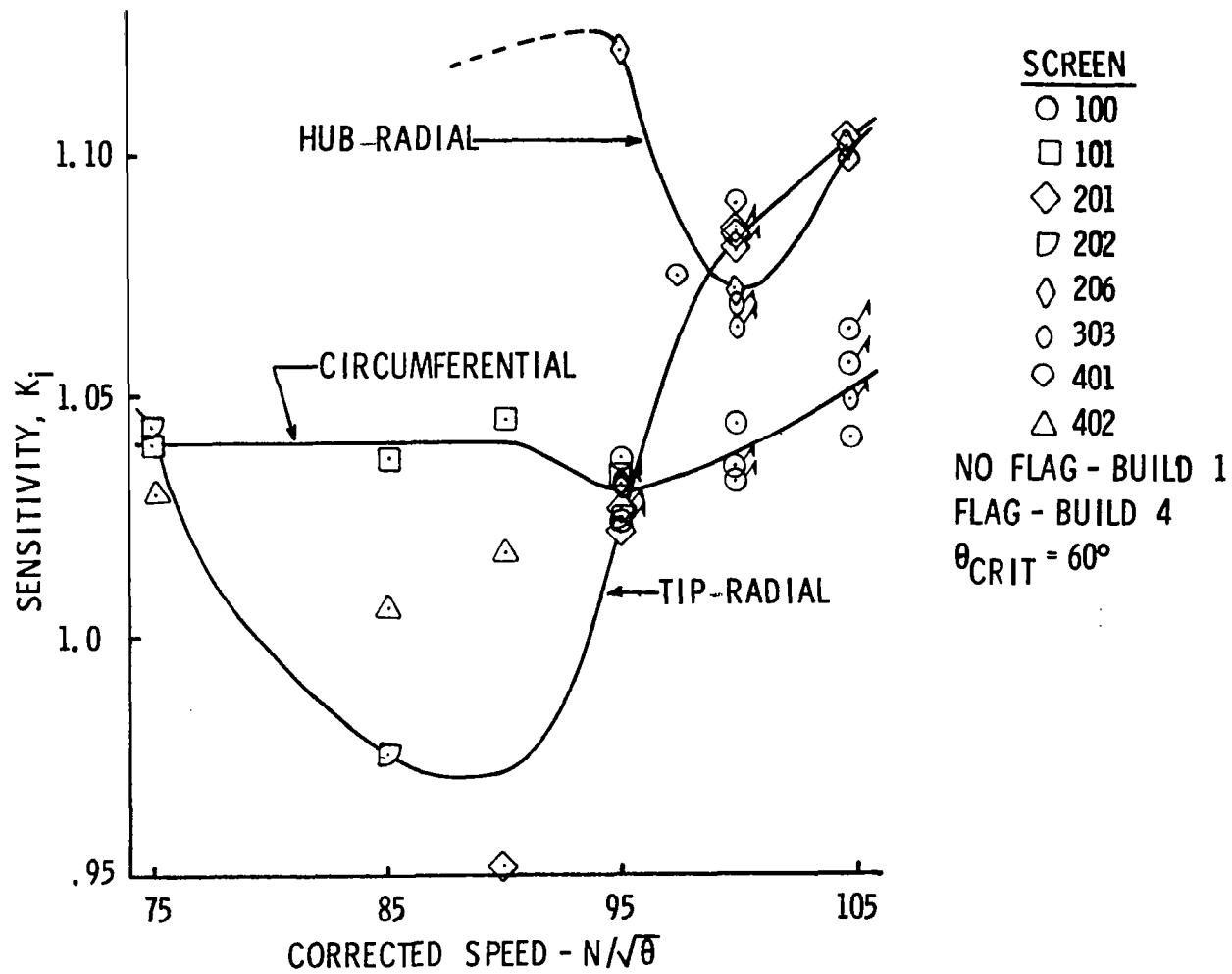
FIGURE 60 – DIDENT SENSITIVITIES AT CONSTANT CORRECTED AIRFLOW FOR
LOW PRESSURE COMPRESSOR RIG TEST – DATA SET E
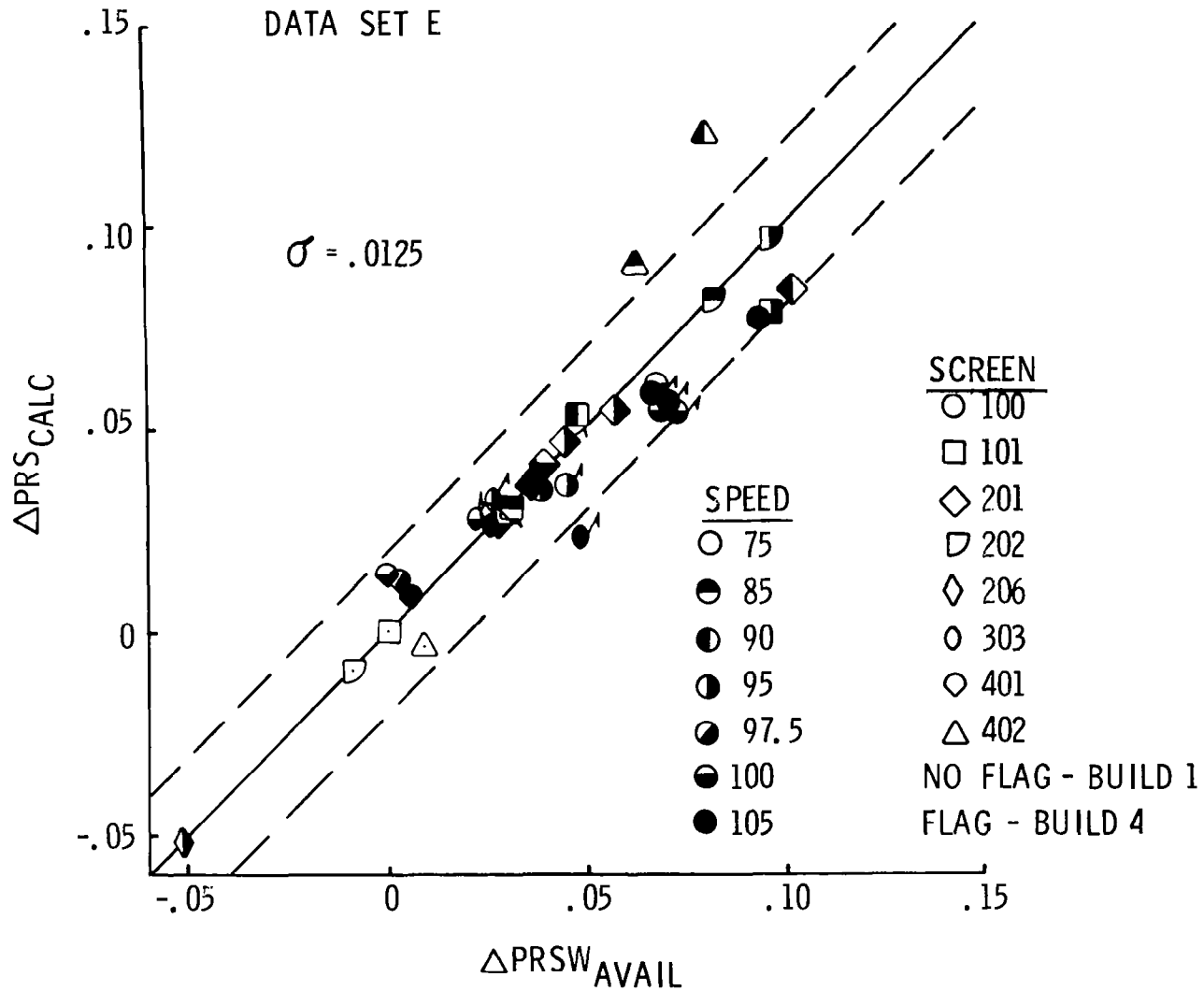
FIGURE 61 – DIDENT CORRELATION OF SURGE PRESSURE RATIO LOSS AT CONSTANT CORRECTED
AIRFLOW FOR LOW PRESSURE COMPRESSOR RIG TEST DATA SET E

METHOD E

FUNCTIONAL BLOCK DIAGRAM
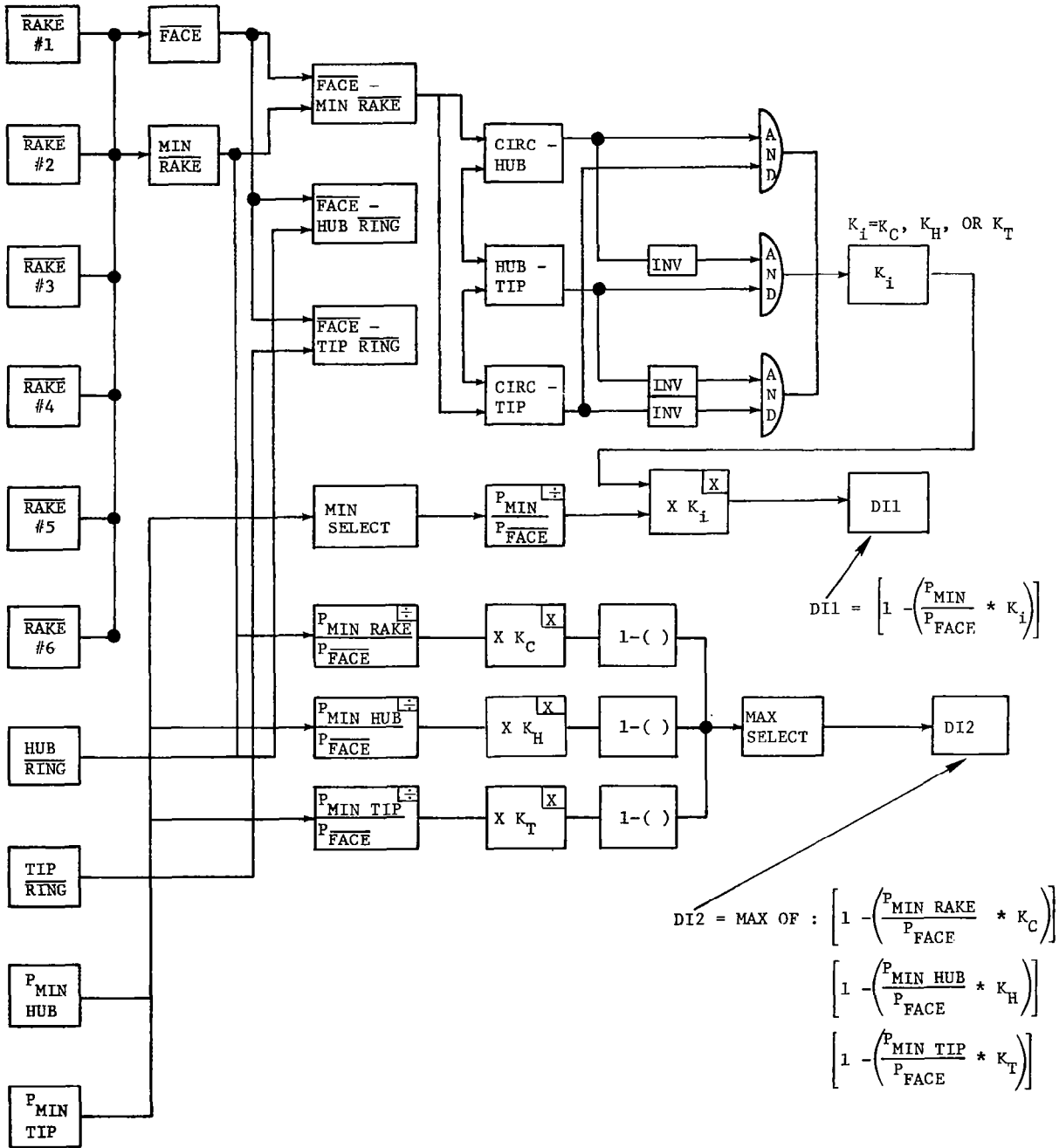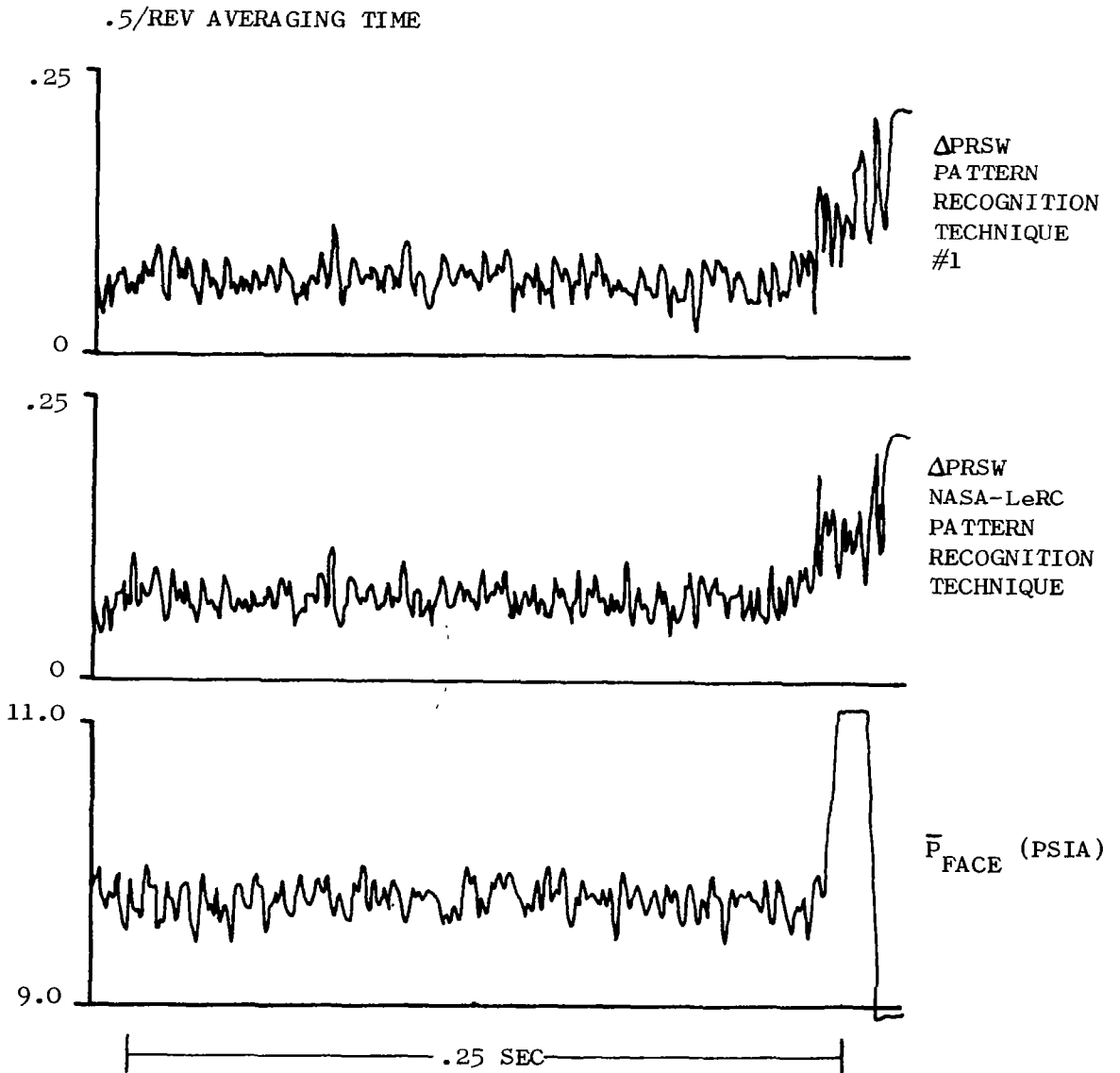


FIGURE 62 – BLOCK DIAGRAM OF METHOD E ANALYSIS IN SMAL

.5/REV AVERAGING TIME
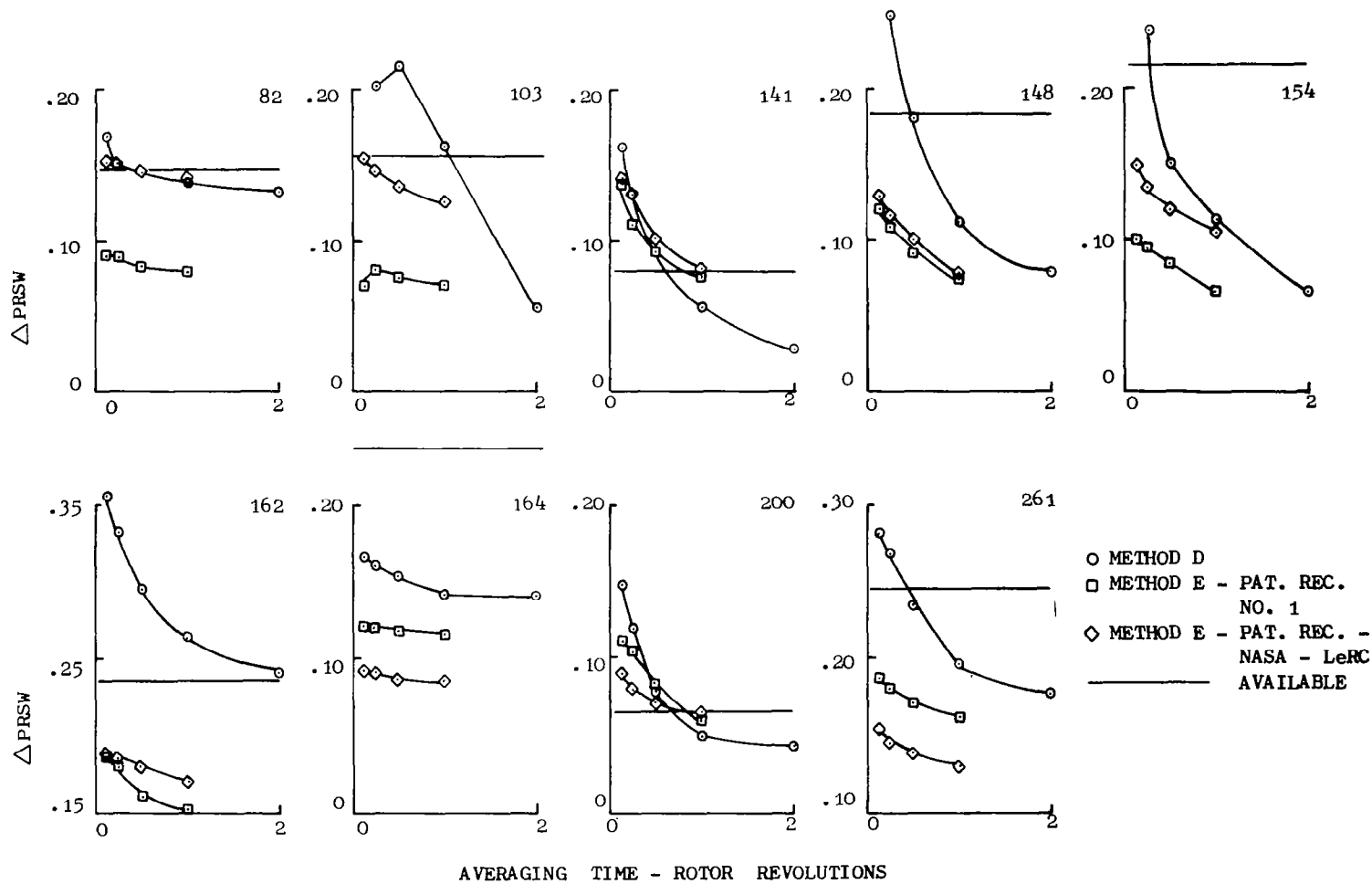


FIGURE 63 - METHOD E ANALYSIS WAVEFORMS, POINT 148, DATA SET A

FIGURE 64 — CALCULATED PEAK ΔPRSW AS A FUNCTION OF AVERAGING TIME

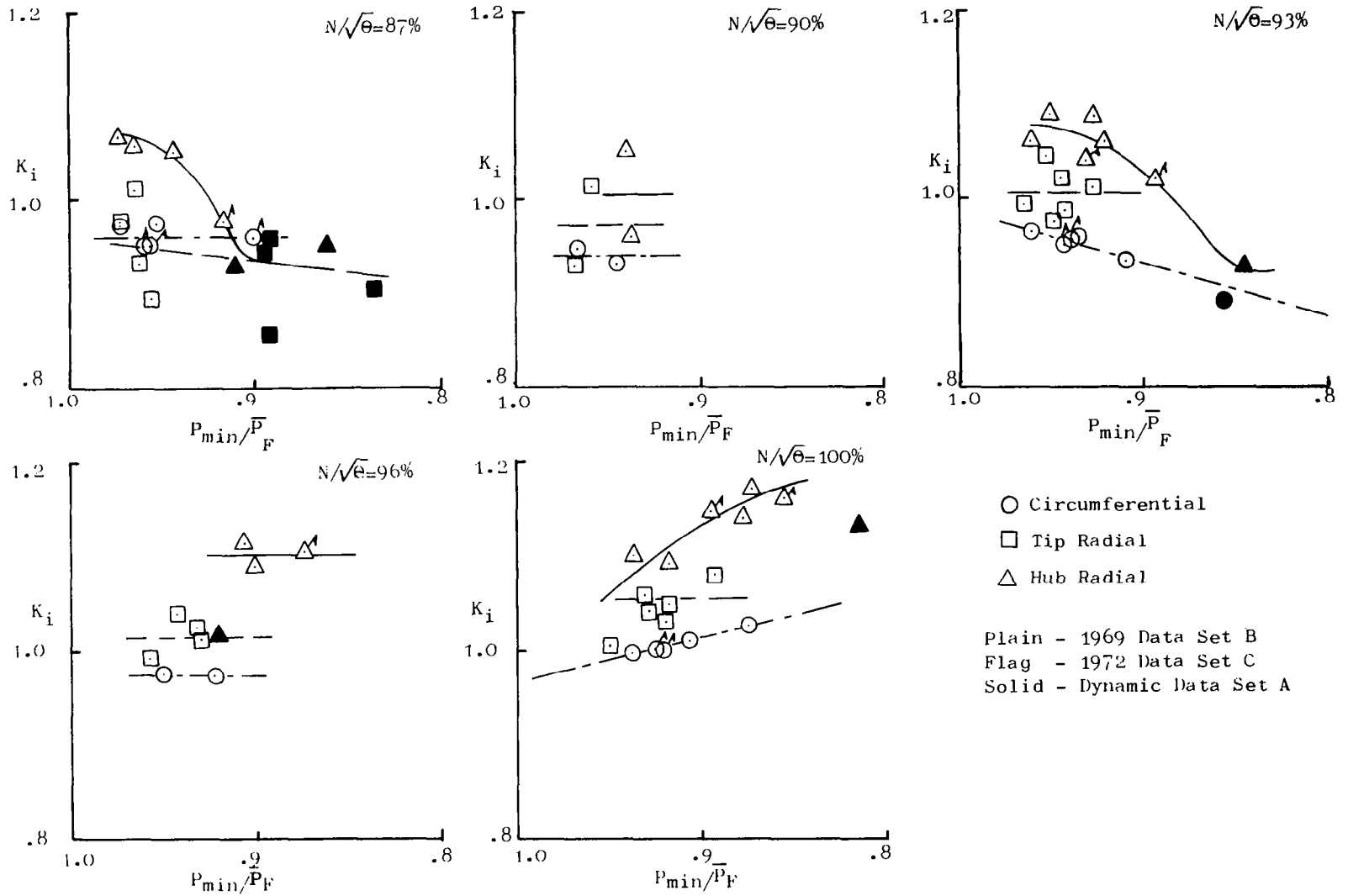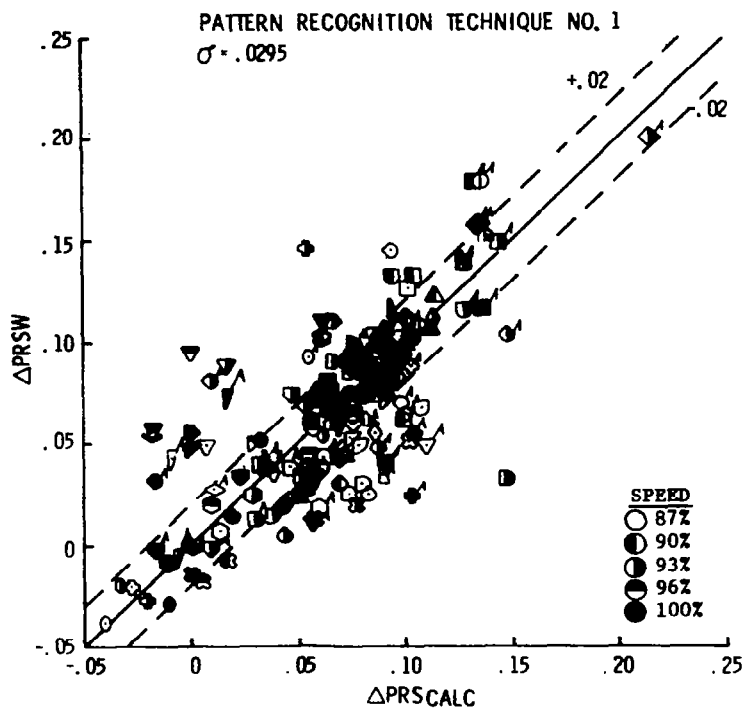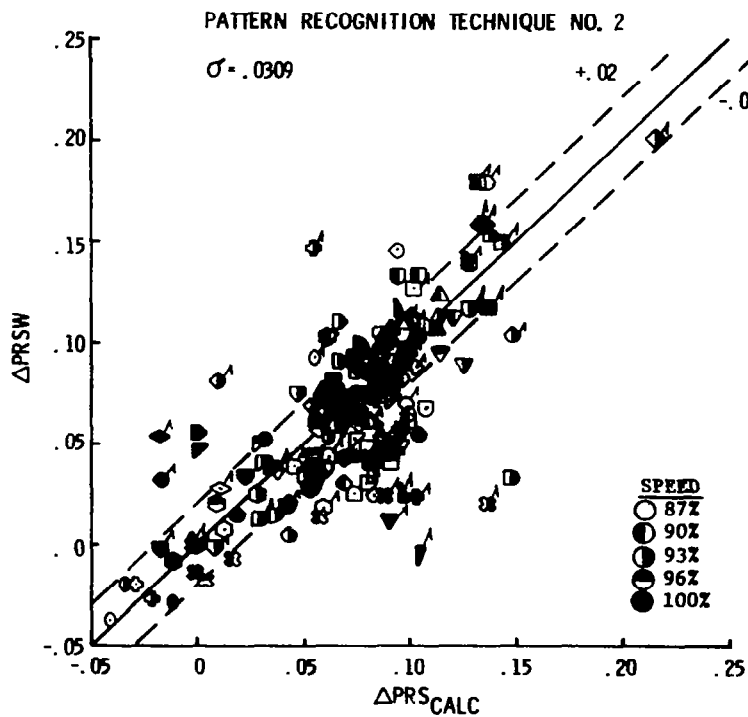FIGURE 65 — METHOD E SENSITIVITIES AS A FUNCTION OF PRESSURE DEFECT

PATTERN RECOGNITION TECHNIQUE NO. 1

$\sigma = .0295$

+.02

.02

SCREEN

| DATA SET A | | DATA SET B |
|---|---|---|
| 1 | | 1 |
| 5 | | 3 |
| 8 | | 2 |
| 2 | | 6 |
| 11 | | 7 |
| 3 | | 8 |
| 10 | | 9 |
| 7 | | 11 |
| 4 | | 12 |
| 9 | | 10 |
| 6 | | 15 |
| 14 | | 14 |
| 13 | | 13 |
| 12 | | 23 |
| 15 | | 25 |
| 23 | | 24 |
| 19 | | 30 |
| 18 | | 16 |
| 24 | | 17 |
| 17 | | 18 |
| 21 | | 31 |
| 22 | | 19 |
| 20 | | 32 |
| 25 | | 29 |
| 26 | | 21 |
| | | 33 |
| | | 5B |

SPEED
- 87%
- 90%
- 93%
- 96%
- 100%

$\Delta$PRSW

$\Delta$PRS$_{CALC}$

PATTERN RECOGNITION TECHNIQUE NO. 2

$\sigma = .0309$

+.02

-.02

SPEED
- 87%
- 90%
- 93%
- 96%
- 100%

$\Delta$PRSW

$\Delta$PRS$_{CALC}$

SCREEN

| DATA SET A | | DATA SET B |
|---|---|---|
| 1 | | 1 |
| 5 | | 3 |
| 8 | | 2 |
| 2 | | 6 |
| 11 | | 7 |
| 3 | | 8 |
| 10 | | 9 |
| 7 | | 11 |
| 4 | | 12 |
| 9 | | 10 |
| 6 | | 15 |
| 14 | | 14 |
| 13 | | 13 |
| 12 | | 23 |
| 15 | | 25 |
| 23 | | 24 |
| 19 | | 30 |
| 18 | | 16 |
| 24 | | 17 |
| 17 | | 18 |
| 21 | | 31 |
| 22 | | 19 |
| 20 | | 32 |
| 25 | | 29 |
| 26 | | 21 |
| | | 33 |
| | | 5B |

FIGURE 66 – CORRELATION OF DATA SETS B AND C AS ONE DATA SET

L/D = 1.486→          ←L/D = .352

DISTORTION RAKES

SCREEN



345°          30°          33.9 CM
                          32.2 CM
                          28.4 CM
                          24.0 CM
300°                      18.6 CM
                          10.7 CM

255°                      75°

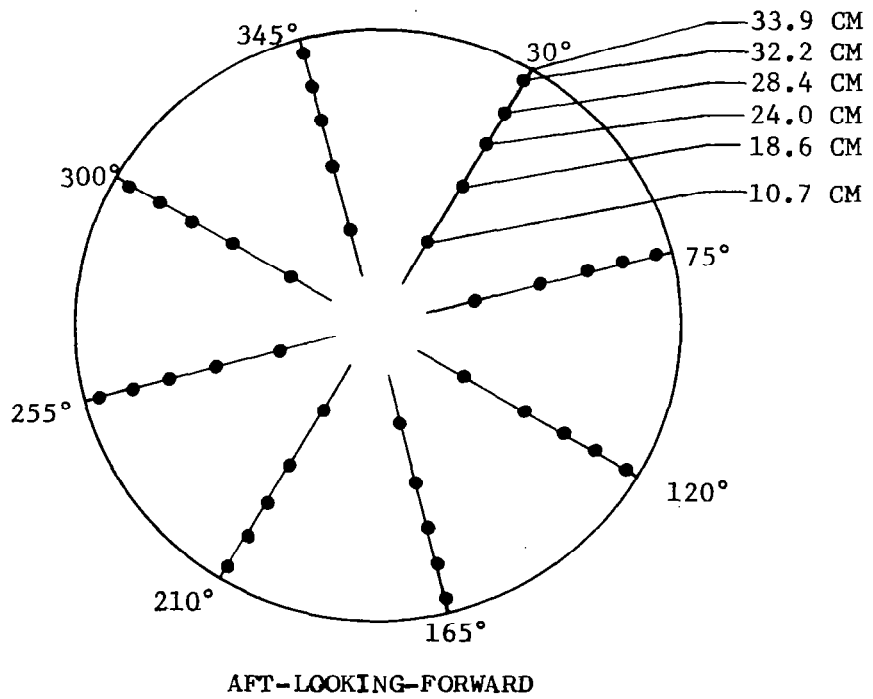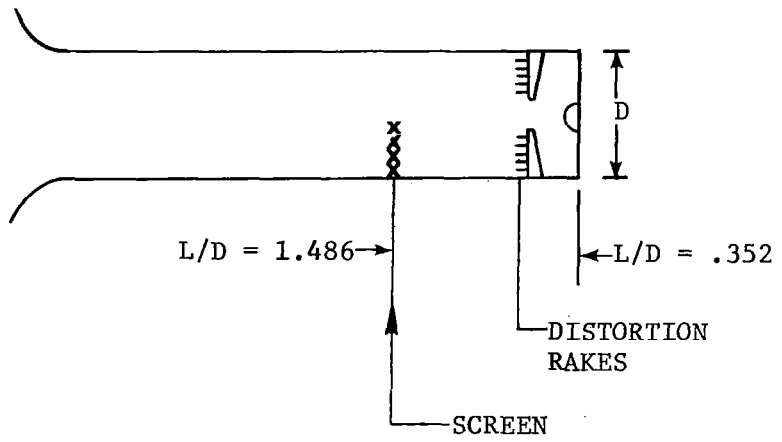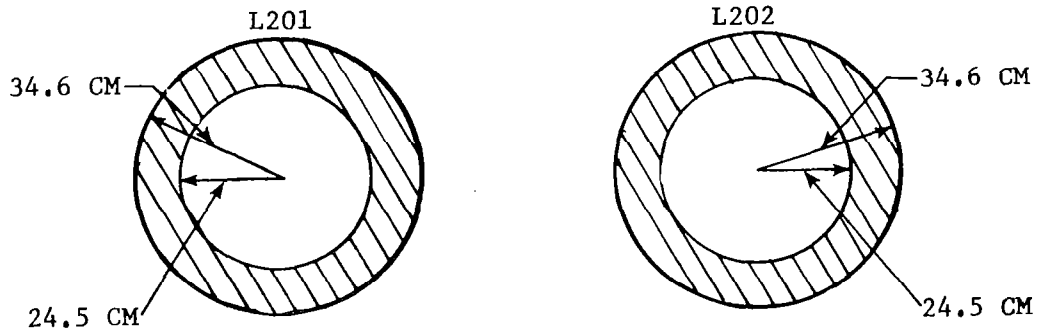                          120°
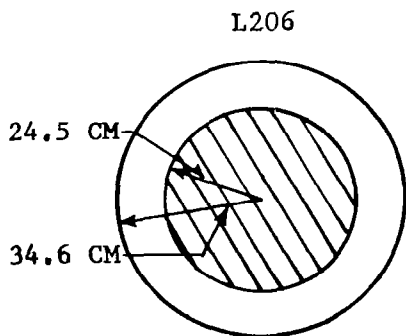
210°
          165°

AFT–LOOKING–FORWARD

FIGURE 67 – INSTRUMENTATION FOR DATA SET E

94

ONE PER REV

L100

L101

34.6 CM

34.6 CM

TIP-RADIAL

L201

L202

34.6 CM

34.6 CM

24.5 CM

24.5 CM

HUB-RADIAL

COMBINED

L206

L303

24.5 CM

$P_1$

23.0 CM

$P_2$

34.6 CM

5.2 CM

34.6 CM
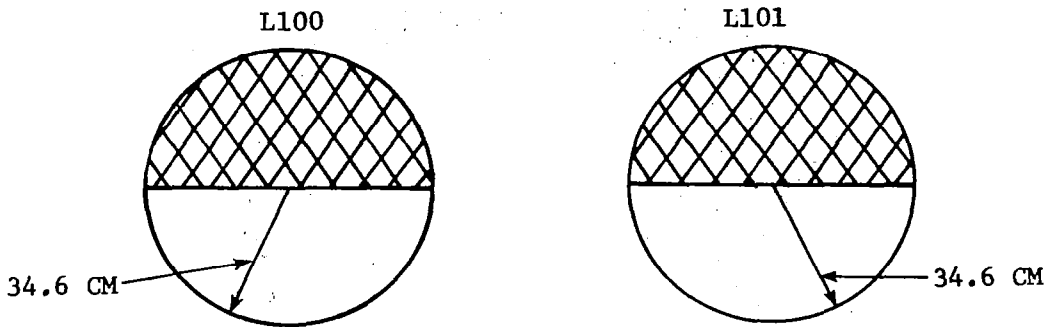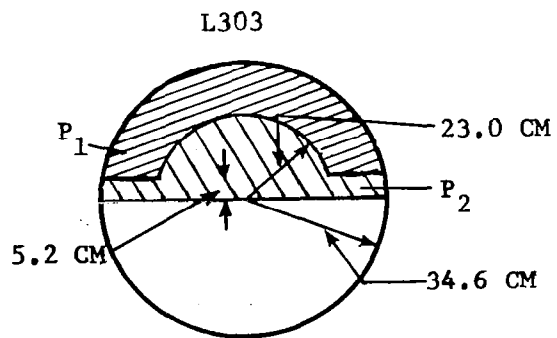
FIGURE 68 — DISTORTION SCREENS FOR DATA SET E

SCREEN L401



64.4%

51.0%

23.8%

ORIENT THIS SECTION OF
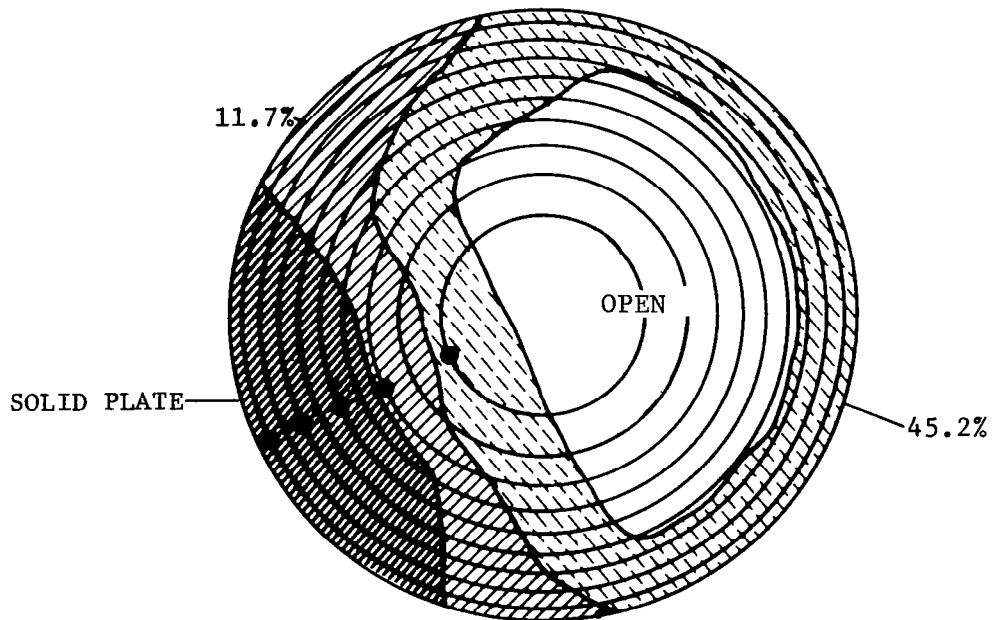SCREEN BEHIND PROBE

SCREEN L402



11.7%

OPEN

SOLID PLATE
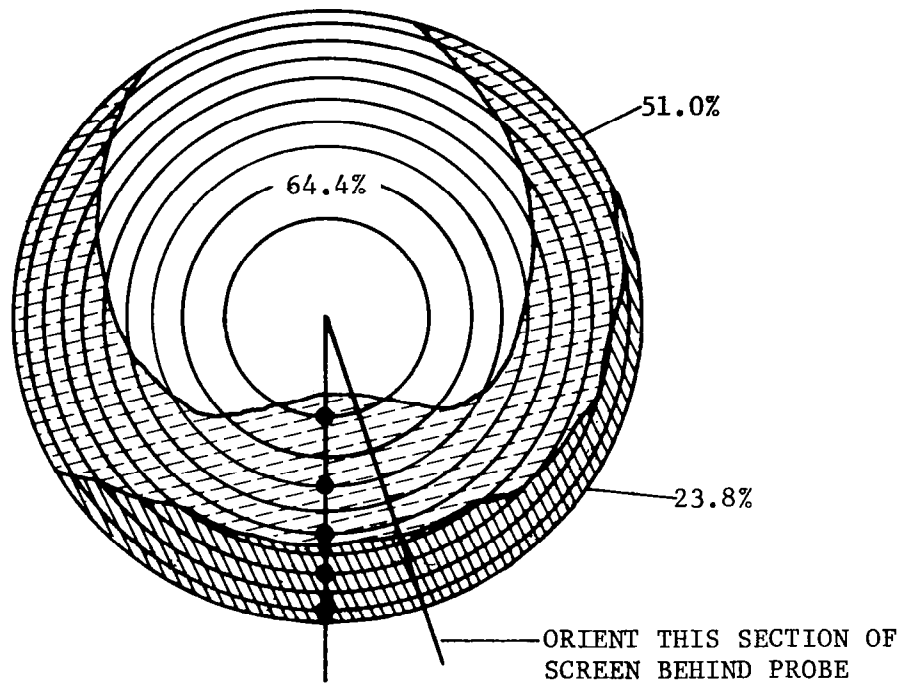
45.2%

FIGURE 69 — FLIGHT PATTERN DISTORTION SCREENS FOR DATA SET E